DYNAMIC PROPERTIES OF COMPACTED SOILS USING RESONANT COLUMN WITH SELF-CONTAINED BENDER ELEMENTS

by

ROSHNARA MOHAMMAD

Presented to the Faculty of the Graduate School of
The University of Texas at Arlington in Partial Fulfillment
of the Requirements
for the Degree of

MASTER OF SCIENCE IN CIVIL ENGINEERING

THE UNIVERSITY OF TEXAS AT ARLINGTON

May 2008

ACKNOWLEDGEMENTS

The author would like to thank his supervising professor, Dr. Laureano R. Hoyos, for all his guidance and unconditional support throughout the course of this research effort.

Thanks are also extended to the other members of her thesis committee, Drs. Anand Puppala, and Dr. MD. Sahadat Hossain for their valuable advice and review of this manuscript. In addition, the author would like to thank the faculty and staff of the Department of Civil and Environmental Engineering at The University of Texas at Arlington for their valuable assistance during his graduate studies.

The author also would like to thank all the geotechnical engineering graduate students in this institution for all their help and support. Special thanks are also extended to the Indian group for their worthy friendship and the good times.

The author would also like to thank Juan, Dr. Rajashekar, Ch. Srinivas, Dr. Sireesh, Sam, Srujan specially for their help during the thesis work.

Finally, and most of all, the author would like to thank her parents and her sister for all their love, encouragement, and great support. It is the best thing in her life to be a part of their family.

April 16, 2008

ABSTRACT

DYNAMIC PROPERTIES OF COMPACTED SOILS USING

RESONANT COLUMN WITH SELF-CONTAINED

BENDER ELEMENTS

Roshnara Mohammad, M.S.

The University of Texas at Arlington, 2008

Supervising Professor: Laureano R. Hoyos

A comprehensive series of resonant column and bender elements tests were simultaneously performed in the developed RC/BE apparatus. RC/BE tests were conducted on compacted specimens of poorly graded sand (SP) and high plasticity clay (CH) prepared at different moisture contents (17.7, 22.1, 25.5, 30.2% by weight for clay, and 5, 10, 15, 20% by weight for sand) and under different confining pressures (0, 2.5, 5.0, and 10.0 psi, or 0, 17.2, 34.4, 69.0 kPa) in order to assess the influence of key environmental factors, such as compaction induced suction and confining pressure, on small-strain stiffness properties of unsaturated soils, such as shear modulus (G_{max}) and damping ratio (D_{min}).

The high PI clay used in this work was obtained from city of Paris, Texas, while poorly graded sand was obtained from a local supplier in the city of Arlington, Texas. Compaction induced suction prior to RC/BE testing was assessed from soil-water characteristic curves (SWCC) obtained for SP and CH soils via PPE technique.

TABLE OF CONTENTS

LIST OF ILLUSTRATIONS

Figure Page

LIST OF TABLES

CHAPTER 1

INTRODUCTION

1.1 Background and Importance

The majority of roadway embankments, pavement subgrades and shallow foundation systems are supported by or made of unsaturated soil materials. The lack of education and training among engineering graduates and practitioners to properly deal with soils under partially saturated conditions has resulted in faulty or excessively conservative designs, and deficient long-term performance of built infrastructure.

The critical role of soil stiffness at small strains in the design and analysis of geotechnical infrastructure (earthdams, embankments, foundations) is now widely accepted. As most soils involved in these structures experience small strains, there is a great need for a better understanding of the small-strain behavior of such soils.

In the United States, various research efforts have been focused on field and laboratory measurements of soil suction, assessment of soil-water characteristic curve (SWCC) and analysis of swell-collapse behavior, but very few efforts have been focused on small-strain response of unsaturated soils and their dynamic characterization. The present thesis work is partly motivated by these research needs.

Small-strain stiffness properties like shear wave velocity (V_s), shear modulus (G_{max}) and material damping (D_{min}) are also the key subsoil parameters for an adequate design or analysis of earth structures subject to non-static loading (figure 1.1). Therefore, a thorough understanding of these stiffness properties is of critical importance.

Conventional geotechnical testing techniques, however, cannot capture this small-strain behavior and, hence, vastly underestimate the true soil stiffness, mainly due to errors in small-strain measurements. More recently, bender element based techniques have proved a viable

way to investigate soil stiffness at very small strains, mostly under dry or saturated conditions (Fam et al. 2002, and Thomann and Hryciw, 1990), Therefore, there is a great need for assessing the feasibility of bender element based techniques for unsaturated soils as compared to more reliable, fully standardized laboratory procedures, such as simple shear and resonant column based methods. The present thesis work is also motivated in part by these research needs.

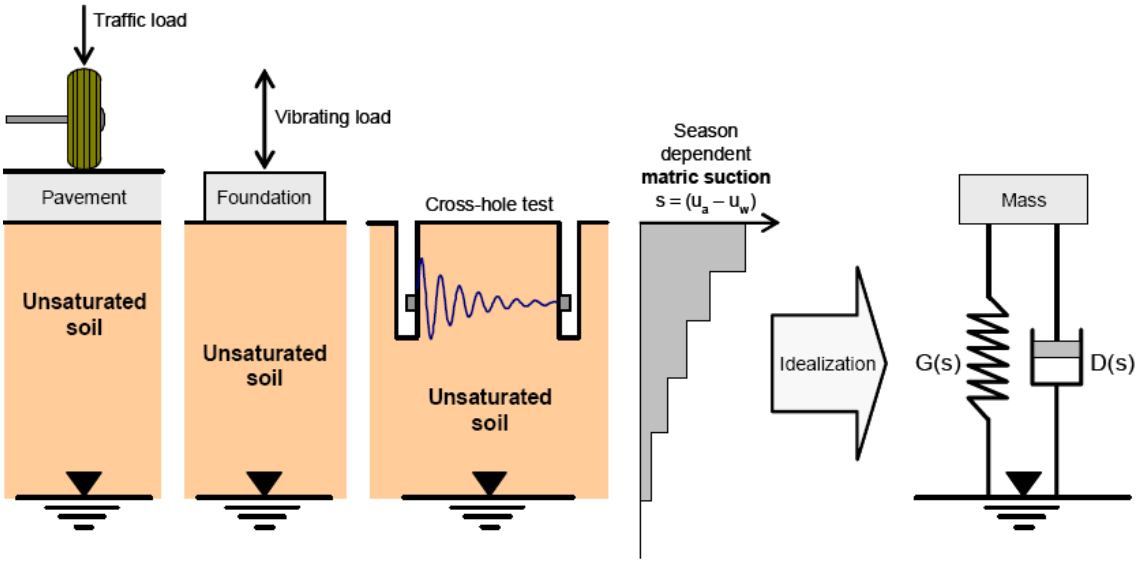

Figure 1.1 Idealization of Unsaturated Soil Under Non-static Loading

1.2 Objective and Scope

The main objective of the present thesis work was threefold: (1) To upgrade an existing resonant column device to accommodate piezoceramic bender elements, hereafter referred to as the RC/BE device; (2) To investigate the influence of key environmental factors, such as compaction-induced suction and confining pressure, on small-strain stiffness properties of unsaturated soils, such as shear modulus G_{max} and damping ratio D_{min}, via simultaneous RC

and BE testing; and (3) To assess the feasibility of BE technique for a wide range of compaction-induced suction states.

In order to accomplish this goal a comprehensive series of resonant column and bender element test were simultaneously performed in the developed RC/BE apparatus. RC/BE tests were conducted on compacted specimens of poorly graded sand (SP) and high plasticity clay (CH) prepared at different moisture contents (17.7, 22.1, 25.5, and 30.2% by weight for clay, and 5, 10, 15, 20% by weight for sand) and under different confining pressures (0, 2.5, 5.0, and 10.0 psi, or 0, 17.2, 34.4, and 69.0 kPa).

The high PI clay used in this work was obtained from city of Paris, Texas, while poorly graded sand was obtained from a local supplier in the city of Arlington, Texas. Compaction-induced suction prior to RC/BE testing was assessed from soil-water characteristic curves (SWCC) obtained for SP and CH soils via PPE technique.

1.3 Organization

A brief summary of the chapters included in this thesis document is presented in the following paragraphs.

Chapter 2 presents the concept of small-strain shear modulus and a brief review of available methods for measuring small-strain shear modulus in the laboratory. This chapter also includes a literature review of previous studies reported in the literature and related to the present work.

Chapter 3 is devoted to describing the fundamentals of resonant column and bender elements testing techniques, including main components of the modified RC/BE device, its step-by-step assembling process, and the typical soil parameters obtained from RC and BE tests.

Chapter 4 presents the basic engineering properties of the testing soils, along with a detailed description of all experimental variables and soil specimen preparation procedures.

Chapter 5 describes the entire experimental program and procedures followed in this work, along with a comprehensive analysis of all RC/BE test results, including the effect of

suction and confining pressure on small-strain shear modulus G_{max} and material damping D_{min}. A comparison of test results from resonant column (RC) and bender element (BE) testing techniques is also included.

Chapter 6 includes a summary of the accomplished work and the main conclusions.

CHAPTER 2

LITERATURE REVIEW

2.1 Introduction

This chapter illustrates the concept of small-strain shear modulus and presents a brief review of available methods for measuring small-strain shear modulus in the laboratory. This chapter also includes a literature review of previous studies reported in the literature and related to the present work.

2.2 Significance of Shear Modulus (G)

A key material property necessary to evaluate the small-strain and dynamic response of soil is the shear modulus, G, which relates shear stresses to shear strains. The relationship between shear stresses and shear strains is shown in figure 2.1. At low strain amplitudes the shear modulus is high as the curve is linear in nature. This modulus is known as the low-strain shear modulus (G_{max}). With an increase in strain, the curve becomes non-linear in nature, and the shear modulus related to these strains is known as the secant shear modulus (G).

Shear modulus is necessary to evaluate various types of geotechnical engineering problems including deformations in embankments, stability of shallow and deep foundation systems, dynamic soil-structure interaction, and machine foundation design (Dyvik and Madshus, 1986). Free-field dynamic response shear wave velocity has also been used to evaluate susceptibility of soils to liquefaction and to predict the ground surface and subsurface sub motions from outrunning ground shock produced by the detonation of high or nuclear explosives.

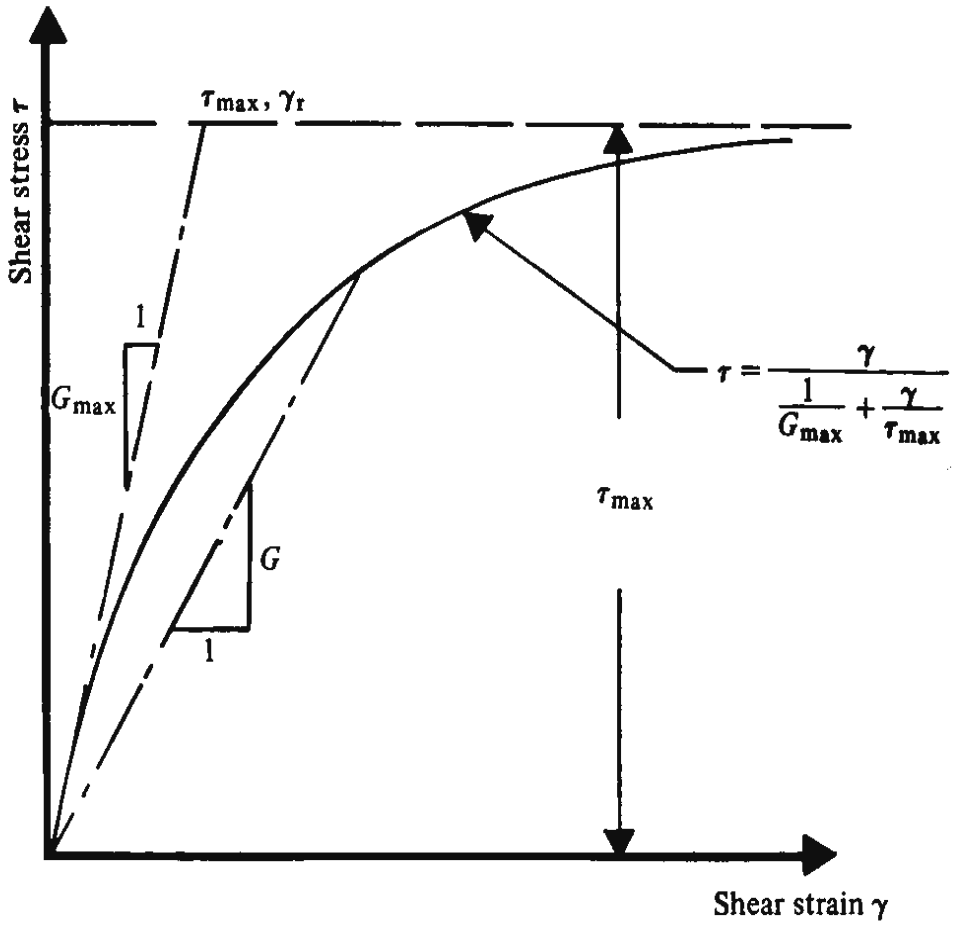

Figure 2.1 Variation of Shear Stress versus Shear Strain
(Hardin and Drnevich, 1972)

The shear modulus may also be used as an indirect indication of various soil parameters, as it correlates well to other soil properties such as density, fabric and liquefaction potential as well as sampling disturbance.

2.3 Laboratory Methods for Measuring G_{max}

2.3.1 Resonant Column

The most common method for measuring shear modulus G and damping ratio D in the laboratory is by the resonant column technique (Stokoe et al. 1978). This requires a special device where a cylindrical specimen is excited torsionally and tuned to resonance. The shear modulus measured by this technique is associated with strain levels of 10^{-5}% - 10^{-3}%.

The analysis of resonant column test is based on the assumption that the behavior of the soil is linear and elastic. The main disadvantage of this technique is that both the driving apparatus used for the excitation of the soil specimen and the motion monitoring instruments must be attached to the soil specimen. This alters the boundary conditions so that the interpretation of the test is based on the assumption that the attachments are lumped into a mass which oscillates with the soil specimen.

The RC test, however, has proved to yield reliable results and has been standardized by the American Society for Testing and Materials (ASTM D 4015-92).

2.3.2 Bender Element

The bender element method is the most simple and fast technique to obtain small strain shear modulus (G_{max}) of the soil, by measuring the velocity of propagation of a shear wave through a sample. Bender element systems can be set up in most laboratory apparatus, like oedometer or in direct simple shear devices, but are particularly versatile when used in the triaxial test (Dyvik and Madshus, 1986). In this technique the shear modulus is measured at strain levels below 10^{-3}%.

The main disadvantage of this test is that there is no direct methodology to find the damping ratio and shear modulus at higher strain levels. The BE technique, however, has been proved to yield reliable results in dry or saturated specimens, as shown in the literature review summarized in the following section.

2.4 Previous Work

Dyvik and Madshus (1986) installed bender elements in a Drnevich resonant column device at NGI. Values of G_{max} measured simultaneously by both methods on the same specimen were compared.

Five tests were performed on five different clay samples: tests 1 to 3 on off-shore clays, test 4 on a specimen of Drammen clay, and test 5 on a specimen of Haga clay, at different confining stress levels. The comparison of the results with G_{max} measured by resonant column technique and with bender elements is shown in figure 2.2.

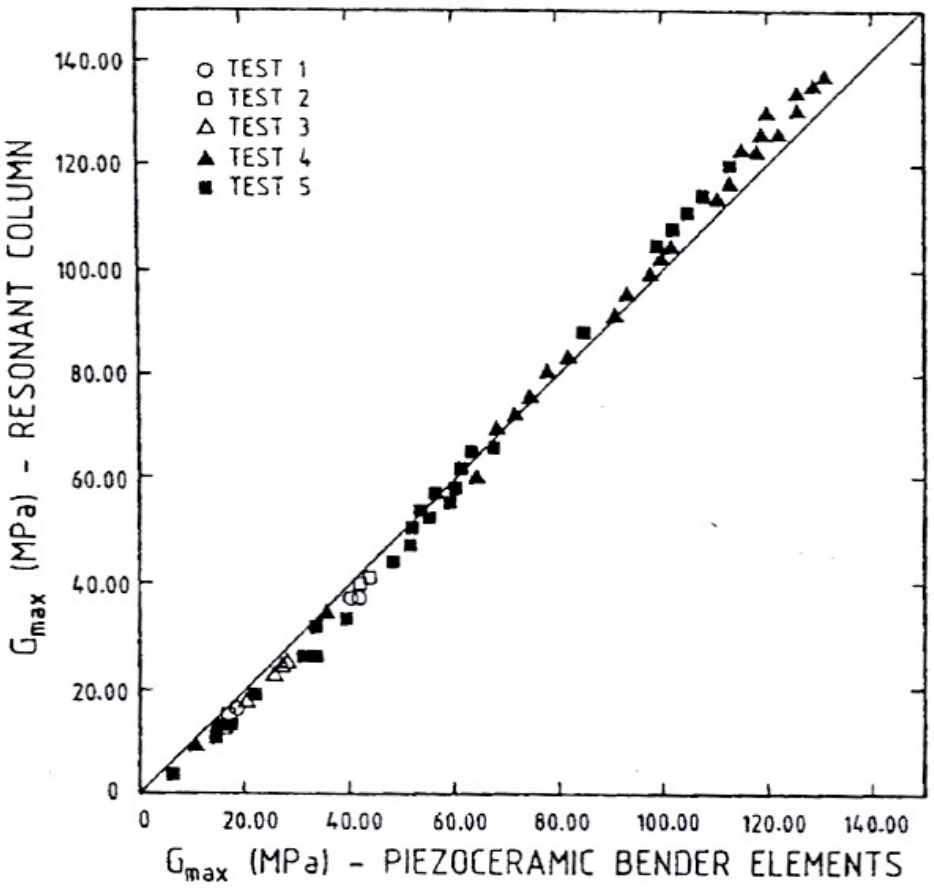

Figure 2.2 Comparison of G_{max} results by the RC and BE techniques
(Dyvik and Madshus, 1986)

The results from both the techniques are seen to cover a wide range of soil stiffness and are in excellent agreement. The G_{max} values match perfectly at a mid-range value of about 75 MPa and slightly deviate at the extremes. Although the resonant column technique is a well established method for determining G_{max} in the laboratory, there is nothing that says these results are exactly correct, so the resonant column and bender element techniques actually serve as a check on each other (Dyvik and Madshus, 1986).

To verify the accuracy of the bender elements system, Thomann and Hryciw (1990) inserted the bender elements in a resonant column apparatus and conducted tests on two cohesionless soils: Ottawa 100-200 and Glacier way silt.

A sample was constructed and the shear modulus was determined by both resonant column and bender element techniques for one day. The confining stress was increased, and the shear modulus was measured again for one day. They performed tests on five samples with confining stress running from 34.5 kPa (5 psi) to 345 kPa (50 psi). The shear wave velocities measured from both the techniques were compared as shown in the figure 2.3. The bender element results show a slightly higher stiffness than the resonant column results. The authors believe that this small discrepancy is due to the slight difference in shear strain levels in the two tests.

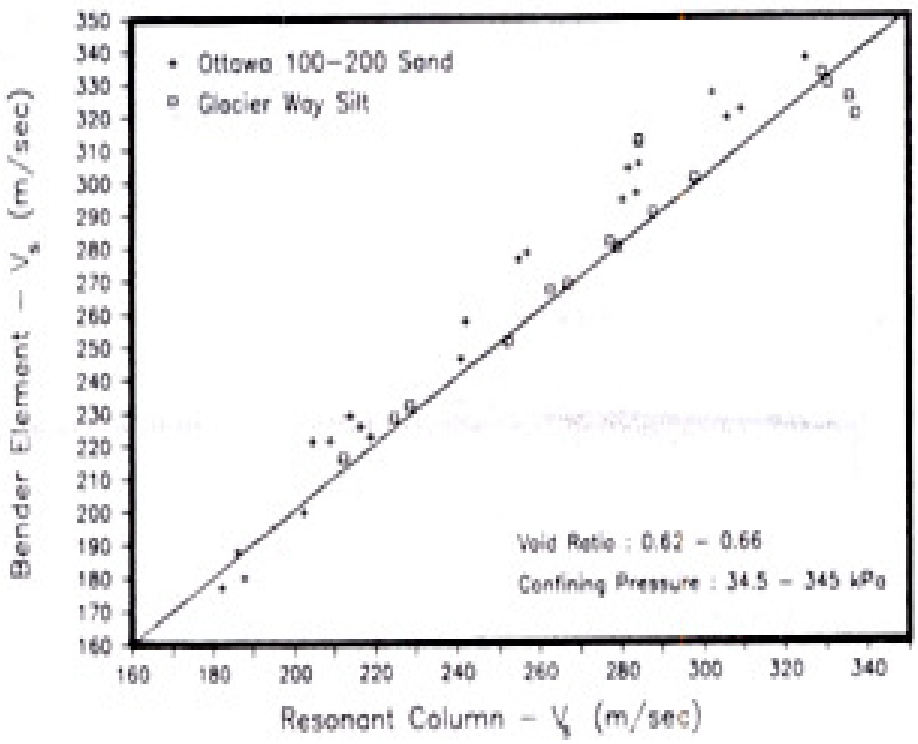

Figure 2.3 Comparison of shear wave velocity from RC and BE
(Thomann and Hryciw, 1990)

A special type of resonant column setup (fig 2.4) was developed by Ozudogru and Souto (1994) to investigate the limits of test conditions using piezocrystals in coarse grained soils in comparison with the resonant column tests. It was a fixed free (fixed end, spring tops) type of equipment supported by a Hardin-type of oscillator, which was originally a rotation prevented stepping motor. Triaxial cell was the main part of the equipment; an oscillator was mounted on the upper part of the cell with in the reaction mass. Both the top and bottom caps of the triaxial sample were equipped with peizocrystals. Cables coming from the resonant column part are connected to the power and charge amplifiers, signal generator, frequency meter accelerometer, linear variable differential meter, voltmeter and oscilloscope and cables coming from bender elements part are connected to pulse generator and computer scope (Souto and Ozudogru 1994). The tests were carried out on the samples at cell

pressures of 10, 25, 50, 100, 150, 200, 300, 400 kPa. The maximum shear modulus G_{max} measured by the two methods gave the similar results up to 100 kPa.

The results from the resonant column and bender elements are shown (figures 2.5 to 2.10). For crushed materials with grain size greater than 8 mm the results from bender elements tests are slightly greater than the results from the resonant column test.

Thus both the resonant column and bender elements tests are reliable for the G_{max} measurements below 8 mm grain size. Above 8 mm grain size resonant column test seems to be more reliable because they are more consistent with previous results and the results from the empirical equations (Souto and Ozudogru, 1994).

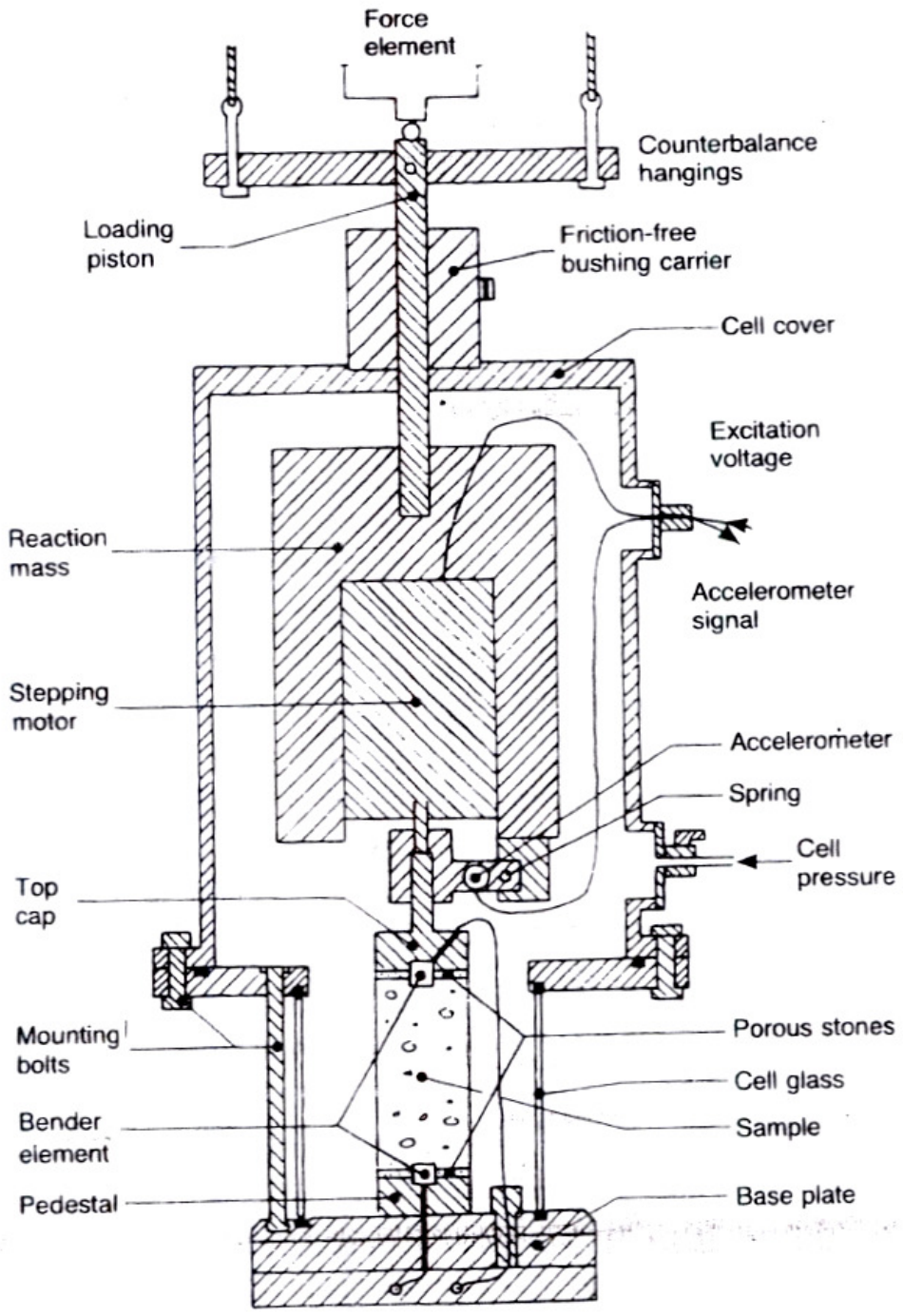

Figure 2.4 Newly developed bender element resonant column testing device (Souto and Ozudogru, 1994)

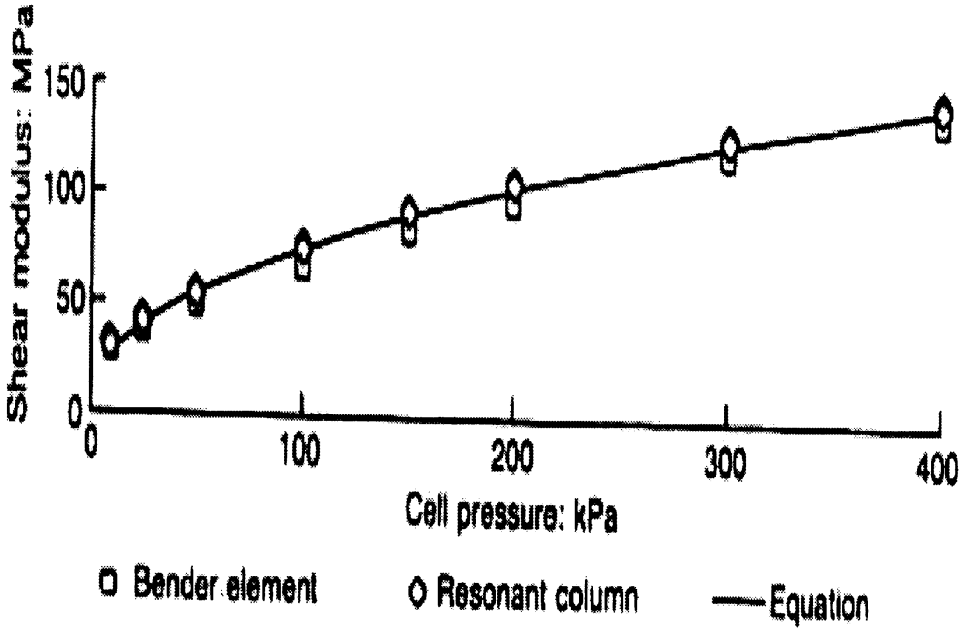

Figure 2.5 Shear modulus of 0-2 mm sand as a function of cell pressure
(Souto and Ozudogru, 1994)

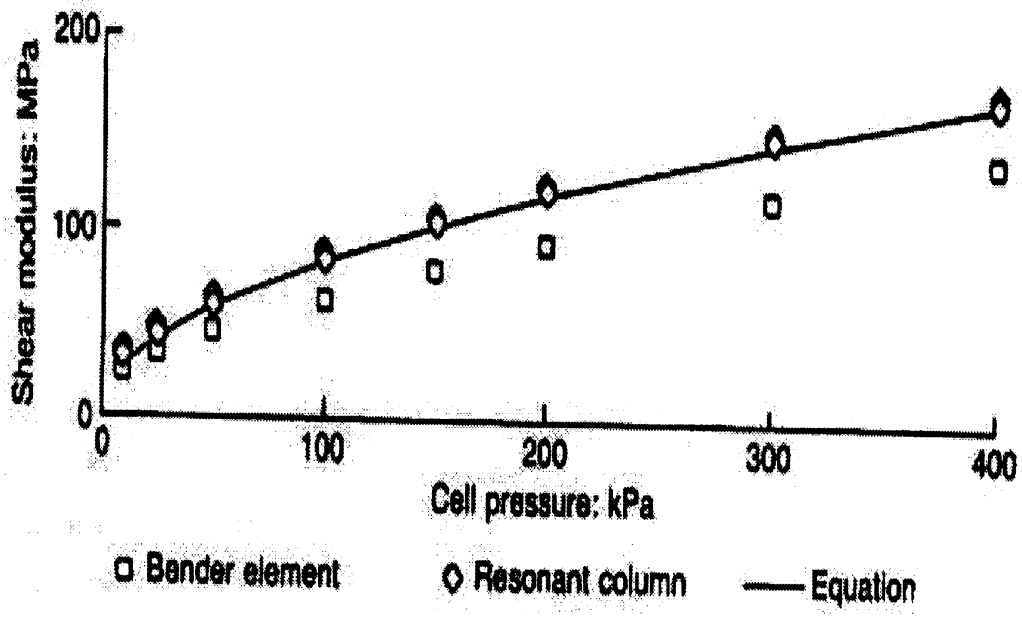

Figure 2.6 Shear modulus of 0-8 mm sand as a function of cell pressure
(Souto and Ozudogru, 1994)

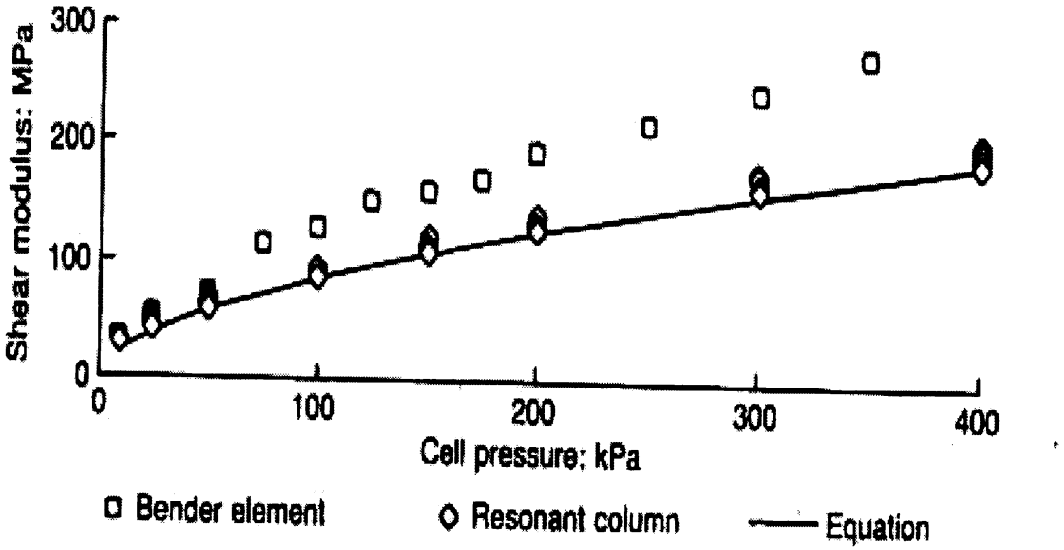

Figure 2.7 Shear modulus of 0-18 mm crushed till (Kaapinsalmi) as a function of cell pressure (Souto and Ozudogru, 1994)

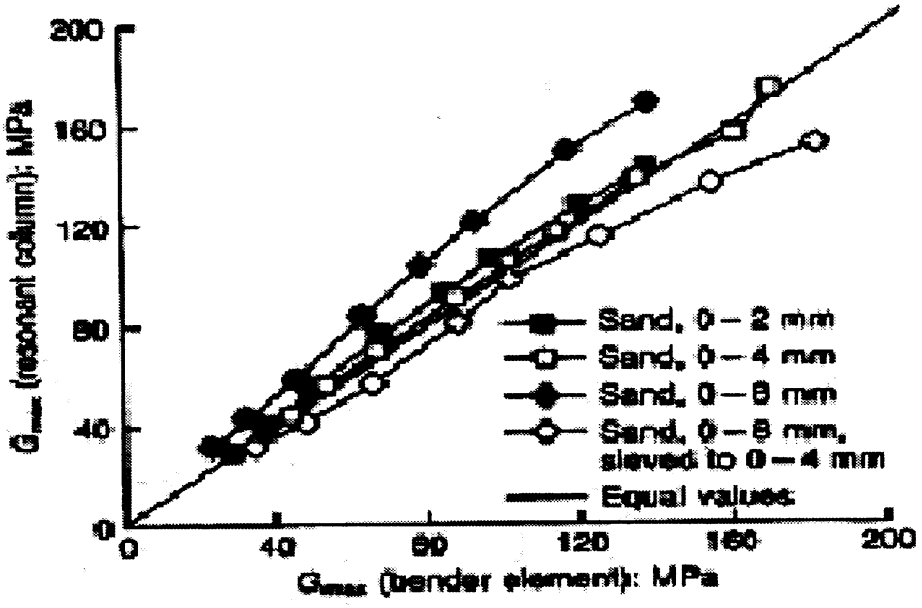

Figure 2.8 Comparison of shear modulus of sands measured by RC and BE tests (Souto and Ozudogru, 1994)

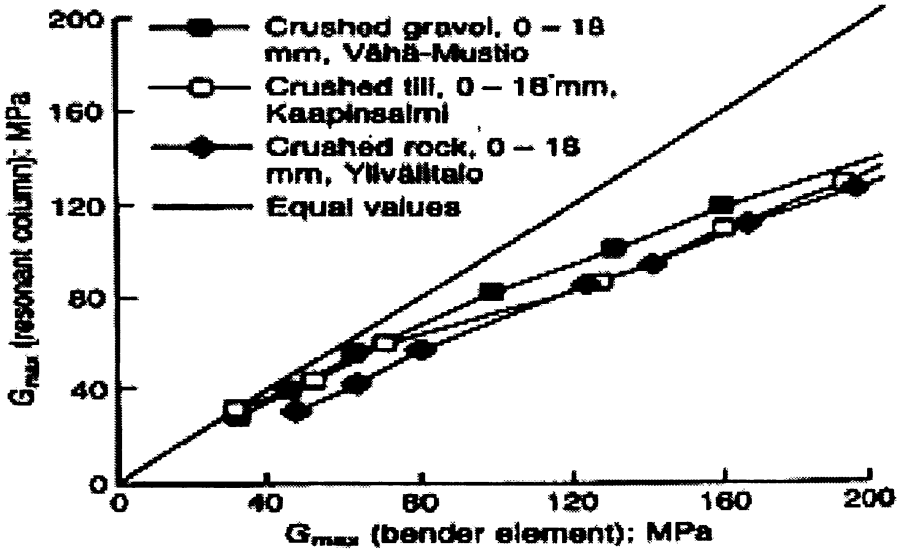

Figure 2.9 Comparison of shear modulus of crushed materials (grain size 0–18 mm) by RC and BE tests (Souto and Ozudogru, 1994)

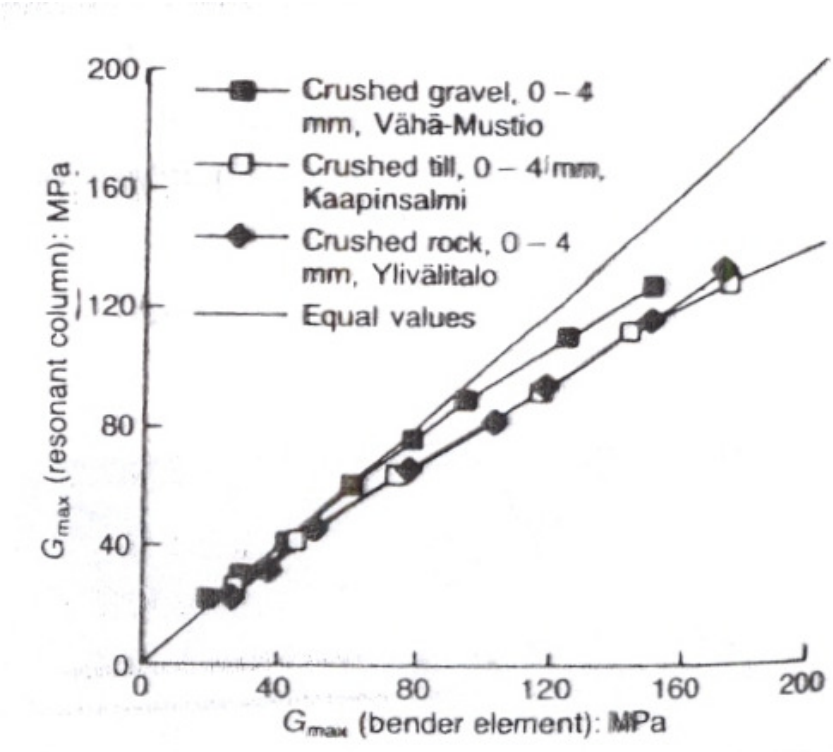

Figure 2.10 Comparison of shear modulus of crushed materials (grain size 0-4 mm) by RC and BE tests (Souto and Ozudogru, 1914).

Fam et al. (2002) conducted resonant column and piezocrystal bender element tests to study small-strain parameters on the fine grained sand. They performed resonant column tests to measure shear wave velocity and attenuation simultaneously and bender element tests were performed to monitor rapid wave velocity changes during particle dissolution.

They performed resonant column tests on two specimens under torsional excitation at small shear strains and instantaneous readings of shear wave velocity were taken during particle dissolution using piezocrystals installed in the top and bottom platens of the resonant column device. The experimental setup used in this work is shown in figure 2.11.

Two specimens of 14 cm long and 7 cm diameter were prepared for small-strain wave propagation testing. The specimen made of pure sand (no salt particles) was referred as the first specimen and the specimen made of sand-salt mixture (5% salt) was referred as the second specimen.

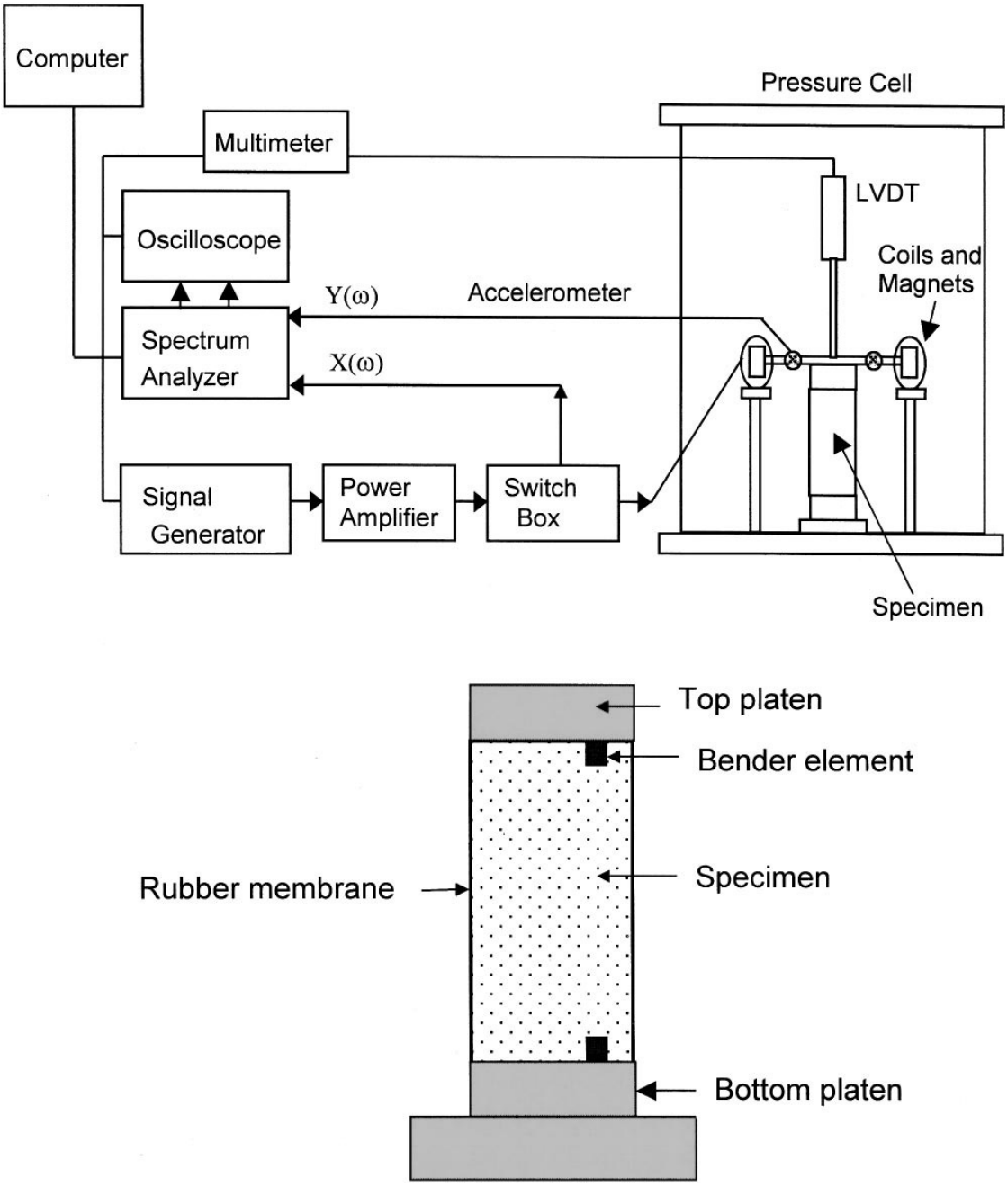

Figure 2.11 Small-strain experimental setup: (a) resonant column and (b) bender elements (Fam, Cascante and Dusseault, 2002)

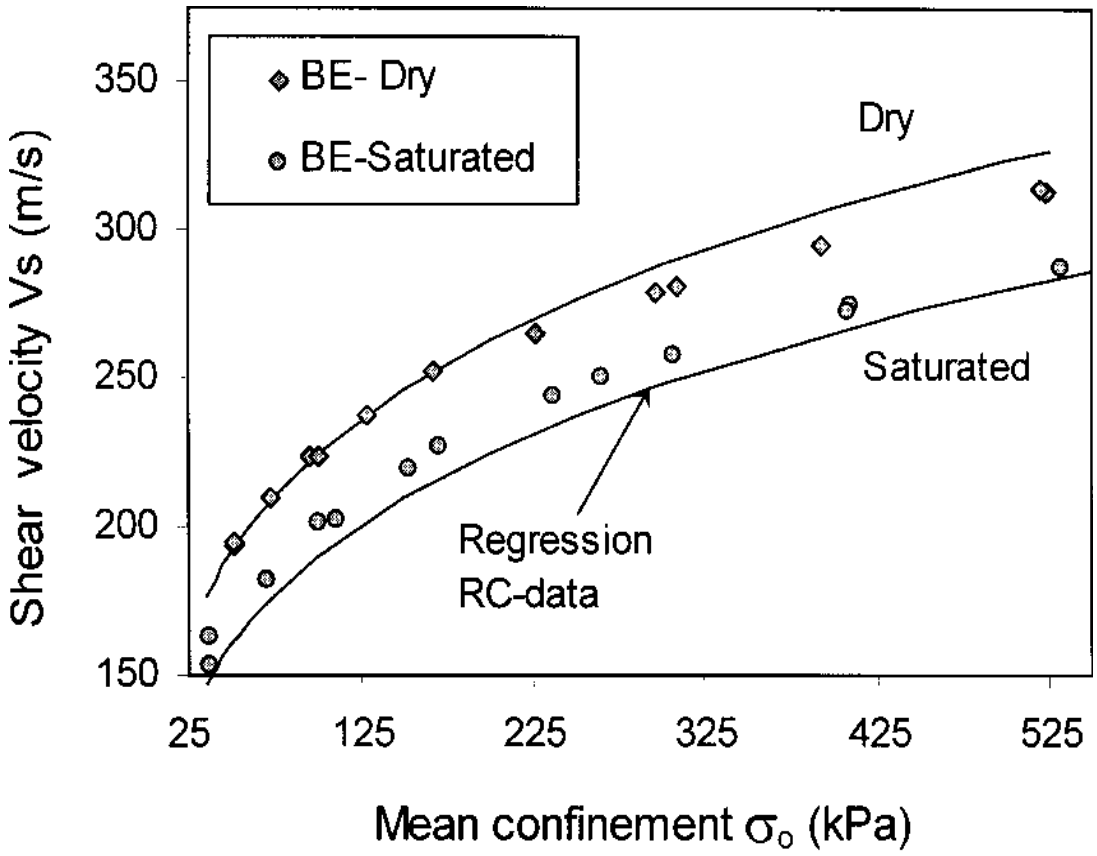

Figure 2.12 Shear velocity from RC and BE tests; second specimen.
(Fam, Cascante and Dusseault, 2002)

Velocity measurements for the dry and saturated specimens from the resonant column device and the bender elements showed good agreement during isotropic loading (figure 2.12). The accelerometer on the driving plate was used as the receiver, and first peak of the acceleration trace was selected as the first arrival of the shear wave. Small-strain test results showed low scatter and high consistency; therefore, it was expected that the conclusions based on the general trends are valid for different levels of salt content.

Phayak Takkabutr (2006) conducted a series of resonant column and bender elements tests to determine the small-strain shear modulus G_{max} and damping ratio D_{min} of partially saturated soils. In this work the bender elements are installed in the top cap and bottom pedestal of the resonant column device. A series of tests were conducted on several sand and clay specimens compacted at

different moisture contents. The sand specimens are compacted at 0%, 5%, 10%, 15%, 20%, 24% moisture contents and clay specimens at 90% dry, 95% dry, optimum, 95% wet and 90% wet of $Y_{d\text{-}max}$ (13%, 17%, 20%, 23% and 27% respectively). The tests are conducted under isotropic air confining pressure (σ_o).

The results of this work are shown in the figure 2.13.

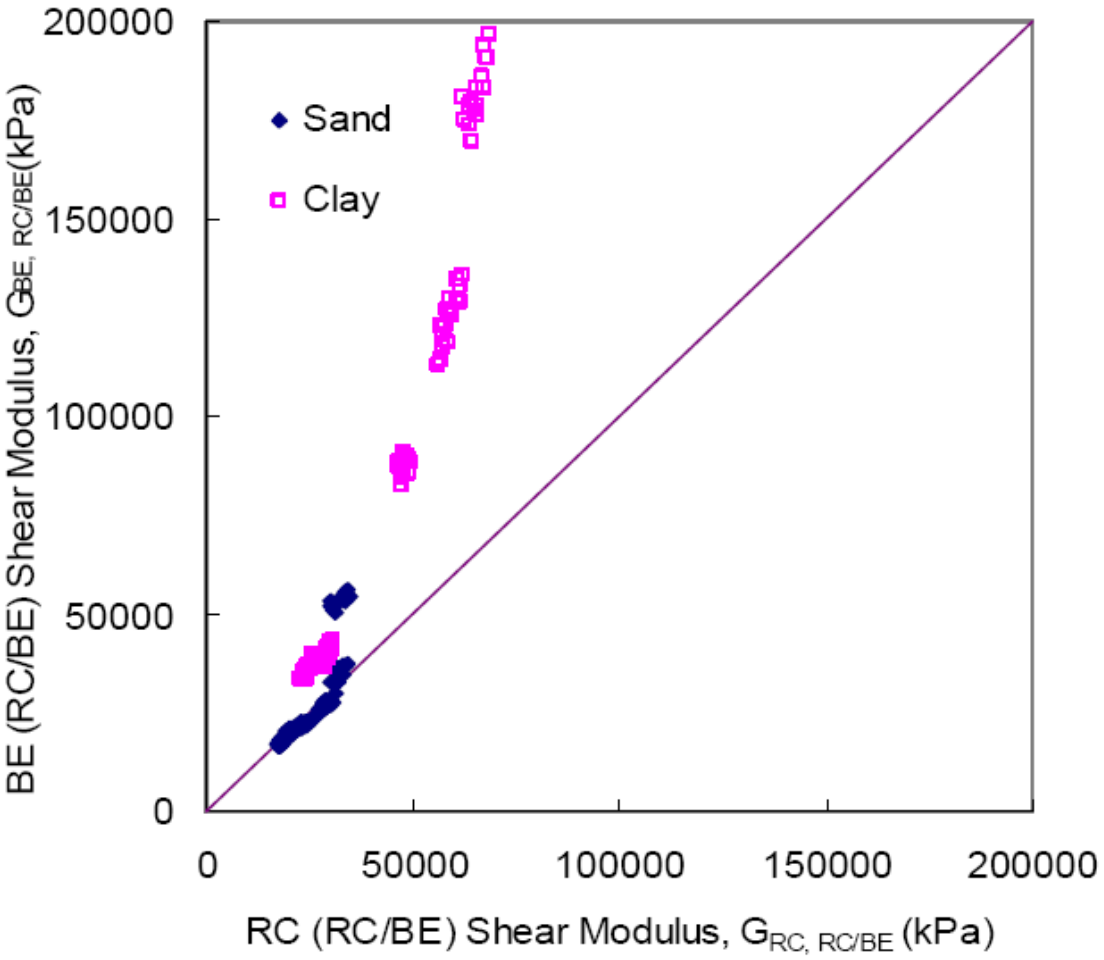

Figure 2.13 Variation of Shear Modulus of RC and BE from RC/BE
(Phayak Takkabutr, 2006)

It is observed that G_{max} values from BE tests considerably deviate from those from RC tests at higher compaction induced suction values.

Phayak Takkabutr used a correction factor to correct the values obtained from the bender element tests to that of the resonant column tests. After application of the correction factor the comparison of the G_{max} from the both the resonant column and bender element tests is shown in figure 2.14.

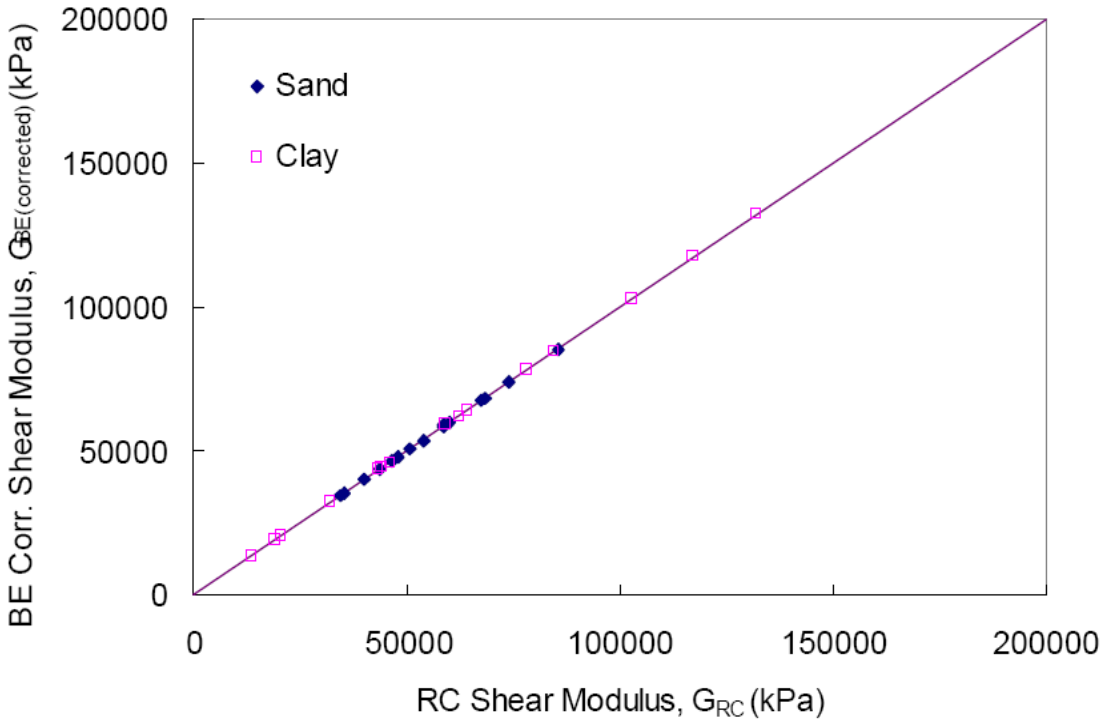

Figure 2.14 Variation of G_{RC} and G_{BE} Corrected for Sand and Clay from RC/BE (Phayak Takkabutr, 2006)

In this work, Takkabutr conducted the tests under air confinement instead of water confining pressure because a wire needs to be connected with the bender element present in the bottom pedestal, which was restricting the placement of the acrylic cylinder for proper application of confinement via water bath.

Ferreira et al. (2007) performed simultaneous resonant column and bender element test on Porto granitic residual soils to obtain the $G_{max.}$ In this work they installed the bender elements in the Hardin oscillator. They used two interpretation methodologies for the bender element results, in order to identify any discrepancies in the measured shear wave velocity.

Figure 2.15 shows the comparison of G_o values obtained from the resonant column and the two bender element tests. The figure shows that the FD domain technique results on G_o values deviate from RC test results by less than 1% in average. The results from the time domain deviate by 2% on an average from RC test results.

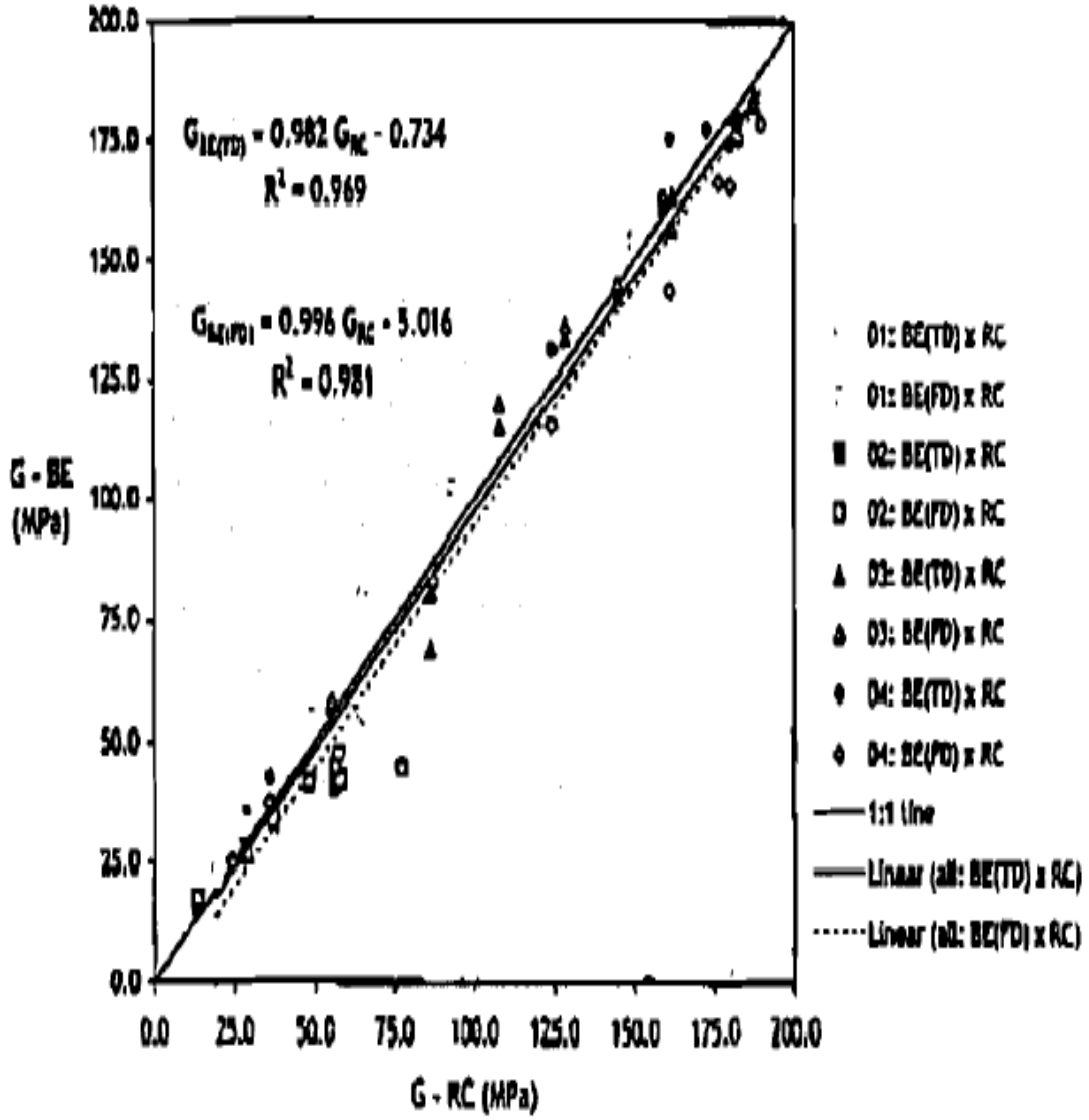

Figure 2.15 G_o Values Derived from the RC Versus from the Two BE Methods (Ferreira, Vianada and Santos, 2007)

In the present thesis work, the bottom pedestal was modified by attaching a custom made metal ring that allows the acrylic cylinder to be tightly secured onto the bottom pedestal without interfering with the BE receiver wiring, as shown in figure 2.16. Therefore, the tests in the present work are conducted under water confining pressure instead of air confining pressure.

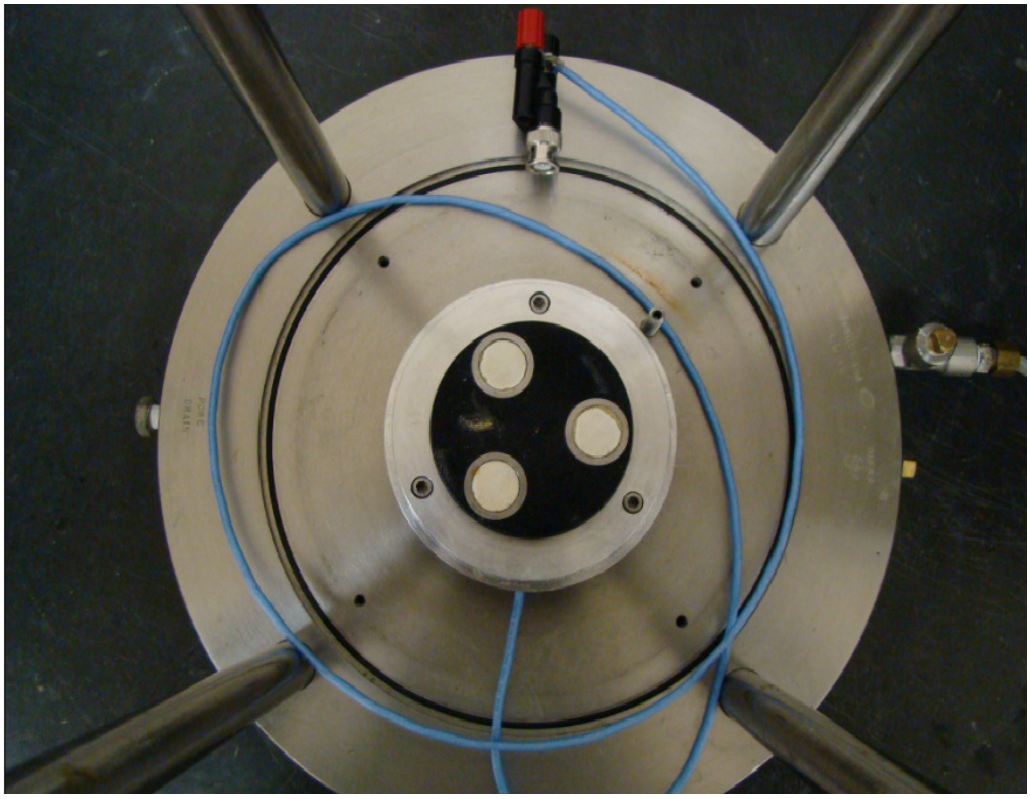

Figure 2.16 Modified Bottom pedestal Attached to the Base Plate in present work.

CHAPTER 3

FUNDAMENTALS OF RESONANT COLUMN AND BENDER ELEMENT TEST METHODS AND DEVELOPMENT OF RC/BE DEVICE

3.1 Introduction

This chapter is devoted to describe the fundamentals of resonant column and bender element testing techniques, including main components of the modified RC/BE device, its step-by-step assembling process, and the typical soil parameters obtained from RC/BE tests.

Stokoe (1978) introduced the resonant column device at UT-Austin, also known as the Stokoe torsional shear/resonant column device (TS/RC), which has been continuously refined in the last three decades. It has become one of the most reliable, efficient and pragmatic laboratory test methods for testing shear modulus G and material damping D of soils.

Shirley and Hampton (1977) introduced the bender element technique to obtain the small strain shear modulus of the soil, G_{max}, by measuring the velocity of propagation of a shear wave through the sample. A bender element is a thin piezoceramic element of two transversely poled plates bonded together with surface electrodes coating it. These bender elements can be incorporated into several laboratory tests like triaxial, shear, oedometer and resonant column tests (Dyvik and Madshus, 1986).

In the present work, bender elements are embedded in the top cap and the bottom pedestal of the resonant column device. Thus the G_{max} from both the resonant column and bender element tests are obtained simultaneously with identical isotropic conditions.

3.2 Fundamentals of Resonant Column Testing

3.2.1 Introduction

The Stokoe torsional shear/resonant column device is a fixed free system (figure 3.1) suitable for testing solid or hollow specimens with shearing strain amplitudes up to 0.4%

(Stokoe et al., 1978). The test specimen is in the shape of a circular cylinder. The bottom of the specimen rests on the rough, rigidly fixed pedestal; the top cap and the torsional drive plate are securely attached on top of the specimen. During resonant column testing the drive plate is allowed to rotate freely so that a torsional excitation is applied at the top of the specimen. The added mass of the top cap and drive plate on the top of the soil specimen has the beneficial effect of linearly distributing the peak torsional displacement throughout the sample, that is, induced shear strains do not vary in the vertical direction.

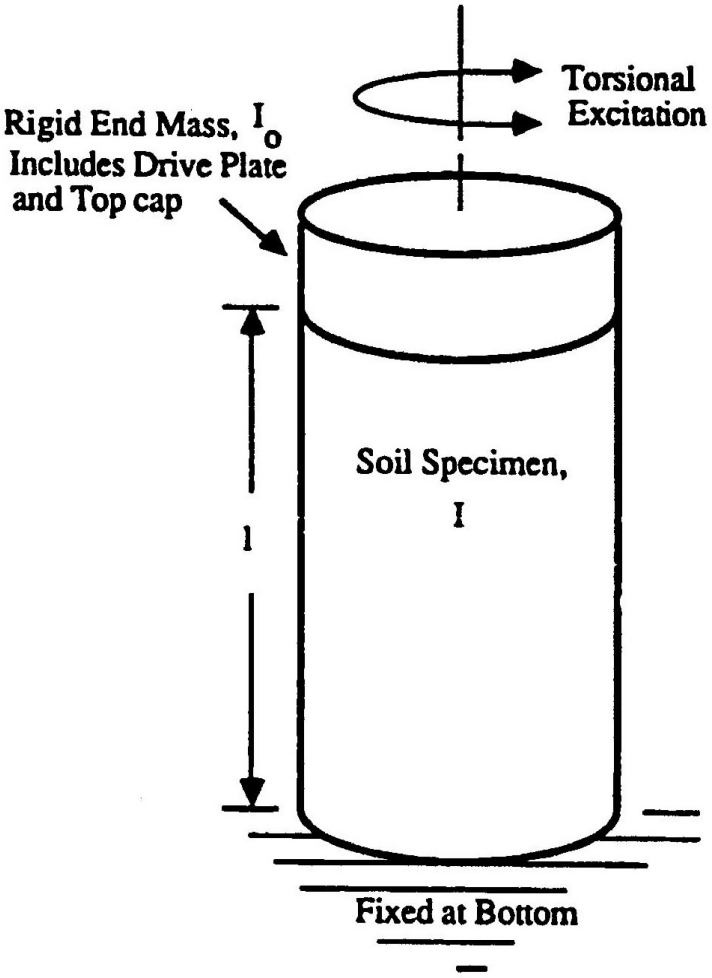

Figure 3.1 Idealization of a Fixed Free RC Device (Huoo-Ni, 1987)

The above testing description corresponds to a cyclic torque of constant amplitude and varying frequency being applied to the top of the specimen. Variations of the peak torsional displacements with varying frequency are recorded to obtain the frequency response curve. The peak torsional displacements are captured using an accelerometer securely attached to the drive plate. The resonant frequency f_r, corresponding to the peak of the curve is then obtained. Typical values of the resonant frequency for soil specimens range from 6 to 150Hz (Stokoe and Huoo-Ni, 1985). Dynamic soil properties like small-strain shear modulus G and damping ratio D can be obtained from the resonant frequency f_r and the frequency response curve, as described in the following sections.

3.2.2 Dynamic Properties from Resonant Column Test

Shear Modulus (G)

For a system undergoing linear vibration, the behavior of the material is linear elastic. That is, soil parameters used to describe the system, such as stiffness or viscous damping are assumed to be constant and independent of frequency and amplitude. For the soil column under torsional vibration, linear vibration theory can be used as long as the peak shearing strain amplitude is less than the threshold limit. Dynamic soil properties below this threshold limit are then considered to be strain independent.

The frequency equation of motion of a fixed-free elastic soil column subjected to harmonic torque at the top is as follows:

$$\frac{\Sigma I}{I_o} = \frac{\omega_n l}{V_s} \tan\left(\frac{\omega_n l}{V_s}\right) \tag{3.1}$$

Where,

$\Sigma I = I_s + I_m + I_w + \ldots\ldots\ldots\ldots\ldots$

And,

I_s = mass moment of inertia of soil column,

I_m = mass moment of inertia of latex membrane,

I_w = mass moment of inertia of central wire (for hollow specimens),

I_o = mass moment of inertia of top rigid mass (top cap + spider),

V_s = composite shear wave velocity in soil column,

ω_n = natural frequency of soil column (rad/sec), and

I = length of soil column.

A detailed analytical description of the equation (3.1) was given by Huoo-Ni (1987). Generally, in equation (3.1) resonant frequency (ω_r) is used instead of (ω_n). This is valid only for those systems presenting no damping. The relationship between natural frequency and resonant frequency is give by,

$$\omega_r = \omega_n \sqrt{1 - 2D^2} \tag{3.2}$$

Where,

D = material damping ratio.

From equation (3.2), as damping increases, the difference between ω_r and ω_n also increases, which yields to an increasing error being introduced by substituting ω_r for ω_n. Yet, fortunately enough, the damping ratio of most of the soils is less than 20%, which results in a difference of less than 4.5% between ω_r and ω_n (Huoo=Ni, 1987).

Now, using the theory of elasticity, the small-strain shear modulus (G_{max}) of he can be obtained from:

$$G = \rho (V_s)^2 \tag{3.3}$$

Where,

V_s = shear wave velocity

ρ = total mass density of the soil (i.e., unit weight divided by gravitational acceleration), $\rho = \gamma/g$. Richart (1975) suggested a simplified method for calculating the shear

modulus (G) using the resonant frequency (f_r), obtained from the soil column and the top cap-driver system. The method can be summarized as follows:

Once the system is under resonance, equation (3.1) can be written as,

$$\frac{\Sigma I}{I_o} = \frac{\omega_n l}{v_s} \tan\left(\frac{\omega_n l}{v_s}\right) \tag{3.4}$$

Where,

$$\omega_r = 2\pi f_r \tag{3.5}$$

for most cases,

$$\frac{\Sigma I}{I_o} \ll 1$$

Therefore, the shear modulus (G) can finally be expressed as,

$$G = \rho (2\pi L)^2 \left[\frac{f_r}{F_r}\right]^2 \tag{3.6}$$

Where,

$$F_r = \sqrt{\frac{I_s}{I_o}}, \text{ a constant} \tag{3.7}$$

In the present work, equations (3.6) and (3.7) were used to calculate linear (small-strain) shear moduli (G). Further details of the resonant column calibration process are presented by Hoyos (1993).

Material Damping Ration (D)

In the present work, the half-power bandwidth method was used to determine the material damping ratio of the soil (Richart et al., 1970). This approach is based on measuring the width of the frequency response curve near resonance. Frequencies above and below resonance (f_1 and f_2), corresponding to response amplitude (A_{rms}), are referred to the half-power points (figure 3.2). Now, the material damping ratio (D) can be determined as,

$$D\ (\%) = \frac{1}{2}\,\frac{f_2 - f_1}{f_r} \qquad (3.8)$$

Where, f_r is the resonant frequency (Hz). Equation (3.8) was used in the present work to calculate linear (small-strain) material damping ratio (D).

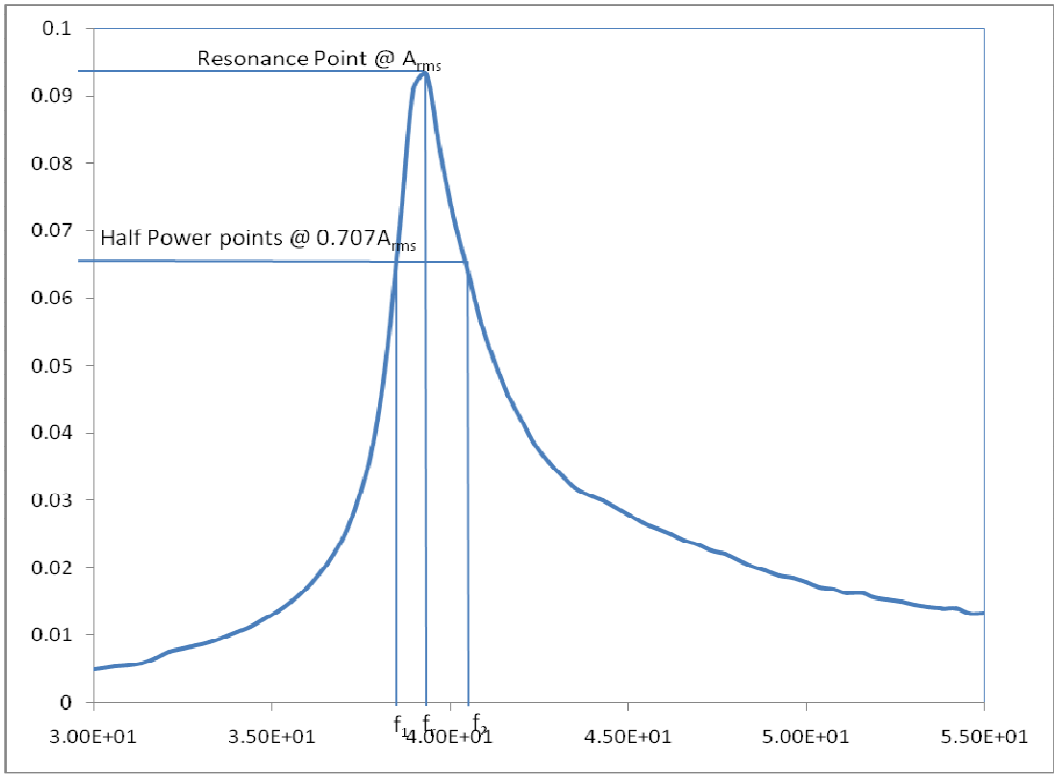

Figure 3.2 Bandwidth Method for Determination Material Damping Ratio, D

Shearing Strain (Y)

When the top of the soil column is subjected to a torsional displacement, the distance between a given point and the center of the soil column effects the shearing strain (Y) at that point with in the soil column. As shown in the figure 3.3, the shearing strain in a fixed-free hollowed specimen subject to a torque can be determined as $Y(r) = r\,\theta_{max}/l$, where r is the radial distance from the central vertical axis of the soil column to the point at which the shearing strain

(Y)is being calculated. The shearing strain increases linearly from 0, at r = 0, to a maximum of $r_o\ \theta_{max}/l$, at $r = r_o$ where r_o is the radius of the soil column (Huoo-Ni, 1987).

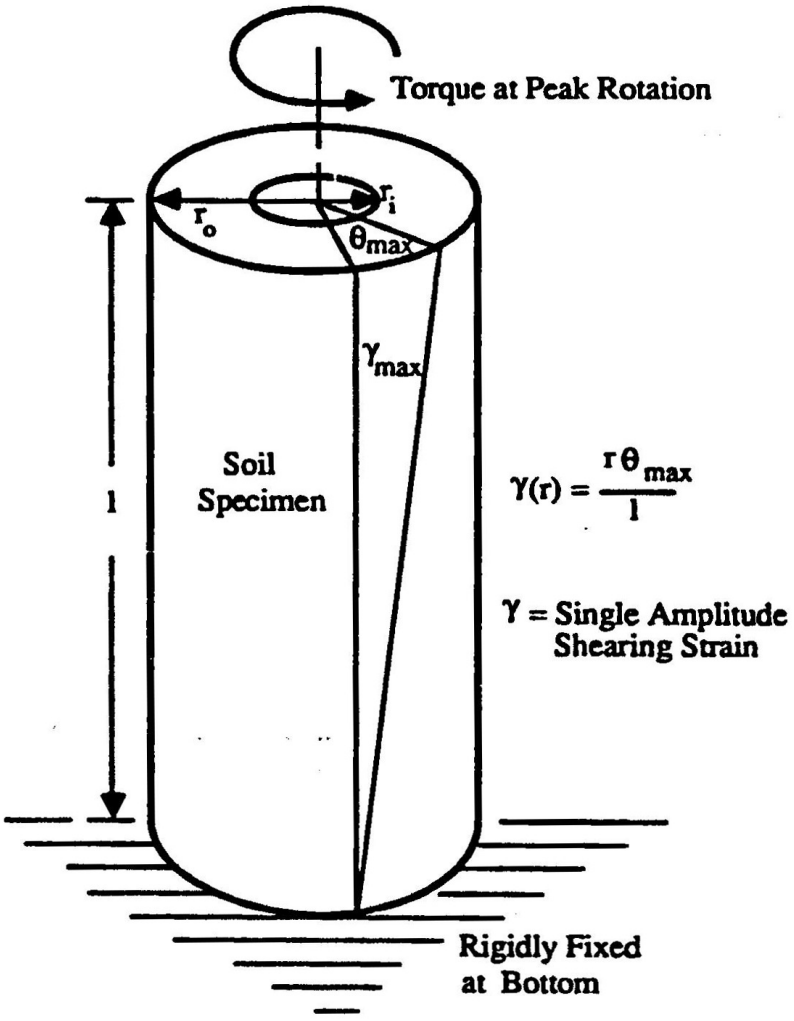

Figure 3.3 Concept of Shearing Strain

Since the shearing strain (Y) is not constant at every point in the soil specimen, an equivalent shearing strain (Y_{eq}) is to be chosen, which may be represented as $Y_{eq}(r) = r_{eq}.\theta_{max}/l$, where r_{eq} is the equivalent radius of a soil specimen used in an actual resonant column test. In

the present work, the shear strains (Y) were calculated at a distance of 0.707(r_o) from the central vertical axis of the resonant column presented by Hoyos (1993) and Chainuwat (2001).

Resilient Modulus (M_r)

In pavement design, resilient modulus (M_r) is the key subsoil stiffness parameter, recommended by the American Association of State Highway and Transportation Officials (AASHTO). Resilient modulus (M_r) is used as the basic material property in the design of multi-layered flexible, rigid or composite pavements, and also as an indication of roughness and potential cracking, rutting, or faulting (AASHTO, 1993).

For practical purposes, the resilient modulus (M_r) is considered to be equal to the elastic young's modulus (E). Therefore, using the theory of elasticity, resilient modulus (M_r), is as follows:

$$M_r = E = 2\,G(1+\mu) \tag{3.9}$$

Where G is obtained from the resonant column test and μ is the Poisson's ratio of the soil.

3.3 Fundamentals of Bender Elements Testing

3.3.1 Introduction

As described earlier bender elements are thin piezoceramic elements and are versatile when used in the triaxial test (Dyvik and Madshus, 1986). These are embedded in the bottom pedestal and the top platen of the triaxial apparatus (Jovicic et al., 1996). Base pedestal and the top platen can be of different sizes those specified by the ASTM. The cantilevering length of the bender elements can also be variable; generally the available sizes are 3mm, 5mm and 9mm. However, the cantilevering length of the bender elements at the transmitting and receiving end should be the same.

Figure 3.4 A Typical Set of Transmitter and Receiver Bender Elements

A pulse generator and a function generator feed the transmitter element with a waveform voltage of 20 V, causing it to bend so hat shear pulse is sent through the sample. A small voltage of 0.1-5 mV is generated by the motion of the receiver element caused by the arrival of the pulse. A digital oscilloscope connected to the personal computer captures the transmitted and received waves, and the G_{max} is calculated from the shear wave velocity, V_s, as it travels through the sample.

Typically a square wave was used as a transmitting wave, but the complexity arises from the fact that a square wave is composed of a spectrum of different frequencies. Viggiani and Atkinson (1995) suggested a sine pulse as the input signal to reduce the degree of subjectivity in the interpretation, and to avoid the difficulty in interpreting the square wave response. Being mainly of one frequency, the output wave was generally of similar shape, which allowed them to apply numerical techniques to reduce the uncertainty in the arrival time to around ±7%. By carefully shielding the cables to the elements a substantial improvement was made in the quality of the received trace, so that neither external amplification of the signal prior to the oscilloscope is needed, nor any filtering or averaging of the data.

3.3.2 Working Mechanism

Bender elements, installed in the end caps of the specimen can generate and measure the shear waves. These bender elements called piezoceramics have the ability to convert electrical impulses to mechanical impulses and vice versa. When a voltage impulse is applied across a single sheet of piezoceramic, it will either shorten or lengthen with a corresponding increase or decrease in thickness. An electrical impulse will cause one side to lengthen and the other side to shorten when two piezoceramic sheets are mounted together with their respective polarities opposite to each other. This result in the bending of the two sheets, hence piezoceramics are given the name bender elements.

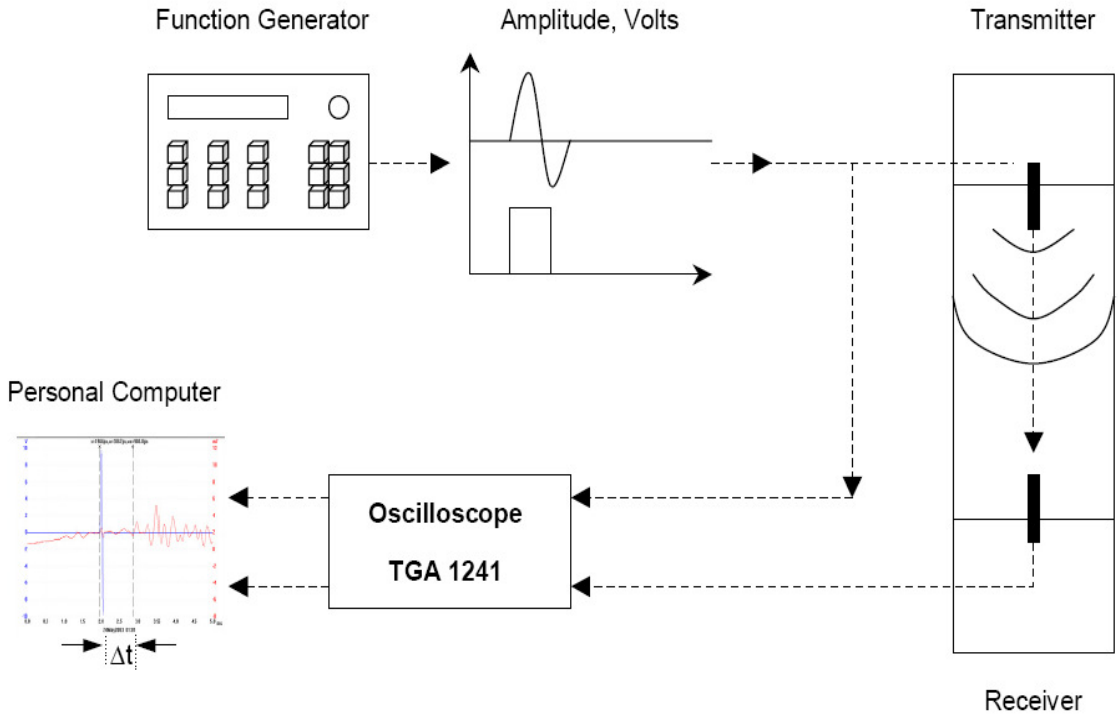

Figure 3.5 Schematic Representation of Principle of Bender Elements

Thus, if an electrical impulse is sent to the bender element mounted in the top cap of a specimen, the bender element will generate the shear wave which propagates through the soil and reaches the bottom of the specimen. Due to this the bender element mounted in the bottom cap vibrates slightly creating an electrical impulse. Using a parallel connection between personal computer and an oscilloscope, the impulse that is sent to the top bender element (transmitter) and the impulse that is generated by the bottom bender element (receiver) can be observed, the time it took the wave to propagate can be measured directly, and is called arrival time.

3.3.3. Factors effecting the arrival time of the shear wave

Near-field Effects

The first deflection of the signal may not correspond to the arrival of the shear wave but to the arrival of the so-called near-field component which travels with the velocity of a compression wave (Sahnero et al, 1986). Brignoli and Gotti (1992) found the evidence for the existence of the near components in the bender element tests. Parametric studies of the propagation of elastic waves in an elastic medium by Mancuso and Vinale (1988) show that the near-field effect may mask the arrival of the shear wave when the distance between the source and the receiver is in the range 1/4 - 4 wavelengths, which can be estimated from $\lambda = V_s/f$ where f is the mean frequency of the received signal. According to Viggiani and Atkinson (1995a), inverting the polarity of the source wave inverts the polarity of all the components, and therefore does not positively identify it.

Bender elements are like antennas which tend to pick up every little electrical noise. Due to this, transmitting wave is followed by the immediate response from the receiving wave. Therefore, in order to get rid of the noise cables should be insulated and grounded properly.

Near-field effects in bender element tests have been recognized by previous investigators (Brignoli and Gotti, 1992, Viggiani and Atkinson, 1995, Jovicic et al., 1996) with references made to the findings of Sanchez-Salinero et al. (1986). Sanchez-Salinero et al.

(1986) considered that “near-field” effects are potentially more complicated in triaxial specimen than in the unbounded 3-D space. This is because:

(1) interpretation methods that use the input signal are similar using d_1/λ of zero (where d_1 is the distance from the source to receiver), and so near field waves will be stronger than were considered in many of their analysis.

(2) the spherically spreading wave fronts that are generated by transmitting bender can reflect from the boundaries and therefore travel between benders by indirect paths and

(3) the transmitting bender is not a point source. Consequently, the assumption of planar wave fronts moving one-dimensionally between the caps will introduce errors that are in addition to the near-field effects identified by Sanchez-Salinero et al. (1986). Furthermore the transfer functions relating the physical waveform to the measured electrical signals introduce significant phase or time lags that are different at the transmitting and receiving benders (Arulnathan et al., 1998).

Time of Flight

The principal problem with bender elements method has always been the subjectivity of the determination of the arrival time used to measure shear wave velocity. Researchers have faced considerably greater difficulty in establishing a procedure for accurately evaluating the travel time of the shear wave. The shape of the arriving wave can vary substantially depending on the geometry and fabrication of the apparatus, the specimen properties, and the nature of the transmitted pulse, making a precise interpretation of the travel time difficult.

Travel time of first direct arrival in the output signals

Travel time of an impulse wave between two points in space may be taken as the time between the first direct arrival of the wave at each point. This method of interpretation assumes plane wave fronts and the absence of any reflected or refracted waves (Arulnathan et al., 1998).

In applying this approach to bender element tests, travel time has been estimated as the time between the start of voltage pulse input to be transmitting bender and the deflection in the output signal from the receiving bender.

Travel time between characteristic peaks off input and output signals

Travel Time of an impulse wave between two points in space may be taken as the time between characteristic points in the signals recorded at these two points, again based on the assumption of plane wave fronts and the absence of any reflected or refracted waves. The most commonly used characteristic points are the 'first peak', 'first trough', or 'zero crossings' of the input and output signals.

Travel time by cross-correlation of input to output signals

Travel time of an impulse wave between two points in space may be taken as the time shift that produces the peak cross-correlation between signals recorded at these two points, again based on the assumption of plane wave fronts and the absence of any reflected or refracted waves. For an impulse wave that has been recorded at two spaced points will reach maximum value for the time shift τ that equals the travel time of the impulse between two points.

It is convenient to calculate cross-correlation in the frequency domain using the Fast Fourier Transform (FFT). The calculations take only a few steps in commercial mathematics program and are no longer of onerous task.

Travel time using the second arrival in the output signals

An improved method of measuring the shear wave velocity of soil specimens using piezoceramic bender elements is proposed using reflections of a transmitted shear wave having a carefully controlled waveform which relies solely on data obtained by the receiving element. By relying only on multiple responses at the receiving element, the technique circumvents uncertainties associated with identifying the initial arrival of the shear wave. The second arrival is just the input wave after it reflects from the receiver cap (first arrival), travels back to the transmitter cap where it reflects again, and then returns to the receiver cap a second time.

Assuming plane wave propagation, the time between the first and second arrivals in the output signal is equal to twice the travel time of the wave from cap to cap (Riemer et al., 1998). To obtain useful data, it is important not only to generate a sufficiently strong wave to detect the reflections, but the shapes of the subsequent reflections must be sufficiently similar to identify equivalent points on them.

For the cross-correlation method it was useful to decompose the output signal into two dummy signals, both being modified copies of the original output signal. The first dummy signal is modified by setting the signals equal to zero outside the time window that contains the first arrival. The second dummy signal is modified by setting the signal equal to zero outside the time window that contains the second arrival. Then these two dummy signals can be cross-correlated to obtain the travel time for twice the cap-to-cap distance.

Analytical solutions for the body waves generated by point sources in a 3-D elastic space were used to show that the wave fronts spread in a spherical manner and involved coupling between waves that exhibited the same particle motion but propagated at different velocities (compression or shear wave velocity) and attenuated at different rates. The coupling of these waves was shown to obscure the first direct arrival of shear waves and to affect travel times calculated using characteristic peaks, cross-correlation, or phase velocity methods at locations near the source. The cross-correlation method was shown to be accurate for determining shear wave velocities for cases where the distance from the source to the first receiver (d_1) was greater than one shear wavelength (λ) and the distance from the source to second receiver (d_2) was twice d_1. The phase velocity method was shown to develop significant errors for a typical receiver spacing of $d_1/d_2 = 2$ when the ratio of d_1/λ was less than 1.

The frequency of the input signal is commonly selected by manually varying it to visually optimize the strength and clarity of the output signal. Experience from bender element tests in a variety of soils suggests that the optimum range of input signal frequencies often corresponds to λ/l_b ratios of about 8 to 16. (l_b is the length of the bender element). This range of

frequencies appear to balance the following competing factors: (1) the transmitting bender may appear most like a "point source" for λ/l_b values much larger than 4; (2) the system of waves generated by the transmitting bender can be more complex a λ/l_b values near 4 and decreases as λ/l_b increases, (3) the distortion of the output signal due to wave interference theoretically increases as λ/l_b increases, and (4) minimizing the near-field effect requires maximizing the value of L_{tt}/λ and hence minimizing λ/l_b (where L_{tt} is the tip to tip distance between bender elements) (Arulnathan et al., 1998).

It is recommended that several excitation frequencies and interpretation methods to be used for at least the first set of cantilever-type bender element tests on a given soil in a given device for the first time. The results can be used to identify cases where the choice of interpretation method and input signal frequency are of practical importance and provide insight for arriving at final estimate of V_s. Further experimental and analytical research is needed to provide more structures guidelines for the interpretation of cantilever-type bender element tests and to evaluate alternative configurations of piezoceramic sensors. In practice, first significant inversion of received signal represents true arrival of shear wave velocity. In this research study, the first significant inversion of received signal is considered as the arrival time of shear wave.

3.3.4 Dynamic Properties from Bender Elements Test

Small Strain Shear Modulus (G_{max}) Measurements

In recent years, a technique using bender elements was developed by Dyvik and Madshus (1985), Thomann and Hryciw (1990), Jovicic et al. (1996), Viggiani and Atkinson (1995) to investigate the small strain shear modulus, (G_{max}). This is an important parameter for many geotechnical analyses in earthquake engineering and soil dynamics. The value of G depends on a number of parameters, including void ratio, confining stress, soil structure, degree of saturation, temperature, stress history, and time. The stiffness of soils is often measured by the tangent shear modulus obtained from stress-strain relationships. At strains within the elastic

range, typically 10^{-4}% or less, the stiffness is represented by the small strain shear modulus, G_{max}. This parameter is very important in soil structure interaction problems and earthquake engineering where it is necessary to know how the shear modulus degrades from its small strain value as the level of shear strain increases.

The small strain shear modulus can be determined from the theory of elasticity, and can be written as (Baxter, 1999)

$$G = \rho * V_s^2 \qquad (3.10)$$ where

G = small strain shear modulus

ρ = mass, or total, density

V_s = shear wave velocity

$$V_s = L / \Delta t \qquad (3.11)$$

L = effective distance between tip of bender elements

Δt = travel time for the shear wave

The travel length (L) is taken as the bender element tip to tip distance within the soil specimen i.e. total specimen height minus the protrusion of the transmitter and receiver bender elements into the specimen. Because the bender elements protrude into the soil from the surface of the end caps, it is not intuitively apparent whether the travel path length is the full specimen height, the distance between the tips of the bender elements, or some intermediate "effective" length. Dyvik and Madshus (1985) showed that using the distance between the tips of the bender elements as the travel path length of the shear wave gave the best agreement with the other measurements of the modulus. Viggiani and Atkinson (1995) performed a series of bender element tests on specimens of varying heights, and reached the same conclusion. As a result of these studies, it is standard practice to adopt the tip-to-tip distance between the elements as the effective length of the travel path.

As the specimen height is much greater than the bender element protrusion, the net G_{max} value is relatively unchanged even if the total height of the specimen is considered as a

travel length for the shear wave. Also near-field effects should be taken into account for determining correct arrival time of the shear wave.

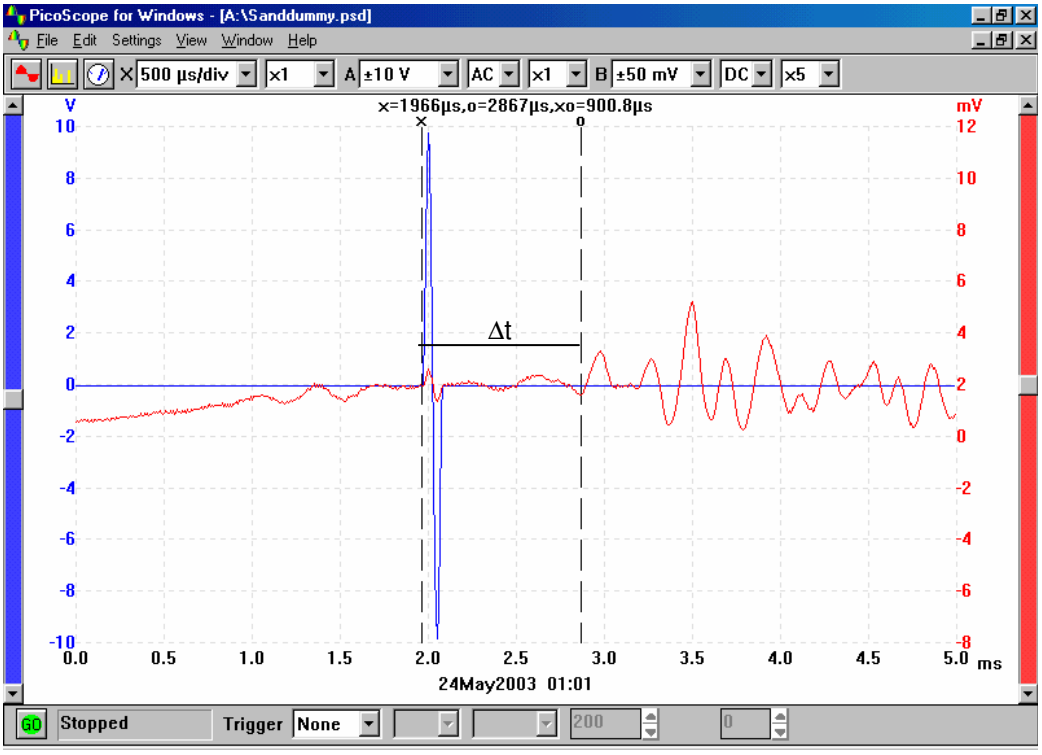

Figure 3.6 Typical Transmitted and Received Signals from Monitor

Damping Ratio Measurements Using Bender Element

Bender element consists of two thin piezoceramic plates rigidly bonded to a central metallic plate. Two thin conductive layers, electrodes, are glued externally to the bender. The polarization of the ceramic material in each plate and the electrical connections are such that when a driving voltage is applied to the element, one plate elongates and the other shortens. The net result is a bending displacement (Pyl and Degrande, 2000). On the other hand, when

an element is forced to bend an electrical signal can be measured through the wires leading to the element. A transmitter element and a receiver element are respectively placed in the bottom and top cap of a triaxial cell.

The basis for the analysis of the frequency response of the soil sample is the identification of different modes of vibration at resonance. The damping ratio D is calculated at these points of the response spectrum in the neighborhood of a resonance peak. The bender element is excited with a steady sine signal of constant voltage and amplitude is measured at the receiver element. To make this value independent from the source amplitude it is normalized by this amplitude. This process is repeated at different frequencies until the whole spectrum of soil sample is defined. The damping ratio is estimated at the points of the curve around the natural frequency of the shear mode. For this purpose different techniques are available such as the half-power and circle-fit method.

Half-Power Method

The most common method of measuring damping uses the relative width of the response spectrum. The application of latter expression is usually called the half-power method. This measurement need use the continue sine waveform to produce the vibration to the receiver bender element. Then, the peak-to-peak amplitude from received signal is collected at different frequency near the highest amplitude. The typical signal and measurement from the received signal are shown in figure 3.7.

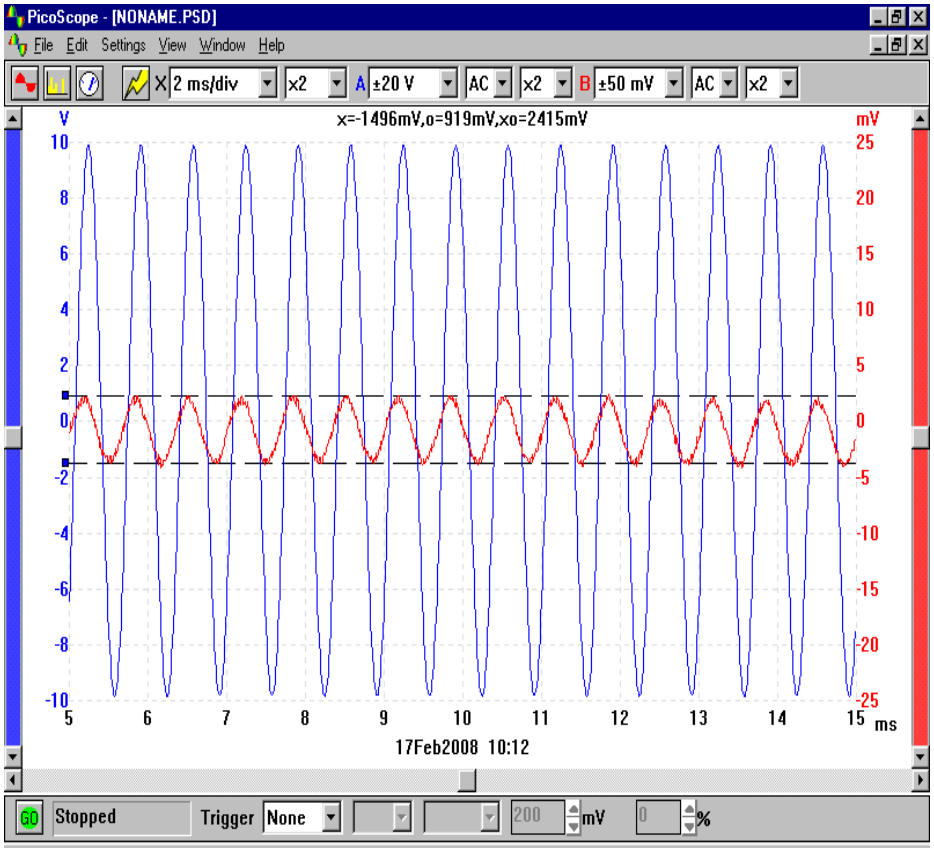

Figure 3.7 Typical Amplitude Measurement from BE Test

The figure 3.8 has shown the typical frequency and amplitude result from the bender element test. After creating the resonant frequency curve, the half-power method is performed to calculate the damping ration, D from equation 3.12:

$$D\ (\%) = \frac{1}{2}\,\frac{f_2 - f_1}{f_r} \qquad (3.12)$$

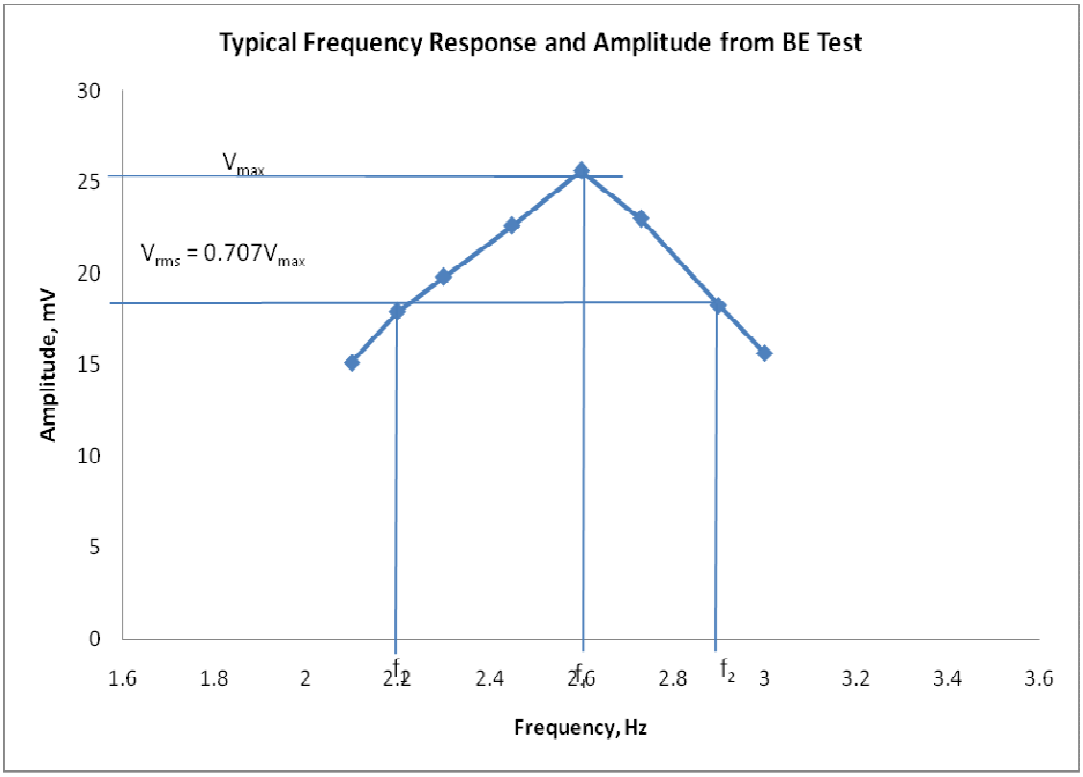

Figure 3.8 Typical Resonant Curve with Variables for Half Power Method

Circle-Fit Method

The circle-fit method, described in Ewins (1988) is able to calculate the damping ratio with very few points around the resonance peak and the amplitude of the peak has only little influence on the result. This is an advantage in cases were different modes have frequencies close to each other.

The Nyquist plot of the response spectrum of a single degree of freedom system leads to a circle as shown in figure 3.9. Even though the sample is not such a system it behaves for selected frequency sections in the same way. The material damping can be calculated from

points close to that corresponding to the maximum amplitude using the following expression (equation 3.13):

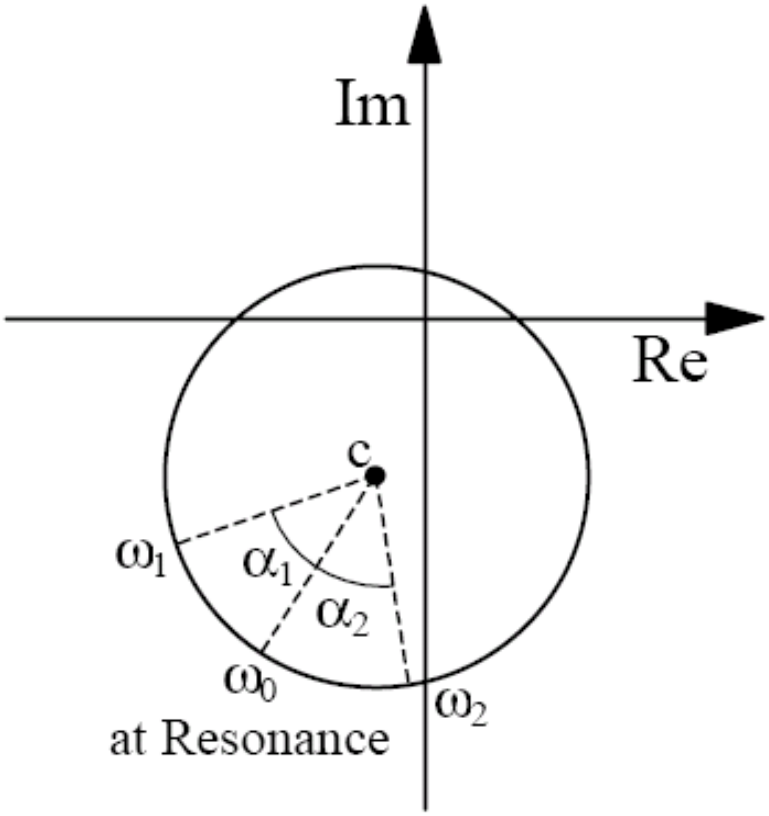

Figure 3.9 Nyquist Plot Used in the Circle-Fit Method

$$D = \frac{\omega_2^2 - \omega_1^2}{2\omega_0\left[\omega_2 \tan\frac{\alpha_2}{2} + \omega_1 \tan\frac{\alpha_2}{2}\right]} \qquad (3.13)$$

where:

ω_o = angular frequency corresponding to the maximum angular sweep velocity

ω_1, ω_2 = angular frequencies

α_1, α_2 = angles at both sides of ω_o

A circle is fitted to the points of the response curve close to the resonant frequency to find the center. Knowing this point makes it possible to determine the necessary angles α (Pyl and Degrande, 2000).

3.4 Basic Components of Upgraded RC/BE Test Device

In this thesis work the resonant column and bender element tests are performed simultaneously in order to simulate the identical isotropic conditions during both the tests. Consequently, the comparison of the results from both the methods can be determined accurately.

The confining chamber of the conventional resonant column was modified by drilling two small holes and replacing them with the sealed 50 psi bulkhead BNC connectors to prevent air leak during the test. These holes are drilled in order to connect both the top and bottom bender element wires with the oscilloscope. The bottom pedestal is modified by attaching a steel metal piece in order to accommodate acrylic cylinder. These modifications are shown in the figures 3.10 and 3.11.

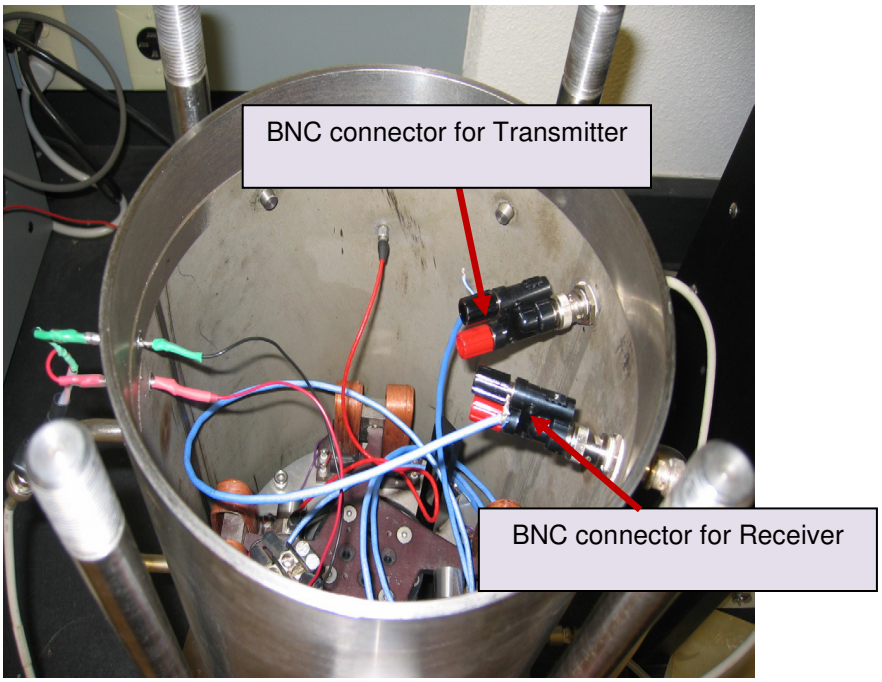

Figure 3.10 Sealed 50Psi Bulkhead Connectors

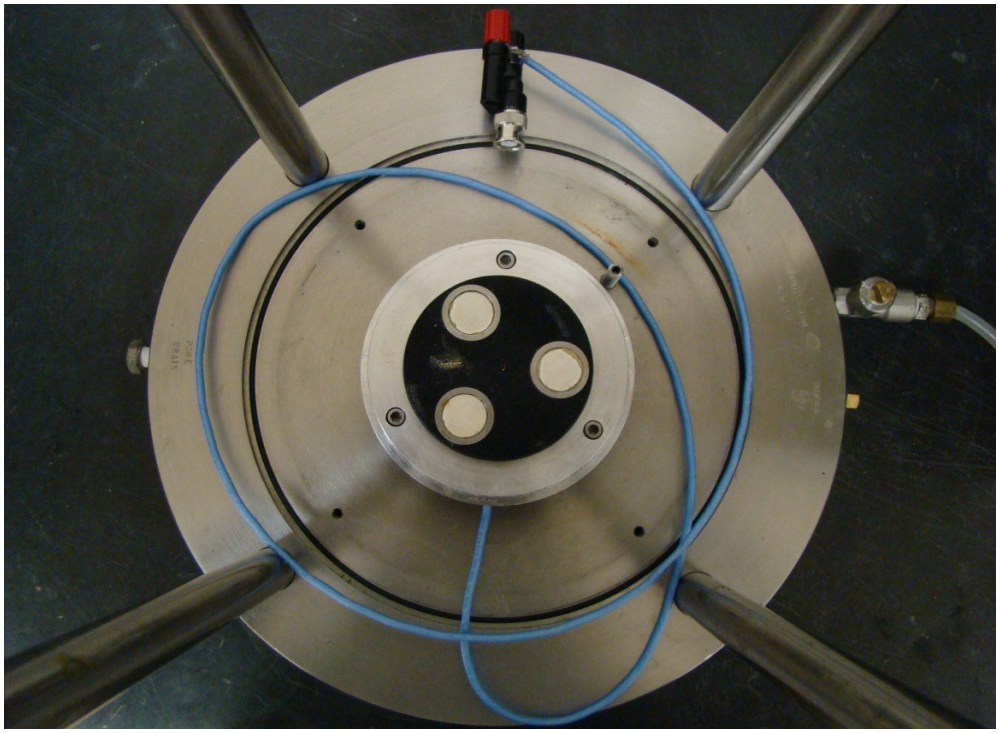

Figure 3.11 Modified Bottom Pedestal Attached to the Base Plate

The main components of the RC/BE testing device used in this thesis work are: confining chamber, torsional drive mechanism, torsional motion monitoring system, oscilloscope, receiving signal converter, bender element, and personal computer. A brief description of these components is presented individually in the following sections.

3.4.1 Confining Chamber

The RC confining chamber is composed of a thin-wall hollow cylinder, a base plate, a cover plate, and four guide rods used to secure the base and cover plates to the hollow cylinder. All components are made of stainless steel. The hollow cylinder has an outside diameter of 8.5 in (21.6 cm), a wall thickness of 0.25 in (0.64 cm), and a height of 18 in (45.7 cm). A fully assembled chamber is shown in figure 3.12

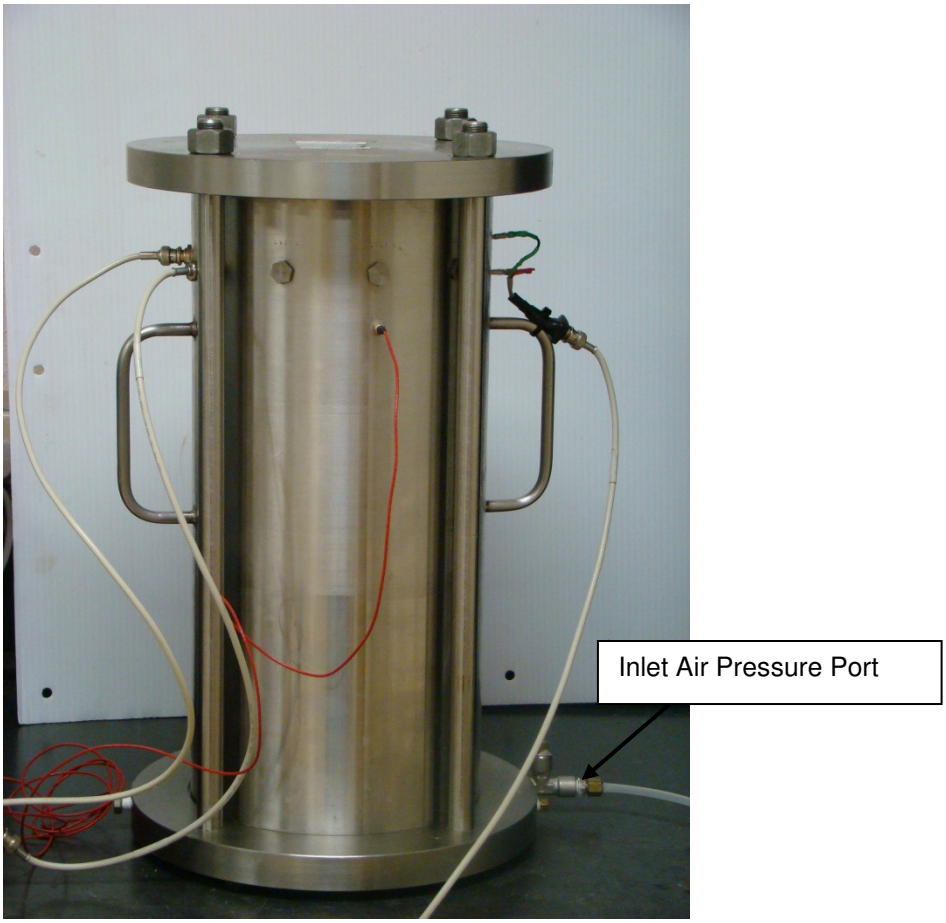

Figure 3.12 Fully Assembled Confining Chamber

Prior to RC testing, the soil specimen, along with the remaining components of the RC device, are placed inside the confining chamber and pressurized with air at the desired isotropic confining pressure. This chamber has been designed to withstand a maximum air pressure of 600 psi (4,173 kPa). To this chamber air pressure is supplied via an inlet air-pressure port located at the base plate shown figure 3.12.

3.4.2. Torsional Drive Mechanism

The torsional drive mechanism (driver) includes a flat aluminum four-armed plate (spider), with a cubical magnet encircled by a pair of drive coils at each end, and an input signal current connection. The magnets are securely attached to the four ends of the spider, which

allow the magnets to move during soil consolidation. The top and side views of the torsional drive mechanism (driver) are shown in figure 3.13

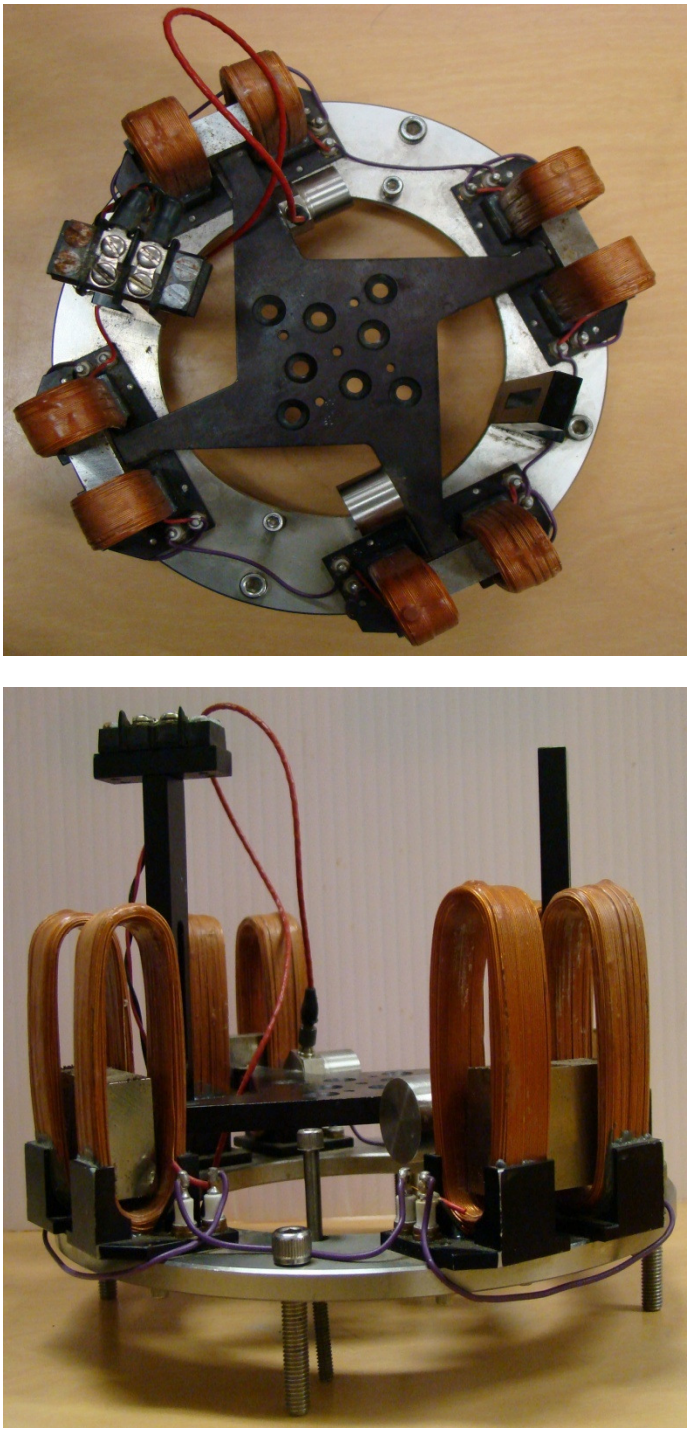

Figure 3.13 Top and Site Views of the Torsional Drive Mechanism (Driver)

The spider and drive coils form a torsional motor that excites the specimen in torsional motion. During RC testing, the spider is fixed to the top cap resting on top of the specimen. The top cap has a rough surface on the side making contact with the specimen to insure that no slippage occurs between the specimen and the driver during torsional excitation. The set of eight drive coils is fixed to a cylindrical cage that is securely attached to the base plate of the chamber (figure 13.14)

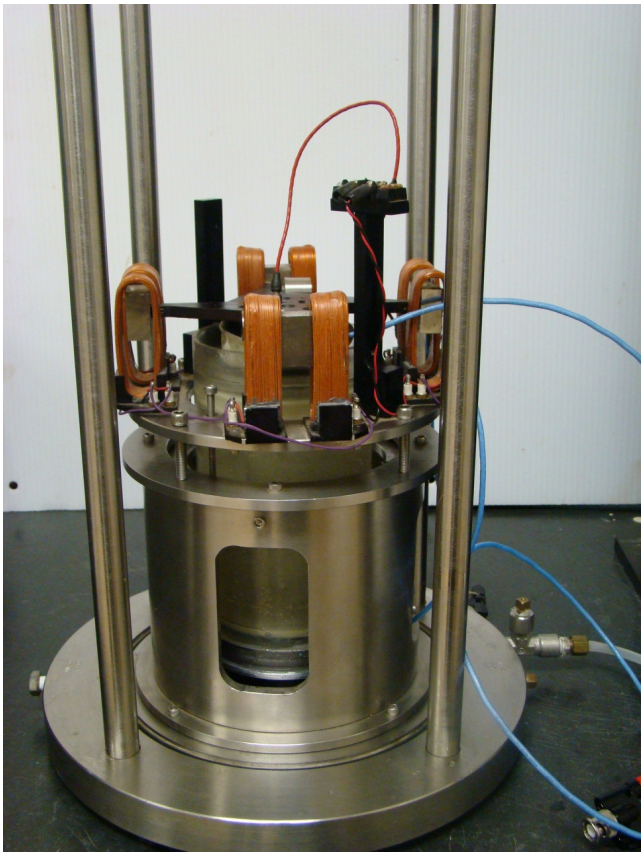

Figure 3.14 Cylindrical Cage Supporting Set of Drive Coils

3.4.3 Torsional Motion Monitoring System

The torsional motion monitoring system is used to capture the frequency response of the soil column during RC testing, and includes an accelerometer rigidly attached to one of the arms of the spider, and an associated counterweight installed on the opposite side of the four-

armed spider as shown in figure 3.13. The voltage response of the accelerometer is sent to a charge amplifier and then recorded by a dynamic signal analyzer, as explained in the following section.

Frequency Response Measurement System

The frequency response measurement system used in this thesis includes a dynamic signal analyzer, a charge amplifier box, and a PC-based computer terminal. The analyzer is a dual-channel SR785-model dynamic signal analyzer acquired from Stanford Research Systems, Inc. The amplifier is a 4102M-model charge amplifier box acquired from Columbia Research Laboratories. The analyzer and charge amplifier box (resting on top of the analyzer) are shown in figure 3.15.

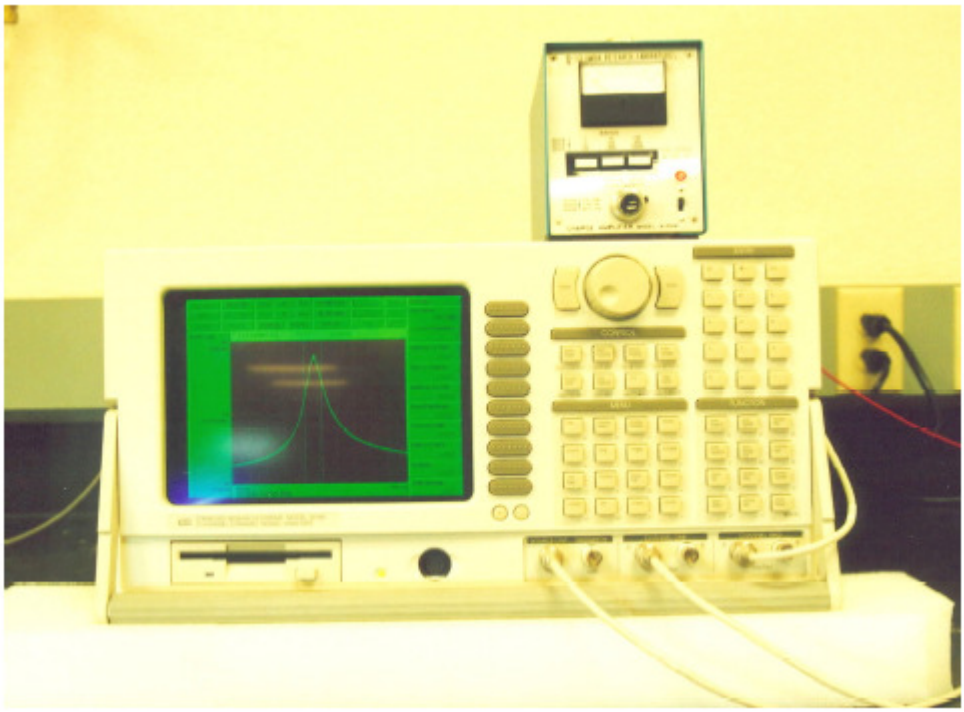

Figure 3.15 SR 785 Dynamic Signal Analyzer and 4102 Charge Amplifier Box

From the dynamic signal analyzer, a constant-amplitude sinusoidal current is sent to the driver (figure 3.12) fixed on top of the soil column. The sinusoidal current travels along a coaxial cable that transmits the signal, via microdot connectors on the thin wall of the confining chamber, to the driver's input current connection. The signal is distributed among the drive coils of the driver system inducing a sinusoidal torsional excitation on the specimen via the reacting magnets of the spider.

The amplitude of vibration is captured by the accelerometer rigidly attached to one of the arms of the spider, and sent to the charge amplifier box in the form of output voltage response. The amplified signal from the charge amplifier is sent back to the dynamic signal analyzer. A frequency response curve is then obtained by sweeping the entire preset frequency scale in the analyzer, and it can be displayed on the screen of the SR785 analyzer as shown in the figure 3.15.

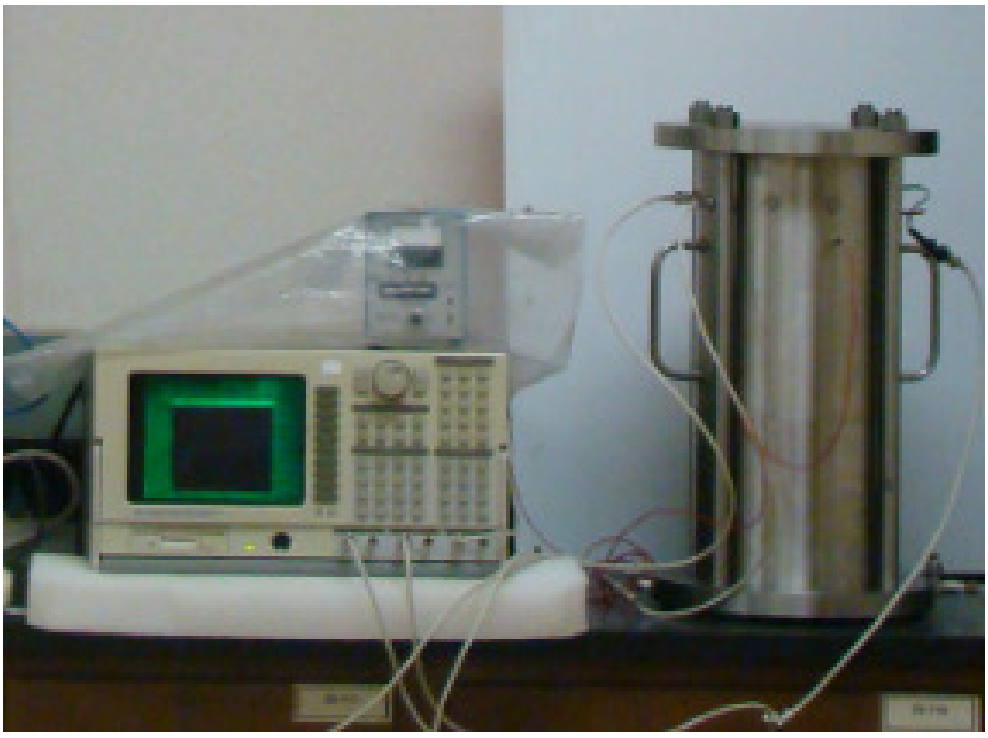

Figure 3.16 Dynamic Signal Analyzer and Charge Amplifier Connected with the RC Device.

The SR785 analyzer allows for storage and graphic display of the captured data in a PC-based computer terminal. The dynamic analyzer and charge amplifier interacting with the RC device is shown in figure 3.16.

3.4.4 Oscilloscope

The oscilloscope used in this thesis is called the Arbitrary Waveform Generator Model TGA 1241(figure 3.17). This oscilloscope can generate any waveform signal at different frequencies varying from 1 to 40MHz; the maximum amplitude is 20 Volts peak-to-peak. However, the frequencies, used in this research, range from 1 to 20 kHz for clay and sand specimens. And, the amplitude was applied at 20 Volts peak-to-peak which is the maximum amplitude available for this oscilloscope, so the received signal can be observed readily and obviously on the computer by not using the amplifier. This oscilloscope not only performs a waveform signal to the top bender element, but also sends the wave form to the receiving signal converter.

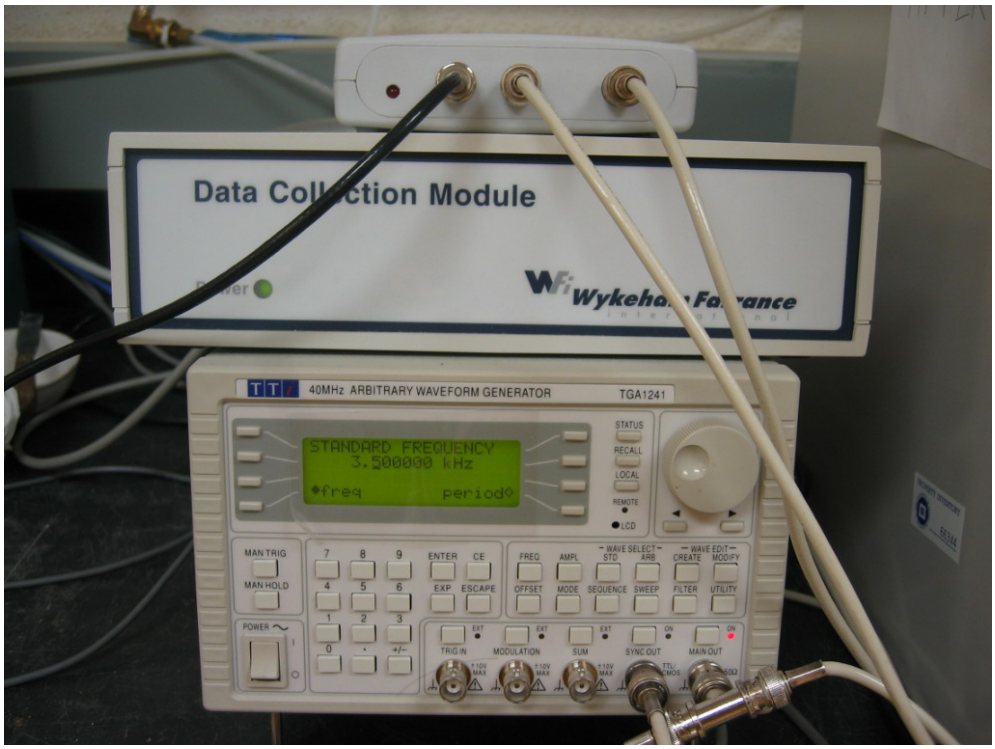

Figure 3.17 Arbitrary Wave Generator and Receiving Signal Converter

3.4.5 Receiving signal converter

Figure 3.17 also shows the receiving signal converter put on the top of the oscilloscope. The major role of the signal converter is to convert the voltage signals from both top and bottom bender elements into digital signals. The digital signals are then sent to a personal computer that has Picowave program installed. This Picowave program is used to view the waveform generated from oscilloscope.

3.4.6 Bender elements set

Bender element set with wires shown in figure 3.18 is used to perform the horizontal vibration through the soil specimen from top to bottom. In other words, the top bender element vibrates when received the signal from the oscilloscope, and then the vibration expands through the soil specimen so that the bottom bender element receives the vibration. Consequently, the elapsed time between the transmitted signal and received signal is measured and calculated.

Figure 3.18 Bender Elements Set

3.4.8 Personal computer

During the bender element test, signals from the converter are sent to the personal computer in order to visualize both transmitted and received signal on the monitor. The Picowave program is used to capture, save, and collect data. Eventually, the shear wave velocity is determined by measuring the elapsed time between the transmitted and received signal normally represented by blue and red lines respectively.

3.5 RC/BE Apparatus Assembly

An illustrated description of the step-by-step assembling process of the RC/BE testing device is presented in the following paragraphs.

1. **Chiseling specimen:** First a soil specimen with dimensions 2.8 inches in diameter and 5.6 inches in height was fully compacted and retrieved from a compaction mold at desired

moisture content. Then the specimen was cautiously chiseled at the top and bottom, of same size and position as a piece of piezoceramic bender element (shown in figure 3.19(a), (b)) in order to keep away from breaking the bender element because sometimes at low moisture content it is unable to put the piece of bender element inside the specimen.

Figure 3.19 (a) Chiseling the Specimen

Figure 3.19 (b) Chiseled Sampled Surface

2. **Specimen placement:** After the specimen was chiseled, it is carefully placed on the base pedestal with bender element (figure 3.20). A latex membrane is then rolled downward by stretcher over the specimen and an O-ring is gently placed at the base pedestal. Next the top cap with bender element is rested on top of the specimen and an O-ring placed is at the top cap (figure 3.21).

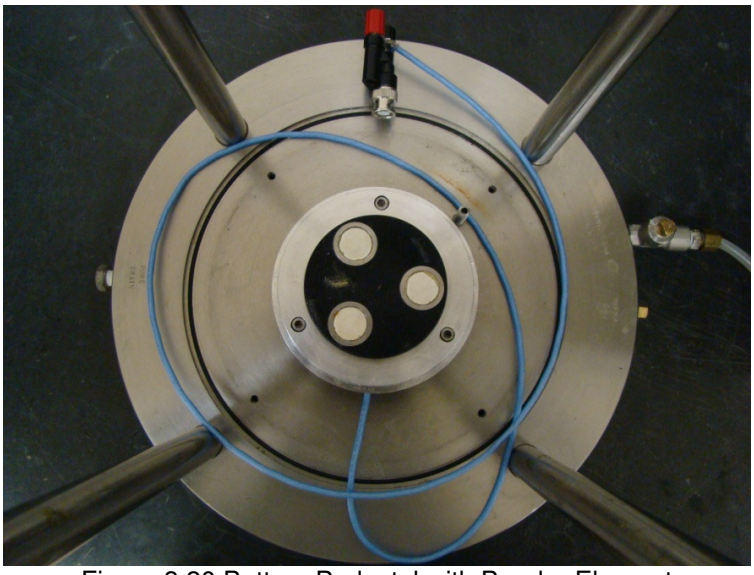

Figure 3.20 Bottom Pedestal with Bender Element

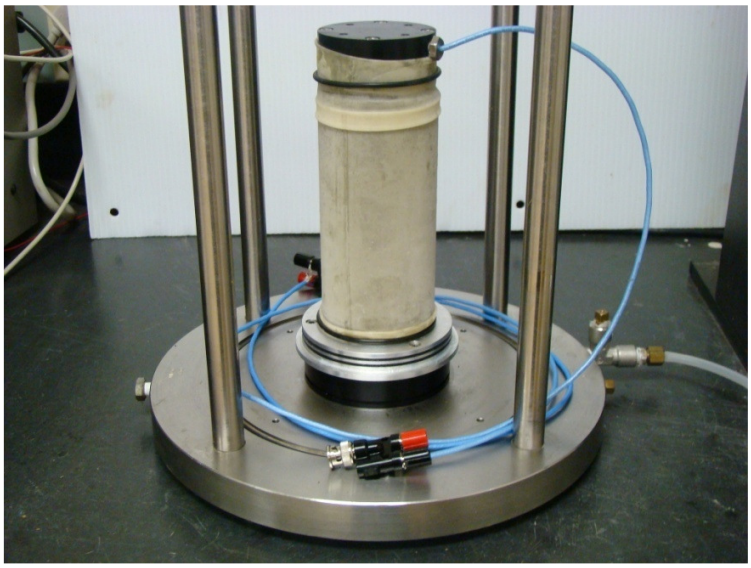

Figure 3.21 Specimen Placed on Bottom Pedestal

3. **<u>Water-bath application</u>:** An inner water-bath acrylic cylinder is placed over the soil specimen and securely fitted into the slip O-ring of the base pedestal until it makes good contact with the base pedestal as shown in the figure 3.22. The gap between the acrylic cylinder and the specimen is filled with water in order to apply the confining pressure uniformly throughout the sample and to minimize extrusion of the latex membrane or air migration through the specimen upon application of confining pressure (figure 3.23).

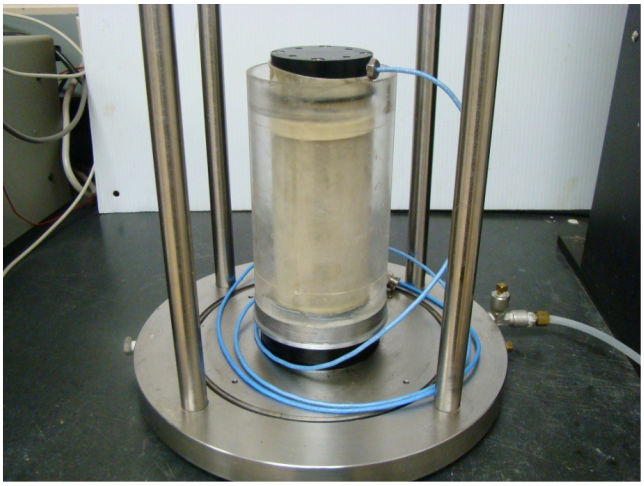

Figure 3.22 Acrylic Cyllinder over Soil Specimen

Figure 3.23 Application of Water between Acrylic Cylinder and Soil Specimen

4. **<u>Torsional driver setup</u>:** The stainless steel cylindrical cage is fitted over the specimen and the acrylic cylinder and securely attached to the base plate as shown in figure 3.24. The torsional driver (coils and spider) is then assembled onto the top cap. The spider is attached to the top cap by means of four flat-head screws. The set of drive coils is accommodated such that each magnet is encircled by a pair of coils without contact. The set of coils is finally secured to the cylindrical cage (figures3.25).

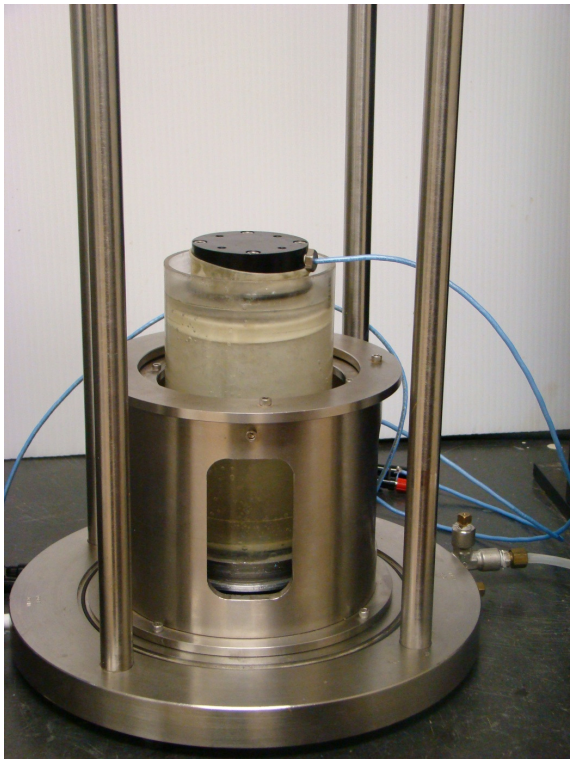

Figure 3.24 Cylindrical Cage over Soil Specimen and Acrylic Cylinder

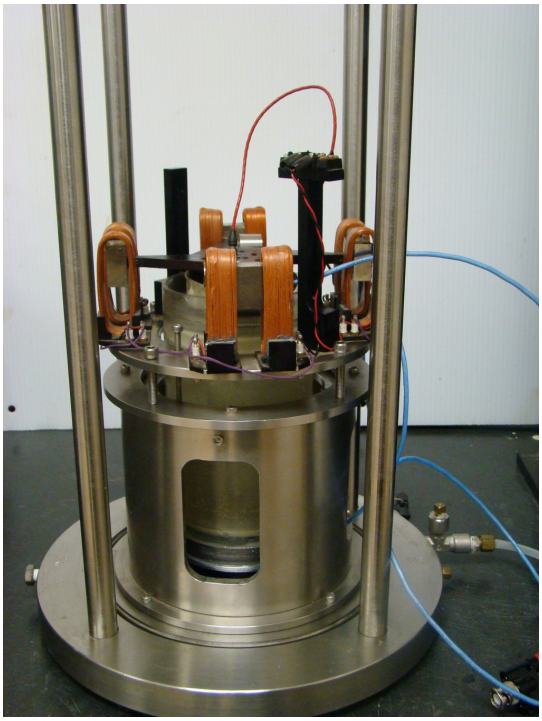

Figure 3.25 Torsional Driver Assembled On Cylindrical Cage

5. **Plugging in the Connection:** A stainless steel cylindrical chamber in which the sample is subjected to an isotropic confining pressure is placed over the soil specimen and securely fitted to the base. Both wires lead from the bender elements in the base pedestal and top cap exit the cell directly through the connection on the side of the chamber. These wires then exit the cell through a pressure-proof fitting connection on the side of the chamber and connected to the oscilloscope and receiving signal converter. For RC testing, the electrical wiring is connected to the corresponding microdot connectors on the inner side of the cylinder, that is, the input signal current wire and the accelerometer output wire. Figures 3.26 and 3.27 show all wires and connections inside and outside the confining chamber. The cover plate is placed over the top of the chamber and bolted tightly with the four guide rods. Then, the soil specimen, along with the remaining components of the RC device, is pressurized with air at the desired isotropic confining pressure (σ_o). Air pressure

is supplied by a HM-4150-model pressure control panel (Humboldt Manufacturing Co.) via an inlet air-pressure port located at the base plate of the confining chamber (figure 3.28).

Figure 3.26 Connections in the Confining Chamber

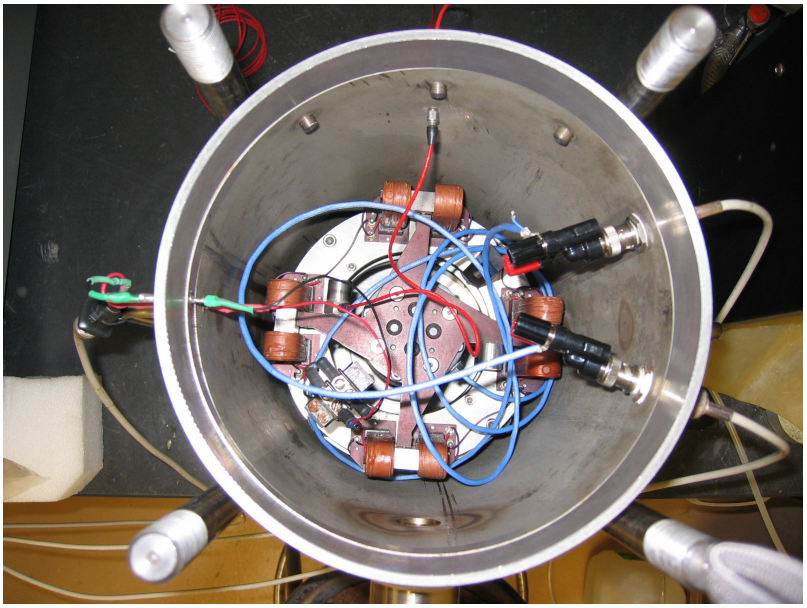

Figure 3.27 Top View of RC/BE Chamber

Figure 3.28 HM - 4150 – Model Pressure Control Panel

6. <u>Measurement setup</u>: The electrical wiring of the SR785 dynamic signal analyzer and the 4102M charge amplifier box is then connected to the corresponding microdot connectors on the outer side of the thin-walled cylinder, that is, the input signal coaxial wire and the accelerometer input wire. The analyzer is then configured at the desired test settings, including amplitude of sinusoidal signal, range of frequency scale, swept-sine testing mode, and number of data points to be recorded.

Once the swept-sine mode RC test has been completed, the frequency response curve and captured test data are transferred to the CPU of the PC-based computer terminal for future data processing using software such as Excel, Grapher, and Statistica.

As mentioned before, the elapse time between transmitted and received signal is enable to visualize and measure by using bender element and resonant column setup. Then the shear wave velocity can be calculated from the travel time of shear wave through the soil specimen. This setup also can collect a measurement of travel time in the personal computer.

This entire setup of the resonant column and bender elements is shown in the following figure 3.29.

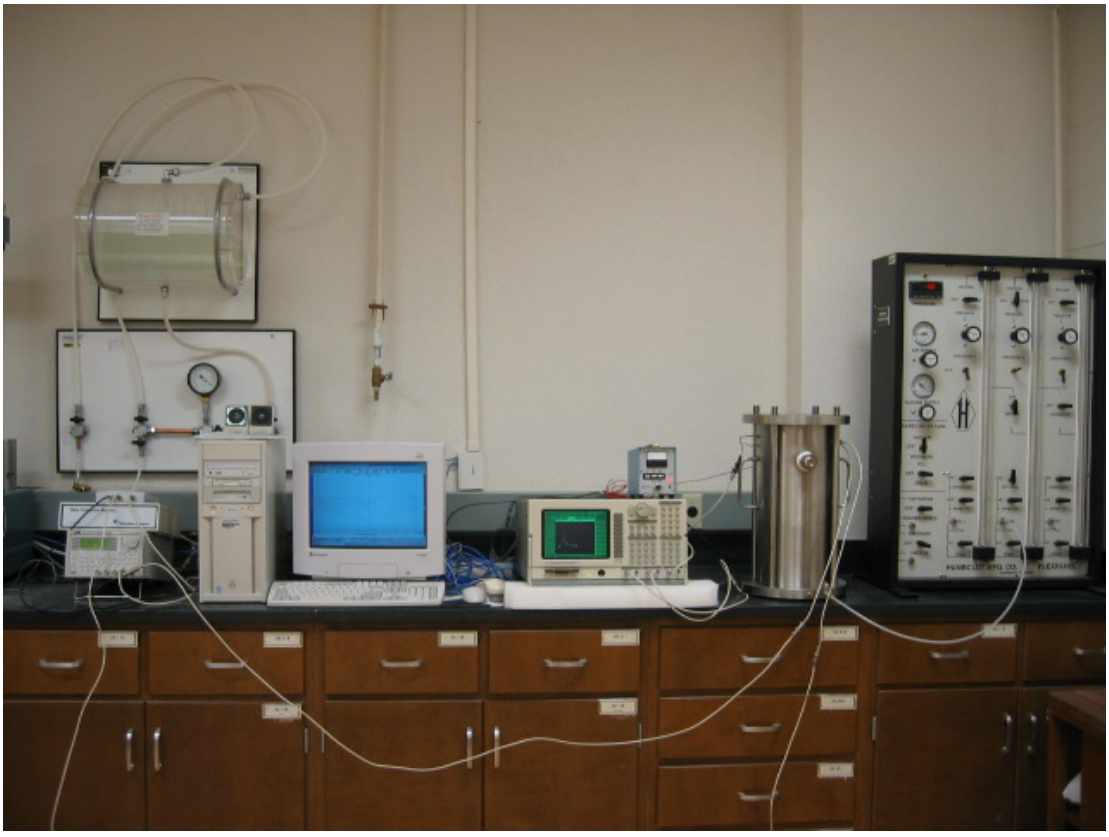

Figure 3.29 Resonant Column with Bender Element Setup

CHAPTER 4

EXPERIMENTAL PROGRAM AND TEST VARIABLES

4.1 Introduction

The experimental program accomplished in this work was designed to assess the influence of key environmental factors, such as suction and confinement, on small strain stiffness properties of unsaturated soils using resonant column and bender element testing techniques. Several identically prepared specimens of poorly graded sand from Arlington, Texas and high plasticity clay from Paris, Texas were tested using resonant column testing device with self contained bender elements as described in Chapter 3. Specimens were prepared at different compaction moisture contents, which are to induce different initial soil suction states. The density of the soil specimens at different moisture contents is maintained constant. The soil specimens are tested at different confining pressures (0, 2.5, 5.0, 10.0 psi or 0, 17.25, 34.5, 68.9 kPa) using resonant column device with self contained bender elements. These confinement values are used in order to represent the shallow foundations and pavement subgrades. SWCCs were determined by using pressure plate extractor and filter paper testing techniques.

The following sections provide the basic engineering properties of the testing soils used in this study, along with a detailed description of all the experimental variables and specimen preparation procedures.

4.2 Test Soils

4.2.1 High-plasticity Clay

The clayey soil used in this investigation was sampled from Paris, Texas. This clay soil is a high plasticity, black in color, with standard proctor optimum moisture content (w_{opt}) of 23% with a maximum dry unit weight ($Y_{d\text{-}max}$) of 92.09 lb/ft^3, specific gravity (G_s) of 2.7, liquid limit (LL) of 60% and plasticity index (PI) of 37%. The soil is classified as A-7-6 and CH according to

AASHTO and USCS, respectively. The basic engineering properties of the testing soil are summarized in table 4.1 and the grain size distribution for clay is shown in figure 4.1.

Table 4.1Basic Engineering Properties of Testing Clay

Properties	Result
Color	Black
Passing No. 200 sieve (%)	81
Specific gravity, G_s	2.7
Liquid limit, LL (%)	60
Plasticity index, PI (%)	37
Standard Proctor maximum dry unit weight, $Y_{d\text{-}max}$ (kN/m^3)	14.48
Standard Proctor optimum moisture content, w_{opt} (%)	23
AASHTO classification	A-7-6
USCS classification	CH

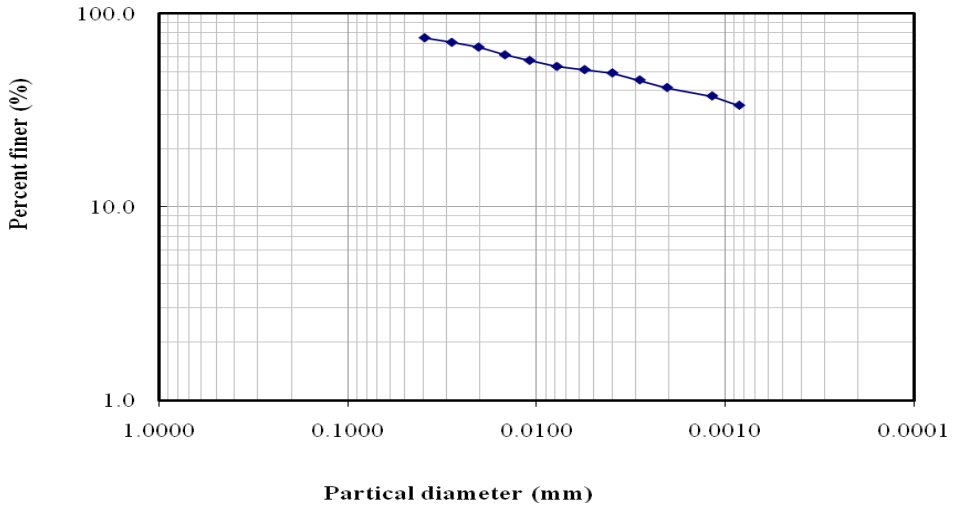

Figure 4.1 Grain Size Distribution for Clay

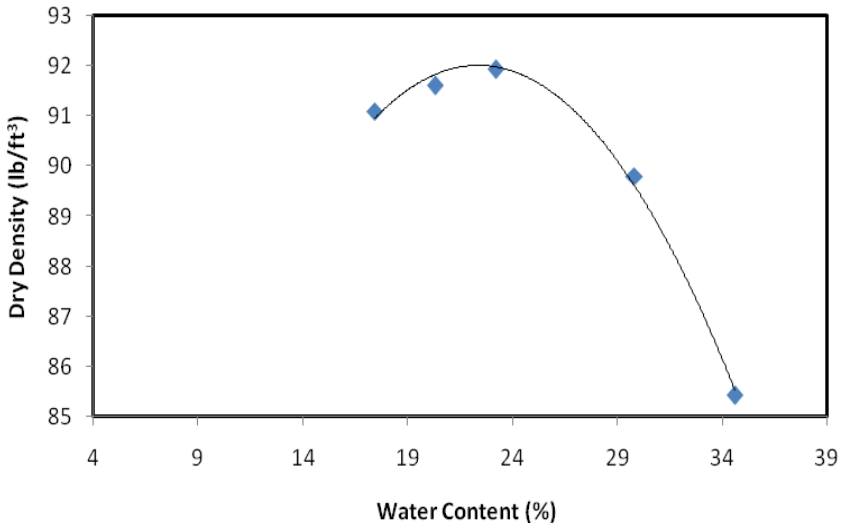

Figure 4.2 Compaction Curve for Clay

4.2.2 Poorly-graded Sand

Clean sand used in this research is a locally available soil. This sand appears as a white crystalline material. This is a poorly graded sand, with standard proctor optimum moisture content (w_{opt}) of 15.5%, maximum dry unit weight of 13.91kN/m^3 and specific gravity (G_s) of 2.7 The soil is classified as A-3 and SP (poorly graded sand) according to AASHTO and USCS, respectively. The basic engineering properties of the testing sandy soil are summarized in table 4.2 and the grain size distribution for the sand in shown in figure 4.2. Figure 4.3 shows an average density of 87.95 lb/ft^3 for SP sand from a combined pluviation-tamping compaction process.

Table 4.2 Basic Engineering Properties of Testing Sand

Properties	Result
Color	White
Passing No. 200 sieve (%)	1.4
Specific gravity, G_s	2.7
Standard Proctor maximum dry unit weight, $Y_{d\text{-}max}$ (kN/m^3)	14.48
Standard Proctor optimum moisture content, w_{opt} (%)	23
AASHTO classification	A-3
USCS classification	SP

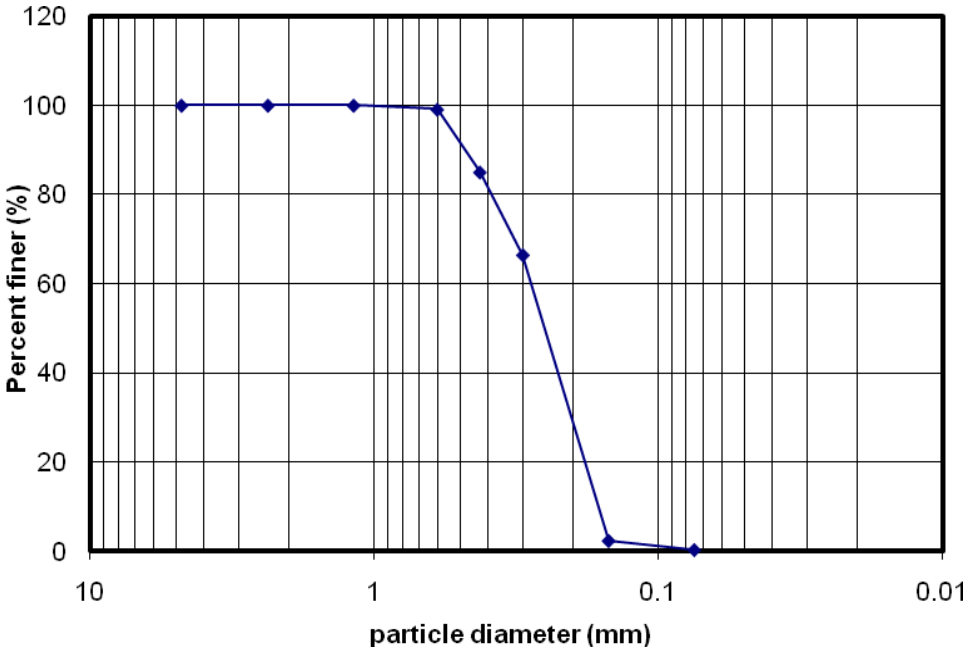

Figure 4.3 Grain Size Distribution for Sand

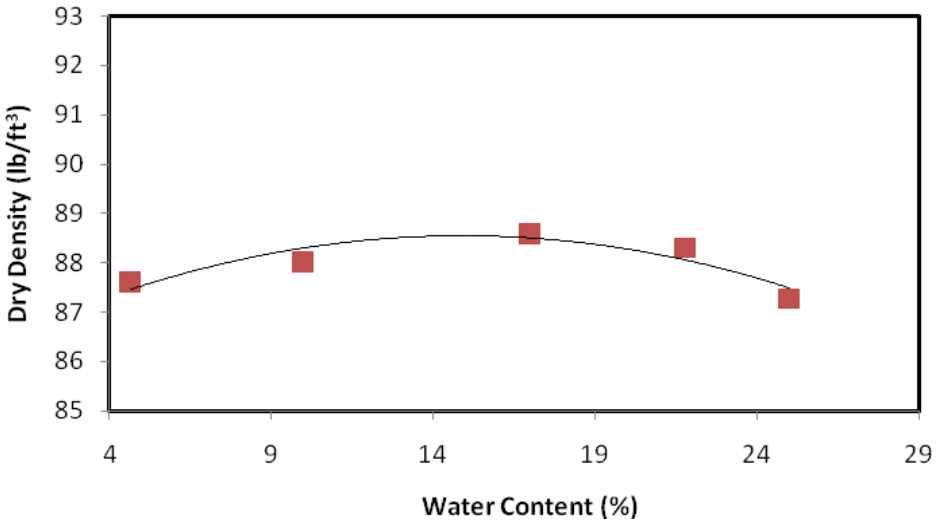

Figure 4.4 Compaction Curve for SP Sand from combined pluviation-tamping compaction

4.3 Experimental Variables

In this thesis work, several clay and sand specimens were tested in the resonant column device with self contained bender elements at four different confining pressures (0, 2.5, 5.0, and 10.0 psi or 0, 17.2, 34.5, and 69.0 kPa). Clay specimens were compacted at four different moisture contents (17.7, 22.1, 25.5, and 30.2% by weight). Sand specimens were compacted in place at four different moisture contents (5, 10, 15, 20% by weight). Even though the moisture contents are changed, the dry density of the testing soil is maintained constant. All specimens were then subjected to resonant column and bender element tests under different constant isotropic confining pressures as described above. The reason for compacting soil specimens at different moisture contents was to attain different matric suction states, assessed via SWCCs from pressure plate extractor and filter paper techniques. The SWCCs of the testing soils are shown in figures 4.3 and 4.4.

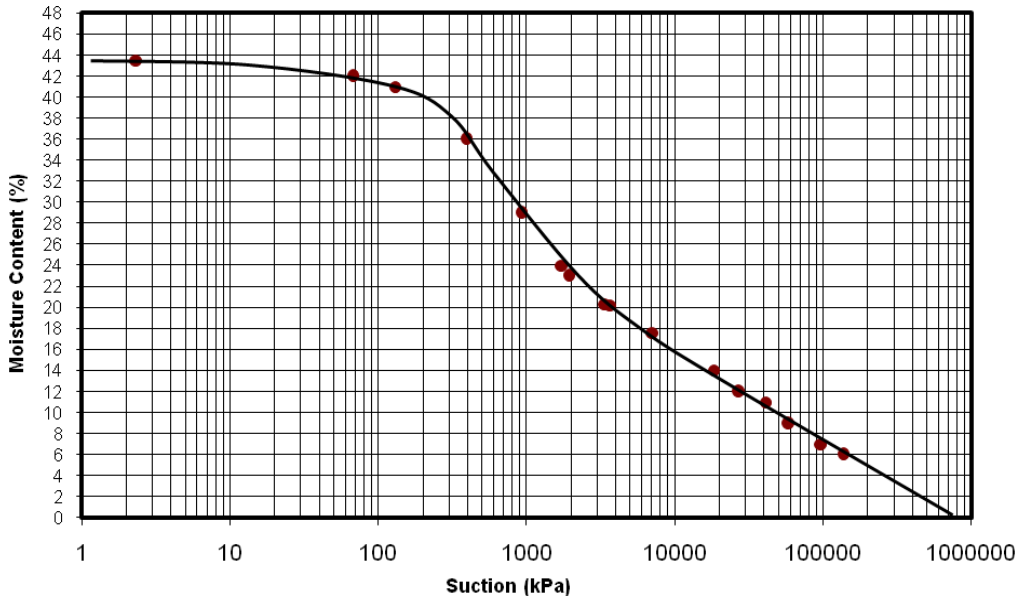

Figure 4.5 SWCC for high-plasticity Clay

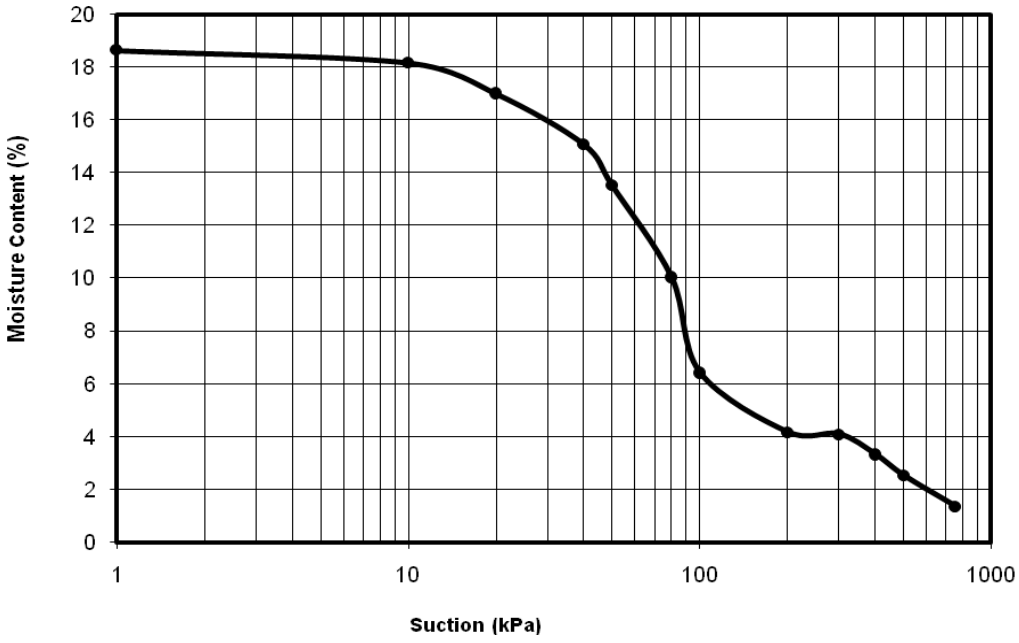

Figure 4.6 SWCC for poorly-graded Sand

4.4 Experimental Program

After the clay and sand specimens were compacted at desired dimensions and moisture contents, three specimens for each moisture content were tested in resonant column device with self contained bender elements to find out the shear modulus (G) and damping ratio (D). Therefore, resonant column and bender elements were performed simultaneously on same specimen at four different confining pressures (0, 2.5, 5.0, and 10.0 psi or 0, 17.2, 34.5, and 69.0kPa). Finally, the results from both the resonant column and bender element tests were compared.

All the resonant column tests were performed by sending a 250mV peak-to-peak sinusoidal signal from the Dynamic Signal Analyzer (DSA) to the torsional drive fixed on top of the specimen (chapter). The frequency of the signal was incrementally changed by sweeping the frequency scale in the DSA until the resonant frequency (f_r) of the soil-driver system was found and the complete frequency response curve was obtained. This low amplitude signal induces a linear response in the specimen and allows the determination of low amplitude values of shear modulus and damping ratio.

The bender tests were carried out by sending the pulse signal from the oscilloscope to the transmitter. The shear wave generated from the top bender element was travelling through the specimen to the receiver, the bottom bender element. Subsequently, the travel time of the shear wave along the height of the specimen was measured by using picowave program on computer monitor. From this the shear wave velocity and shear modulus (G) are calculated by using the equations described in chapter 3.

The damping ratio (D) was determined by sending the continuous sine wave at different frequencies and creating the plot of frequency and amplitude of receiving signal until find the peak. Then, damping ratio (D) was calculated using the half power method as described in chapter 3.

4.5 Sample Preparation

4.5.1 High-Plasticity Clay

Clay specimen in this thesis is first prepared outside and then is transferred into the chamber. During the specimen preparation, the necessary amounts of water, by dry weight of soil, were calculated from the desired moisture compaction moisture contents shown in figure 4.2. Dry soil was first thoroughly mixed with the required amount of water until ensuring homogeneity: figure 4.7(a), and then this soil mix was compacted by following impact compaction method. Specimens were compacted in three equal layers into a 2.875 in diameter and 5.75 in height split miter box reinforced with two clamps: figure 4.7(a). Each layer was compacted using a 5.5 lb, 12 in drop, U.S Army Corps hammer: figure 4.7(a); with uniformly distributed blows as shown in figure 4.7(b), 4.7(c) and the soil specimens were then extruded from the mould (figure 4.8). Then the sample is chiseled to the dimensions equal to that of the bender elements at same positions on both the faces: figure 3.20. The specimen is then transferred to the resonant column chamber.

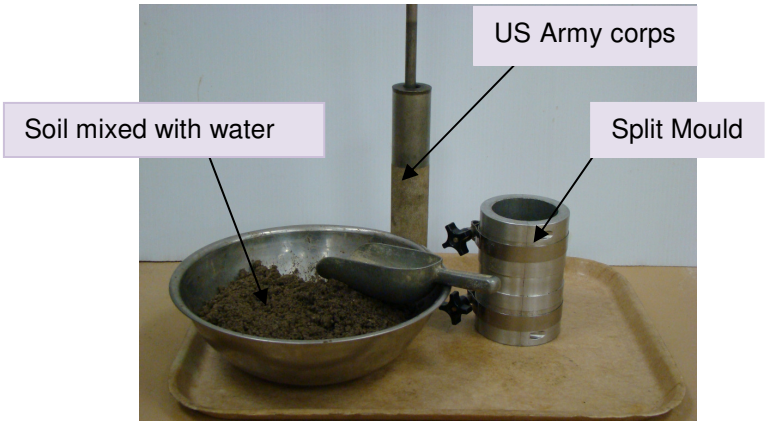

(a)

(b)

(c)

Figure 4.7 (a), (b), (c) – Compaction Process of the Clay Specimen

Figure 4.8 Clay Sample after Extruding from the Mould

4.5.2 Poorly-graded Sand

Sand specimen is prepared in the resonant chamber itself. A rubber membrane which surrounds the soil specimen is put to the split mould and vacuum is applied to hold the membrane. Then the sand is poured into the mould in five layers with light tapping for each layer (figure 4.9(a)). Water is sprinkled on each layer to reach the desired water content (figure 4.9(b)). After that the top cap is placed on the specimen (figure 4.9(c)). Finally the o-rings are placed for both the top and bottom caps, then the vacuum is closed and the mould is removed from the specimen. Figure 4.10 shows the sand specimen between the top and bottom pedestals.

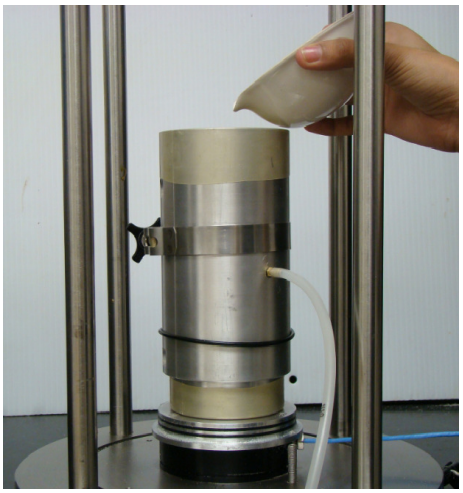

(a)

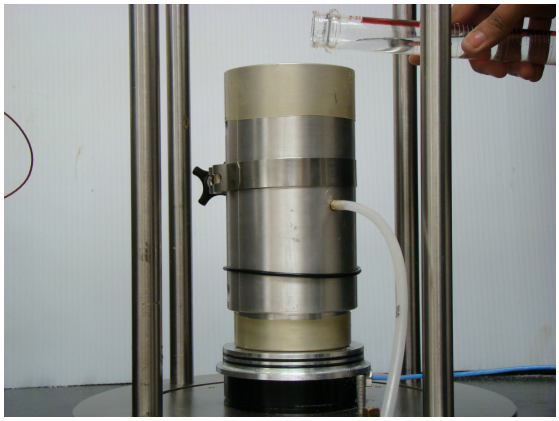

(b)

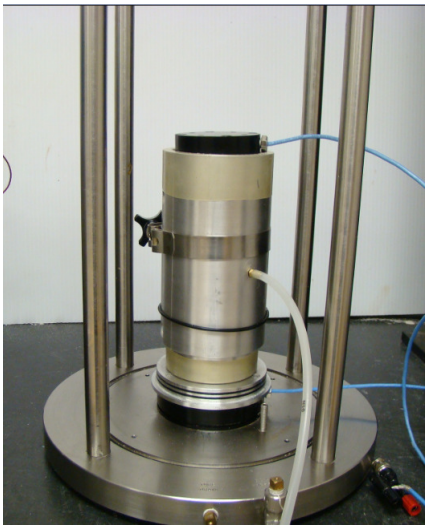

(c)

Figure 4.9 (a), (b). (c) – Sand Specimen Preparation

Figure 4.10 Sand Specimen between Top and Bottom Pedestal

CHAPTER 5

TEST RESULTS AND ANALYSIS

5.1 Shear Modulus Response: SAND

A total of 48 RC/BE tests were performed on 12 specimens of poorly-graded sand compacted via pluviation-tamping at four different moisture contents, 5, 10, 15, and 20%, in order to determine relationships between small strain shear modulus G_{max} with isotropic confining pressures and compaction-induced suction from RC and BE tests in the same confining chamber. Results are presented and analysed in the following sections.

5.1.1 Typical Response Curves

Figure 5.1 shows a typical RC test response at different confining pressures. In this figure it is observed that the resonant frequency increases with increase in the confining pressure. This shows that the value of shear modulus increases with increase in the cofining pressure.

Figure 5.2 shows a typical RC test respone at different compaction-inducednsuctions, i.e at different water contents, at constant confining pressure of 17.2 kPa (2.5 psi). In this figure it is observed that the resonant frequency increases with increase in suction. Consequently the shear modulus increases with increase in suction.

Figure 5.3 shows a typical BE test response at different confining pressures. In this figure it is observed that the arrival time decreases as the confining pressure increases. This shows that the value of shear modulus increases with the increase in the confining pressure.

Figure 5.4 shows a typical BE test response at different compaction-induced suctions, i.e at different water contents. In this figure we can observe that the time increases as the suction decreases. This shows that the shear modulus decrease with the decrease in the suction.

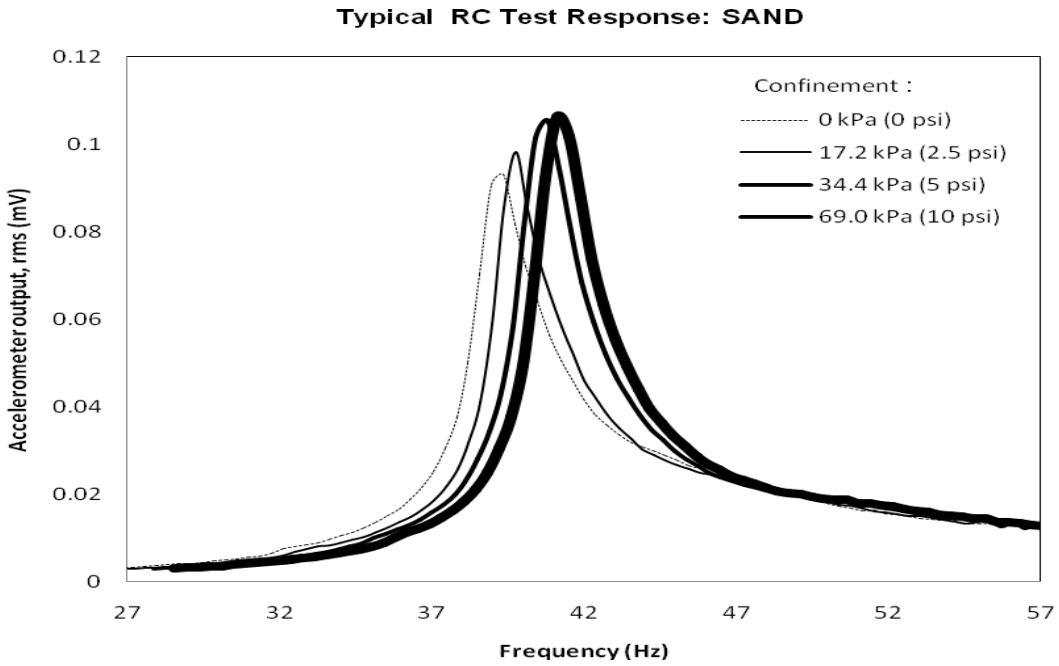

Figure 5.1 Typical RC Test Response from Sand at Different Confining Pressures

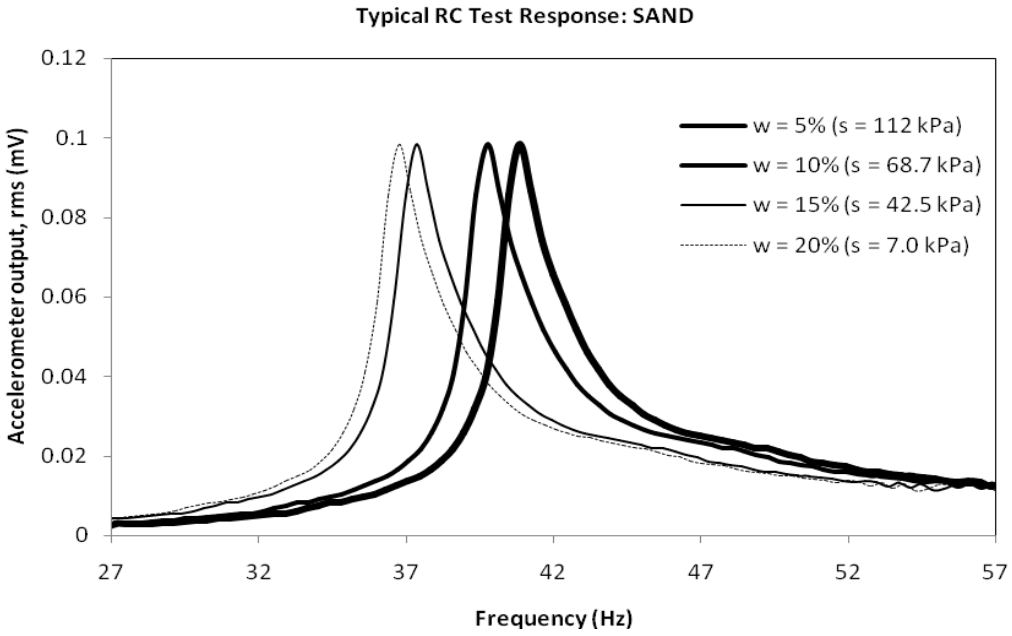

Figure 5.2 Typical RC Test Response at Different Suctions

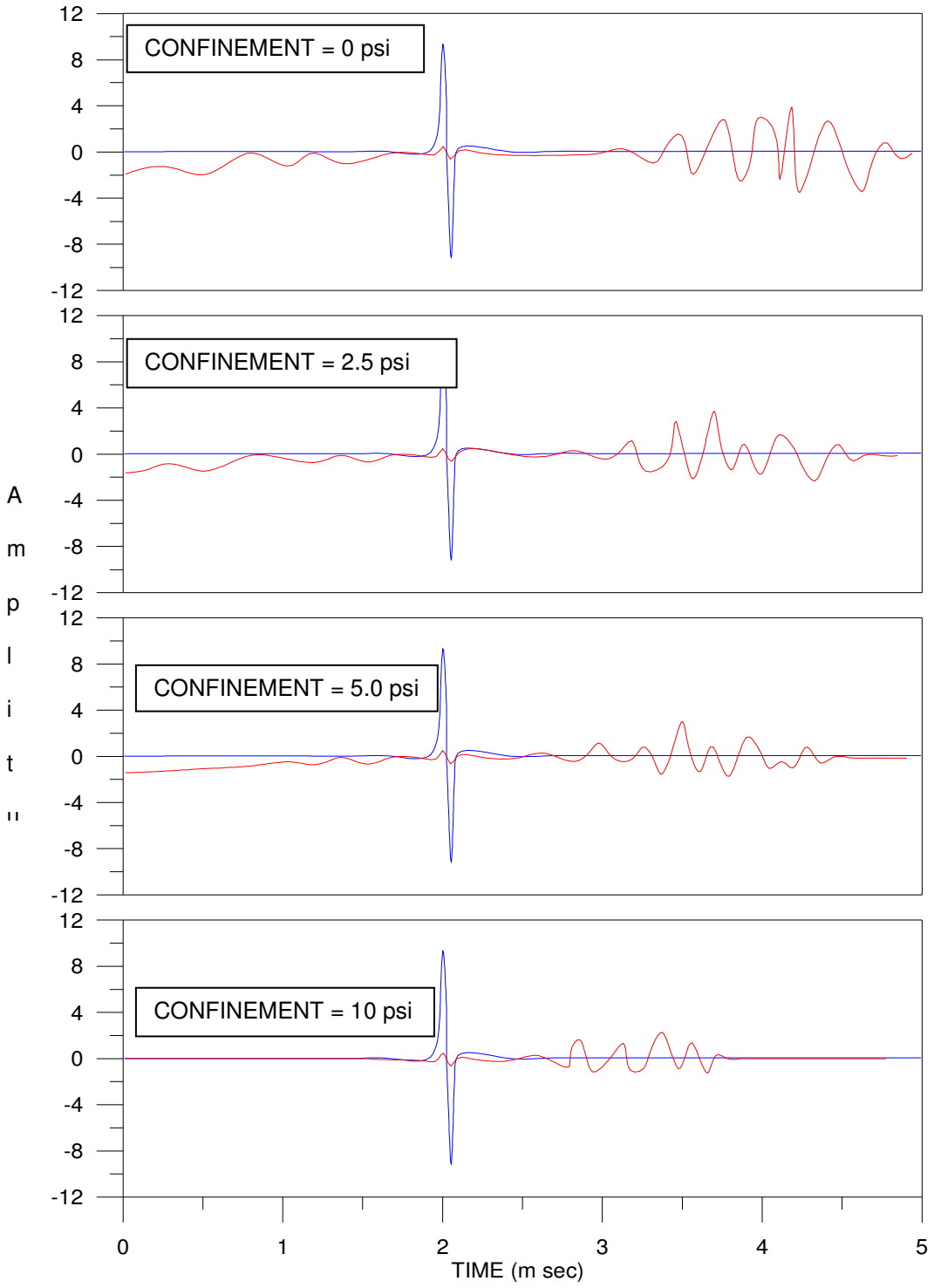

Figure 5.3 Typical BE Test Response from Sand at Different Confining Pressures

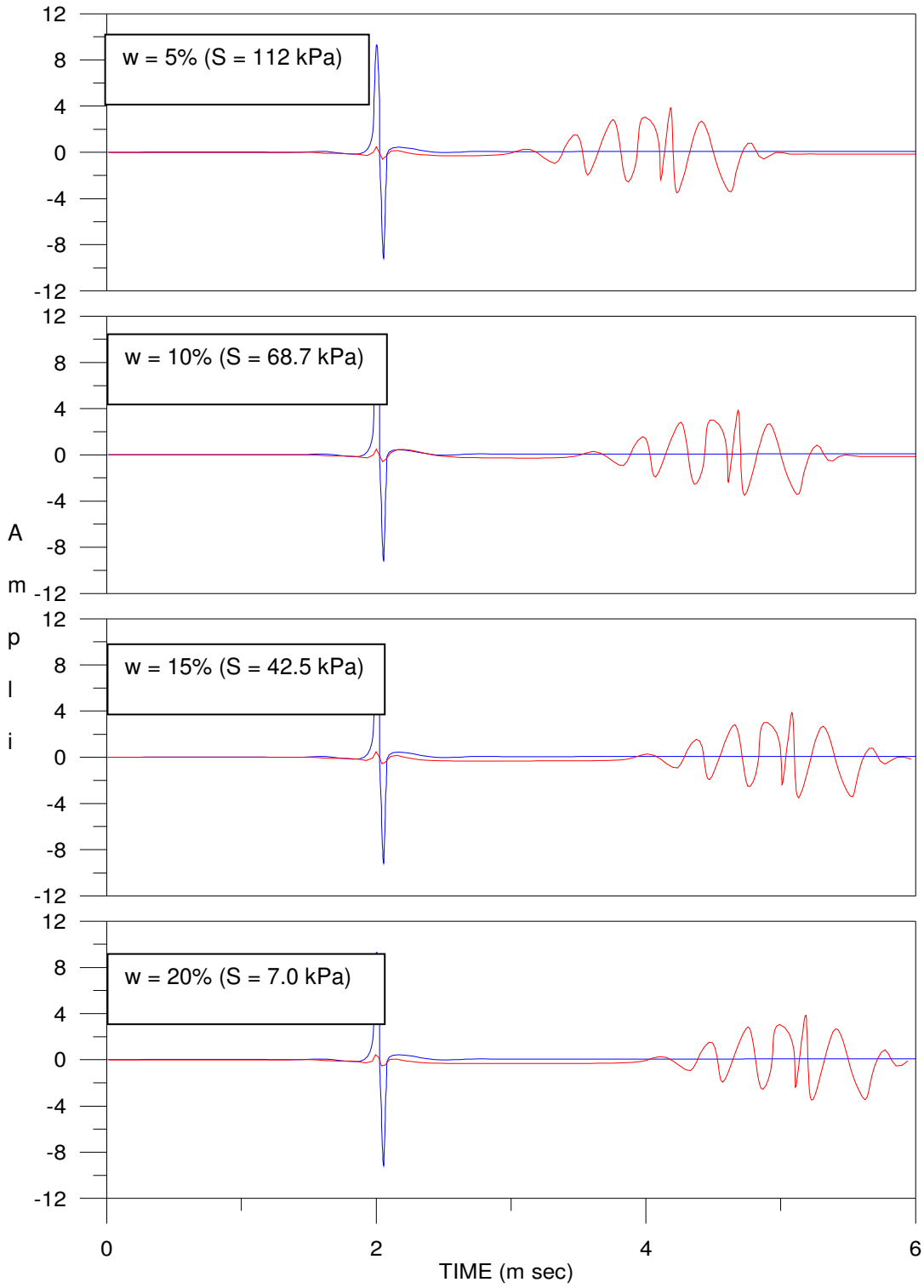

Figure 5.4 Typical BE Test Response at Different Suctions.

5.1.2 G_{max} Results From RC/BE Tests

Tables 5.1 to 5.4 summarize the results of small-strain shear modulus G_{max} of sand specimens at different isotropic confining pressures from both RC and BE methods.

A simple notation for specimen identification was adopted in order to facilitate the reading of all variables intervening in the fabrication/compaction of a specific specimen, particularly those variables referred to soil types, and confinements. For instance, a specimen identified as **"S-00-2"** indicates that this is a specimen made of **S**and, subjected to **0.0**-psi confinement, and labeled as trial specimen number **2**.

Figures 5.5 to 5.6 show the variation of small strain shear modulus at four moisture contents, i.e. at four different suctions, in RC and BE tests. From these figures it can be observed that the shear modulus decreases with decrease in the suction.

Figures 5.7 to 5.10 show the comparison of small strain shear modulus G_{nax} from RC and BE tests. From these figures it can be observed that shear modulus increases with increase in confinement. It can also be noted that at low moisture content, i.e. at high suction value, the shear modulus from BE test tends to be greater than that from the RC test; whereas shear modulus at higher moisture contents, i.e. at lower suction values, from both the RC and BE tests are similar. This explains that the higher the moisture content, the closer the shear modulus values from RC and BE methods.

Table 5.1 G_{max} Results from RC/BE Tests on Sand at w = 5.0% (S = 112 kPa)

Specimen	f_r (Hz)	$G_{max(RC)}$ (MPa)	Avg $G_{max(RC)}$	$SD_{(RC)}$	Time (μs)	$G_{max(BE)}$ (MPa)	Avg $G_{max(BE)}$	$SD_{(BE)}$
S-00-1	40.9	25.89			3412	30.93		
S-00-2	41.6	26.78	26.31	0.366	3408	30.99	30.96	0.029
S-00-3	41.2	26.26			3410	30.96		
S-2.5-1	40.9	25.88			3309	32.88		
S-2.5-2	41.6	26.78	26.31	0.366	3313	32.80	32.84	0.032
S-2.5-3	41.2	26.26			3311	32.84		
S-5.0-1	41.7	26.91			3288	33.30		
S-5.0-2	42	27.29	27.08	0.161	3291	33.24	33.27	0.024
S-5.0-3	41.8	27.03			3290	33.27		
S-10-1	42.6	28.08			3220	34.72		
S-10-2	43.1	28.74	28.39	0.272	3226	34.59	34.66	0.053
S-10-3	42.8	28.34			3223	34.66		

Table 5.2 G_{max} Results from RC/BE Tests on Sand at w = 10.0% (S = 68.7 kPa)

Specimen	f_r (Hz)	$G_{max(RC)}$ (MPa)	Avg $G_{max(RC)}$	$SD_{(RC)}$	Time (μs)	$G_{max(BE)}$ (MPa)	Avg $G_{max(BE)}$	$SD_{(BE)}$
S-00-1	38.8	22.23	22.50	0.237	3767	25.37	25.16	0.173
S-00-2	39.3	22.81			3799	24.94		
S-00-3	39.0	22.46			3783	25.16		
S-2.5-1	39.2	22.69	22.96	0.239	3739	25.75	25.59	0.128
S-2.5-2	39.7	23.28			3762	25.44		
S-2.5-3	39.4	22.92			3751	25.59		
S-5.0-1	39.9	23.51	24.07	0.438	3657	26.92	26.69	0.189
S-5.0-2	40.8	24.58			3682	26.45		
S-5.0-3	40.4	24.10			3673	26.69		
S-10-1	40.9	24.70	24.83	0.099	3623	27.43	27.01	0.338
S-10-2	41.1	24.95			3679	26.60		
S-10-3	40.0	24.82			3651	27.01		

Table 5.3 G_{max} Results from RC/BE Tests on Sand at w = 15.0% (S = 42.5 kPa)

Specimen	f_r (Hz)	$G_{max(RC)}$ (MPa)	Avg $G_{max(RC)}$	$SD_{(RC)}$	Time (μs)	$G_{max(BE)}$ (MPa)	Avg $G_{max(BE)}$	$SD_{(BE)}$
S-00-1	37.1	19.45	19.28	0.130	4187	20.54	20.73	0.158
S-00-2	36.8	19.14			4148	20.92		
S-00-3	36.9	19.24			4168	20.73		
S-2.5-1	37.4	19.76	19.66	0.086	4169	20.71	20.90	0.156
S-2.5-2	37.3	19.66			4131	21.09		
S-2.5-3	37.2	19.55			4150	20.90		
S-5.0-1	37.7	20.08	20.19	0.087	4152	20.88	21.01	0.107
S-5.0-2	37.9	20.30			4126	21.15		
S-5.0-3	37.8	20.19			4139	21.01		
S-10-1	38.3	20.73	20.62	0.088	4136	21.05	21.14	0.075
S-10-2	38.1	20.51			4118	21.23		
S-10-3	38.2	20.62			4128	21.13		

Table 5.4 G_{max} Results from RC/BE Tests on Sand at w = 20.0% (S = 7.0 kPa)

Specimen	f_r (Hz)	$G_{max(RC)}$ (MPa)	Avg $G_{max(RC)}$	$SD_{(RC)}$	Time (μs)	$G_{max(BE)}$ (MPa)	Avg $G_{max(BE)}$	$SD_{(BE)}$
S-00-1	35.8	17.36	17.58	0.256	4422	18.41	18.27	0.114
S-00-2	36.4	17.94			4456	18.13		
S-00-3	35.9	17.43			4439	18.27		
S-2.5-1	36.0	17.55	17.91	0.282	4399	18.60	18.58	0.013
S-2.5-2	36.7	18.24			4403	18.57		
S-2.5-3	36.4	17.94			4401	18.59		
S-5.0-1	36.2	17.74	18.21	0.408	4368	18.87	18.73	0.108
S-5.0-2	37.2	18.74			4399	18.60		
S-5.0-3	37.6	18.14			4384	18.73		
S-10-1	37.1	18.63	19.04	0.331	4257	19.86	19.78	0.071
S-10-2	37.9	19.45			4276	19.69		
S-10-3	37.5	19.04			4267	19.77		

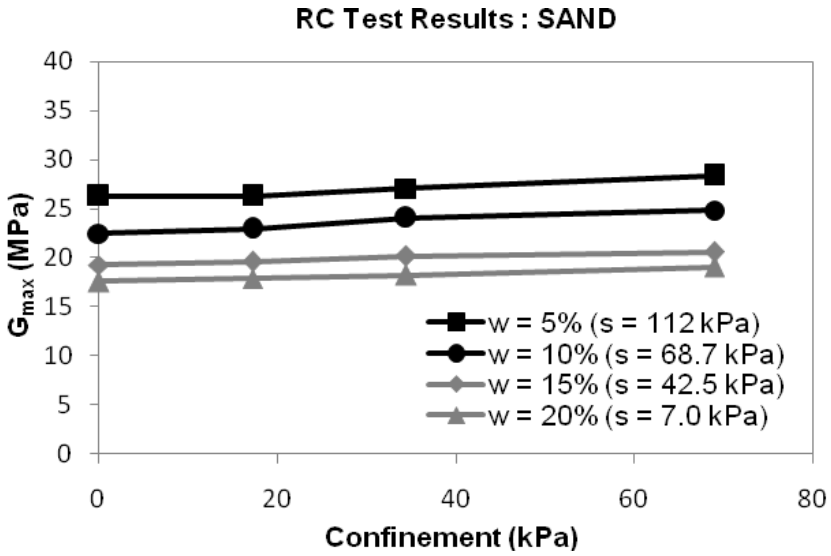

Figure 5.5 Variation of G_{max} with Confinement Using RC Method for Sand

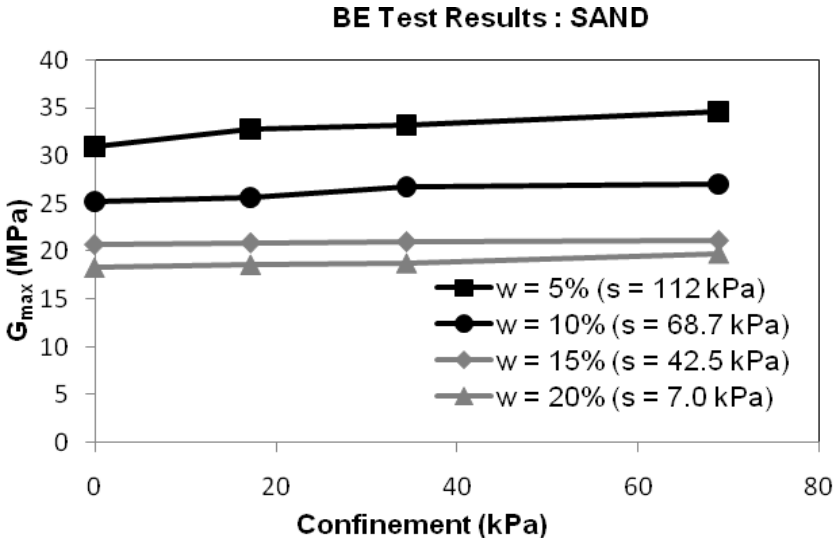

Figure 5.6 Variation of G_{max} with Confinement Using BE Method for Sand

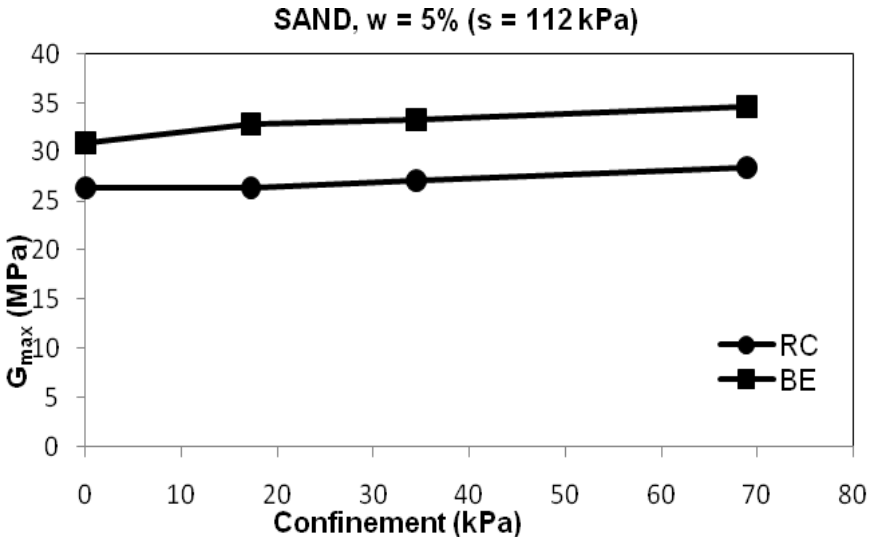

Figure 5.7 Comparison of G_{max} from RC and BE tests on Sand at w = 5% (S = 112 kPa)

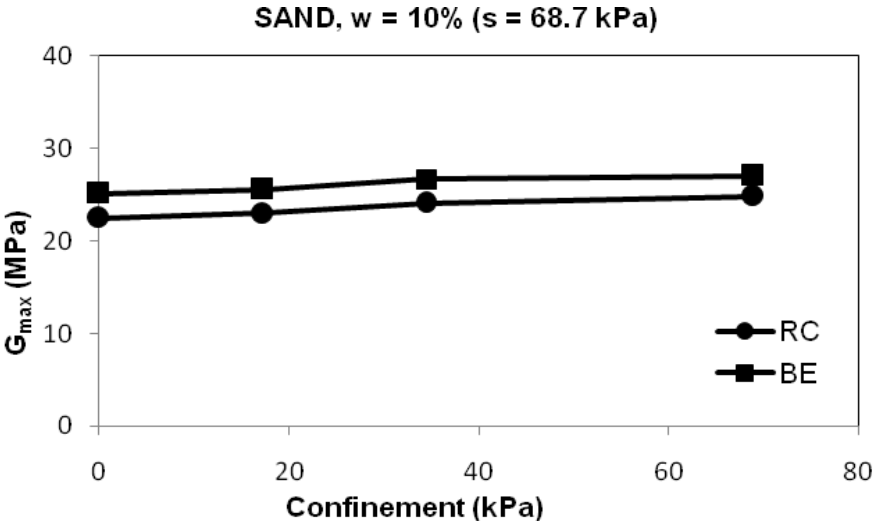

Figure 5.8 Comparison of G_{max} from RC and BE tests on Sand at w = 10% (S = 68.7 kPa)

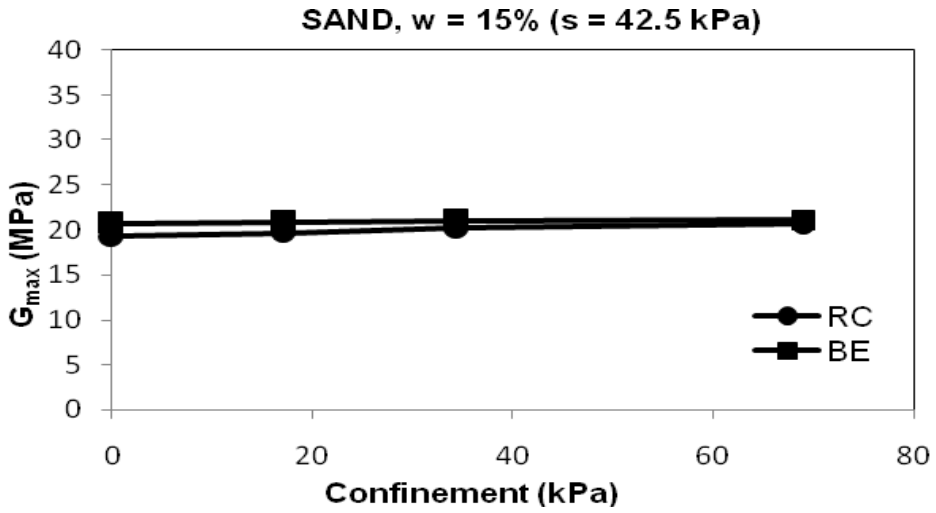

Figure 5.9 Comparison of G_{max} from RC and BE tests on Sand at w = 15% (S = 42.5 kPa)

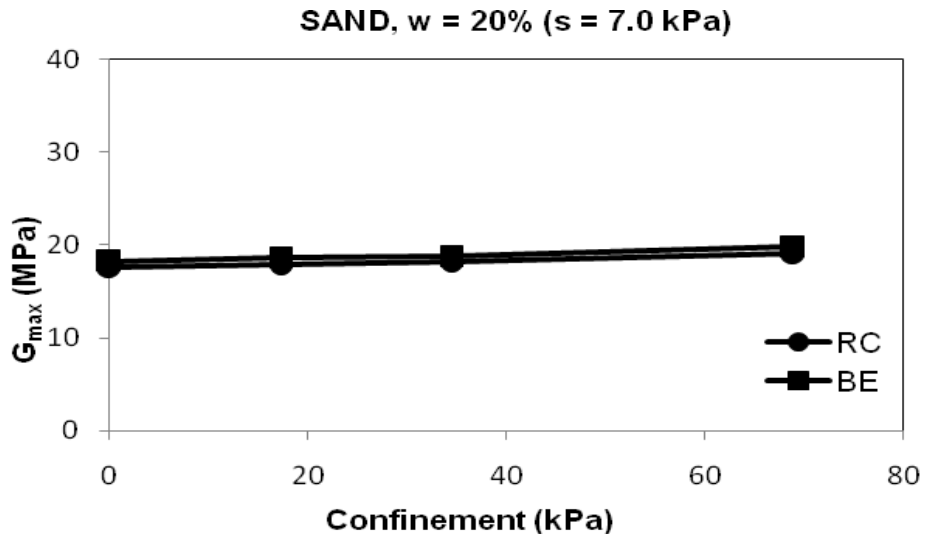

Figure 5.10 Comparison of G_{max} from RC and BE tests on Sand at w = 20% (S = 7.0 kPa)

5.1.3 Normalized G_{max}/σ_o Data as Function of Suction

Figures 5.11 to 5.13 show values of small-strain shear modulus normalized by level of confinement, that is, G_{max}/Confinement values from RC and BE tests presented as functions of compaction-induced suction. In general, the level of confinement has a significant effect on stiffness response of SP soil, i.e. as the confinement increases the normalized G_{max} decreases. It can also be noted the relatively significant influence of compaction-induced suction, with a considerable increase in shear modulus G_{max} at higher values of suction.

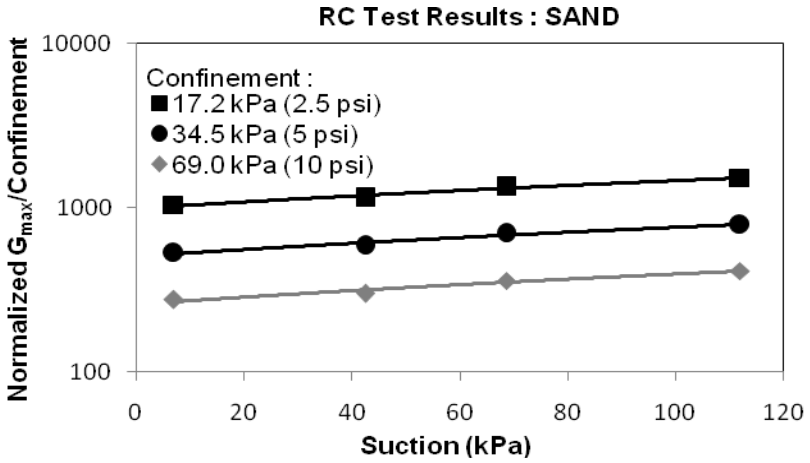

Figure 5.11 Normalized Shear Modulus as Function of Suction for Sand (RC)

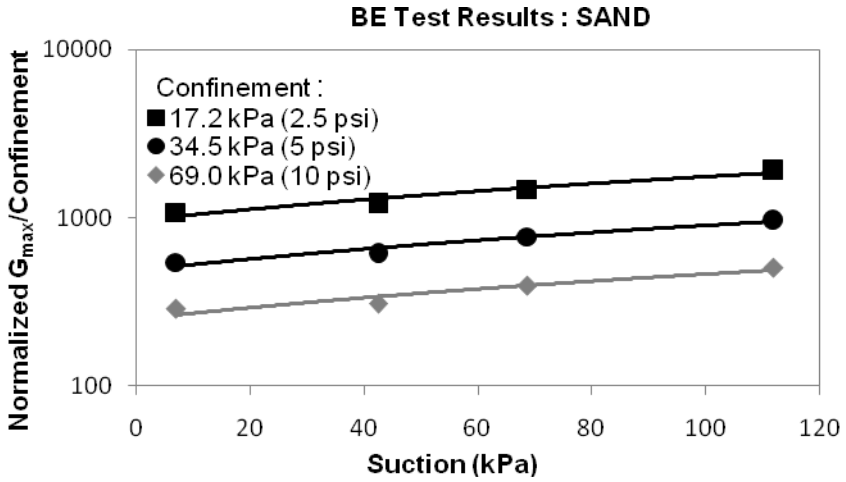

Figure 5.12 Normalized Shear Modulus as Function of Suction for Sand (BE)

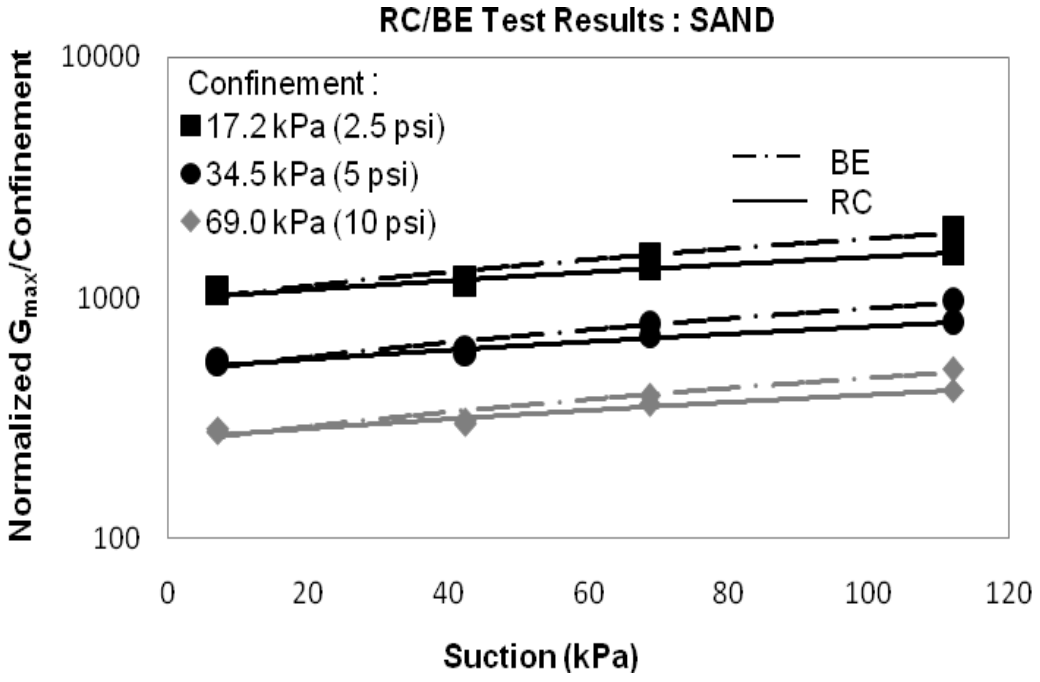

Figure 5.13 Normalized Shear Modulus as Function of Suction for Sand (RC/BE)

5.2 MATERIAL DAMPING RESPONSE: SAND

A total of 48 RC/BE tests were performed on 12 specimens of poorly-graded sand compacted via pluviation-tamping at four different moisture contents, 5, 10, 15, and 20%, in order to determine relationships between damping ratio D_{min} with isotropic confining pressures and compaction-induced suction from RC and BE tests in the same confining chamber. Results are presented and analysed in the following sections.

5.2.1 Typical Response Curve

Figure 5.14 shows a typical Be test response at 17.2kPa (2.5psi) confining pressure and 68.7kPa suction. The resonant frequency (f_r), corresponding to the peak of the frequency

response curve and the half power points (f_1 and f_2) is used to determine matrial damping (D_{min}) for this particular specimen as described in chapter 3.

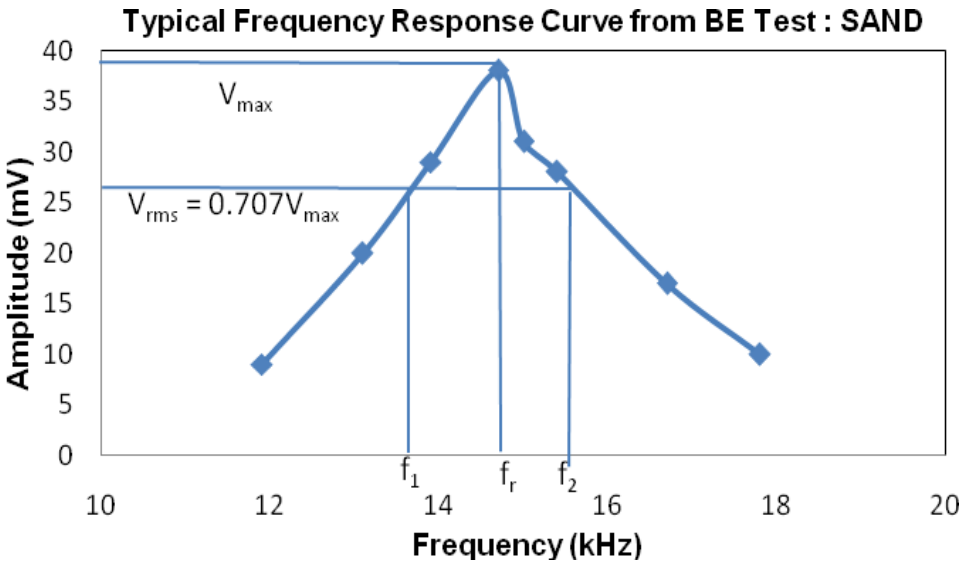

Figure 5.14 Typical BE Test Response from Sand for Damping Ratio

5.2.2 D_{min} Results from RC/BE Tests as Function of Suction

Tables 5.5 to 5.8 summarize the results of material damping D_{min} of specimens at different isotropic confining pressures from both RC and BE methods.

Figures 5.15 to 5.16 show the variation of damping ratio at four moisture contents i.e. at four different suctions, in RC and BE tests. From these figures it can be observed that the damping ratio increases with decrease in the suction.

Figures 5.17 to 5.20 show the comparison of damping ratio D_{min} from RC and BE tests. From these figures it can be observed that damping ratio decreases with increase in

confinement. It can also be noted that at low moisture content i.e. at high suction value, the damping ratio from BE test tends to be greater than that from the RC test and the difference increases with increase in moisture contents, i.e. with decrease in suction values. This explains that the higher the moisture content, the farther the damping ratio values between both RC and BE methods.

Table 5.5 D_{min} Results from RC/BE Tests on Sand at w = 5% (S = 112 kPa)

Specimen	$D_{min(RC)}$ (MPa)	Avg $D_{min(RC)}$	$SD_{(RC)}$	$D_{min(BE)}$ (MPa)	Avg $D_{min(BE)}$	$SD_{(BE)}$
S-00-1	2.32	2.28	0.04	4.73	4.90	0.13
S-00-2	2.22			4.93		
S-00-3	2.30			5.04		
S-2.5-1	2.32	2.28	0.04	4.77	4.71	0.05
S-2.5-2	2.22			4.72		
S-2.5-3	2.30			4.66		
S-5.0-1	2.39	2.23	0.15	4.26	4.22	0.06
S-5.0-2	2.02			4.27		
S-5.0-3	2.27			4.12		
S-10-1	2.23	2.06	0.11	4.17	4.10	0.05
S-10-2	1.98			4.09		
S-10-3	1.98			4.04		

Table 5.6 D_{min} Results from RC/BE Tests on Sand at w = 10% (S = 68.7 kPa)

Specimen	$D_{min(RC)}$ (MPa)	Avg $D_{min(RC)}$	$SD_{(RC)}$	$D_{min(BE)}$ (MPa)	Avg $D_{min(BE)}$	$SD_{(BE)}$
S-00-1	2.56	2.56	0.11	5.52	5.57	0.07
S-00-2	2.42			5.67		
S-00-3	2.69			5.52		
S-2.5-1	2.55	2.47	0.10	5.49	5.47	0.02
S-2.5-2	2.33			5.44		
S-2.5-3	2.54			5.49		
S-5.0-1	2.38	2.34	0.03	5.26	5.40	0.09
S-5.0-2	2.33			5.46		
S-5.0-3	2.31			5.49		
S-10-1	2.32	2.27	0.06	5.28	5.37	0.06
S-10-2	2.19			5.41		
S-10-3	2.31			5.41		

Table 5.7 D_{min} Results from RC/BE Tests on Sand at w = 15% (S = 42.5 kPa)

Specimen	$D_{min(RC)}$ (MPa)	Avg $D_{min(RC)}$	$SD_{(RC)}$	$D_{min(BE)}$ (MPa)	Avg $D_{min(BE)}$	$SD_{(BE)}$
S-00-1	2.56	2.62	0.06	6.41	6.32	0.07
S-00-2	2.58			6.29		
S-00-3	2.71			6.25		
S-2.5-1	2.41	2.50	0.13	6.35	6.16	0.13
S-2.5-2	2.41			6.05		
S-2.5-3	2.69			6.08		
S-5.0-1	2.39	2.38	0.005	6.17	6.10	0.08
S-5.0-2	2.37			5.99		
S-5.0-3	2.38			6.13		
S-10-1	2.22	2.31	0.12	6.08	6.01	0.08
S-10-2	2.23			5.90		
S-10-3	2.48			6.03		

Table 5.8 D_{min} Results from RC/BE Tests on Sand at w = 20% (S = 7.0 kPa)

Specimen	$D_{min(RC)}$ (MPa)	Avg $D_{min(RC)}$	$SD_{(RC)}$	$D_{min(BE)}$ (MPa)	Avg $D_{min(BE)}$	$SD_{(BE)}$
S-00-1	2.65	2.68	0.04	6.37	6.52	0.16
S-00-2	2.74			6.42		
S-00-3	2.64			6.75		
S-2.5-1	2.63	2.52	0.08	6.19	6.26	0.05
S-2.5-2	2.45			6.31		
S-2.5-3	2.47			6.72		
S-5.0-1	2.48	2.45	0.02	6.16	6.19	0.02
S-5.0-2	2.41			6.20		
S-5.0-3	2.45			6.22		
S-10-1	2.42	2.40	0.02	5.89	6.02	0.09
S-10-2	2.37			6.05		
S-10-3	2.40			6.11		

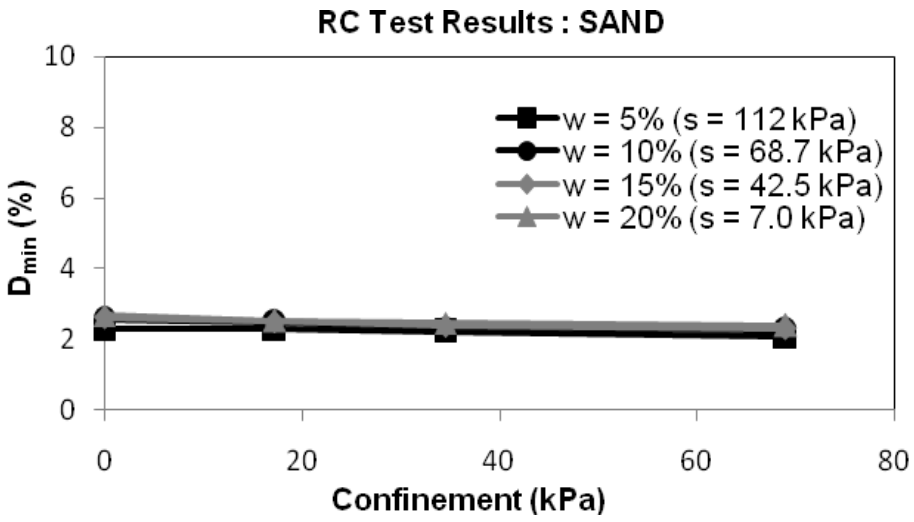

Figure 5.15 Variation of D_{min} with Confinement Using RC Method for Sand

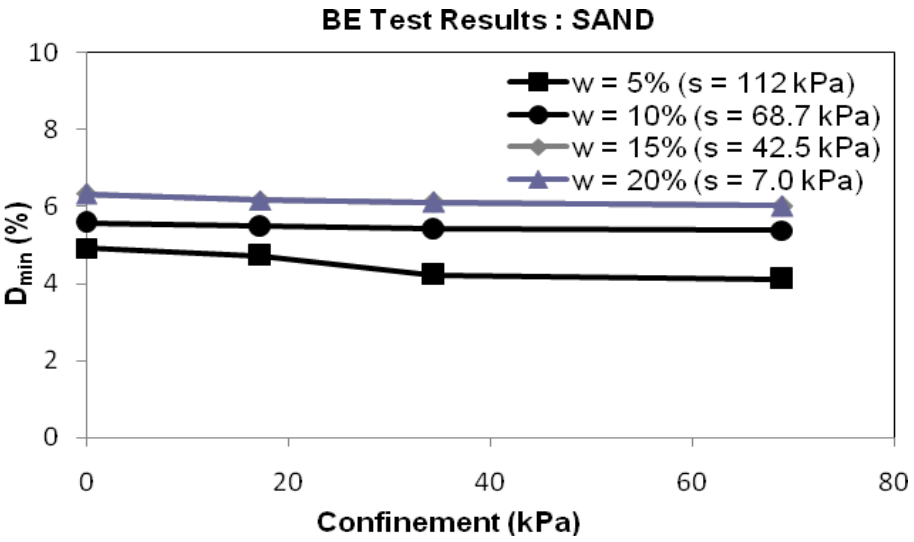

Figure 5.16 Variation of D_{min} with Confinement Using BE Method for Sand

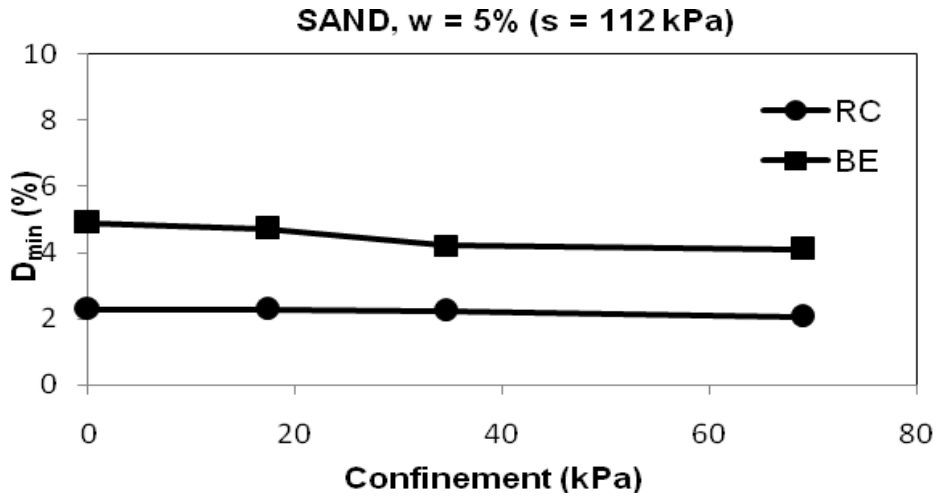

Figure 5.17 Comparison of D_{min} from RC and BE tests on Sand at w = 5% (S = 112 kPa)

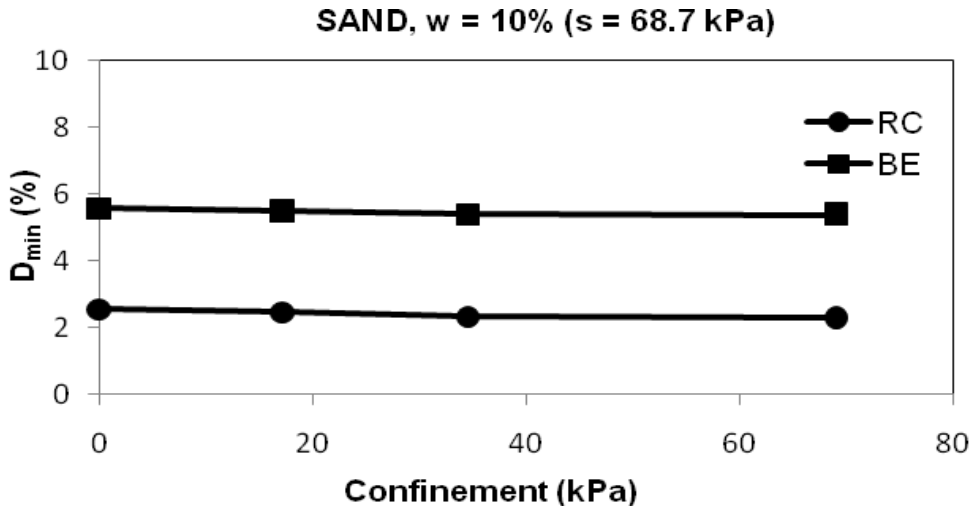

Figure 5.18 Comparison of D_{min} from RC and BE tests on Sand at w = 10% (S = 68.7 kPa)

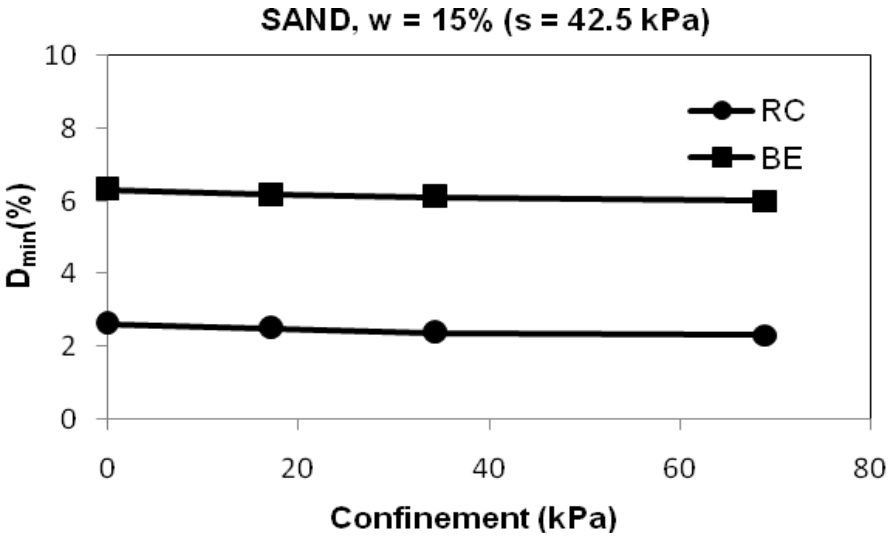

Figure 5.19 Comparison of D_{min} from RC and BE tests on Sand at w = 15% (S = 42.5 kPa)

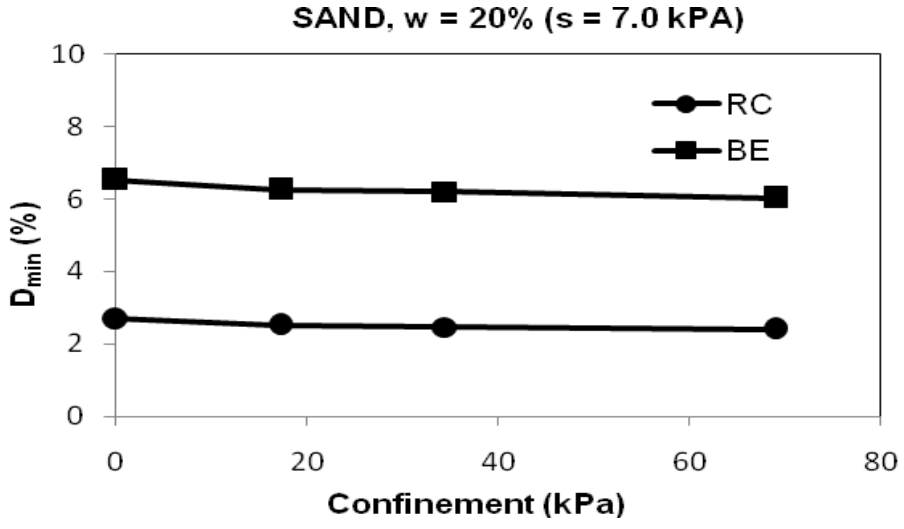

Figure 5.20 Comparison of D_{min} from RC and BE tests on Sand at w = 20% (S = 7.0 kPa)

5.2.3 Normalized D_{min}/σ_o Data as Function of Suction

Figures 5.21 to 5.23 show values of normalized material damping D_{min}/Confinement from RC and BE tests presented as functions of compaction-induced suction. As expected, the level of confinement has a significant effect on stiffness response of SP soil, i.e as the confinement increases the normalized D_{min} decreases. It can also be noted the relatively significant influence of compaction-induced suction, there was a considerable decrease in the damping ratio D_{min} at higher values of suction.

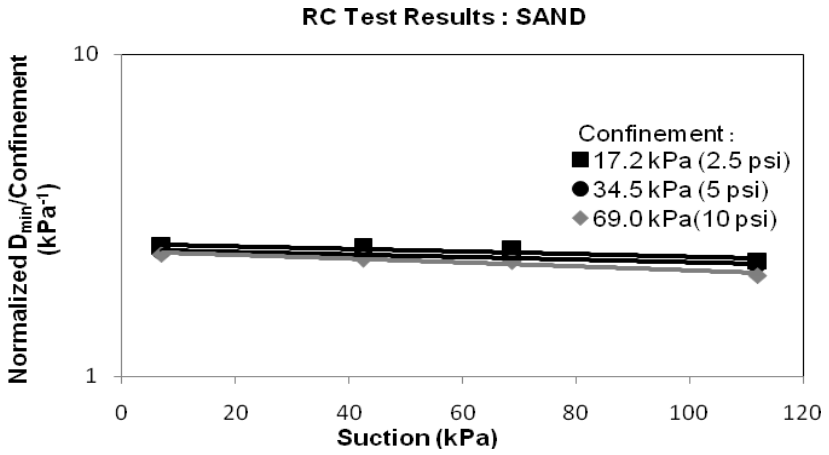

Figure 5.21 Normalized Damping Ratio as Function of Suction for Sand (RC)

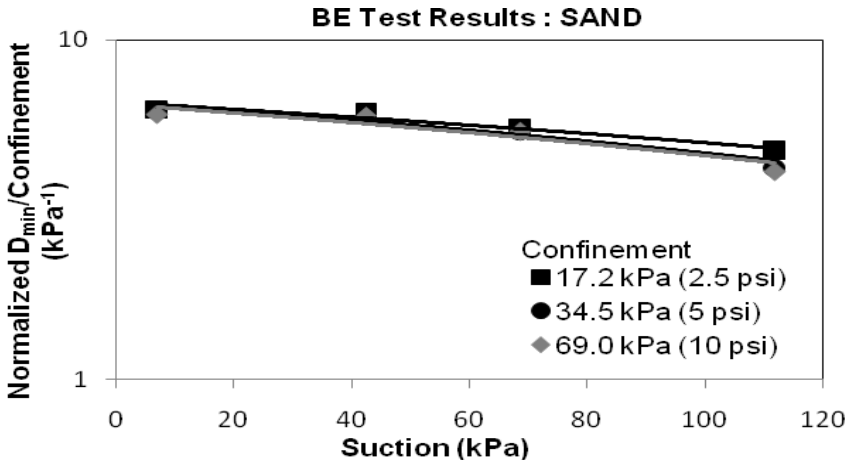

Figure 5.22 Normalized Damping Ratio as Function of Suction for Sand (BE)

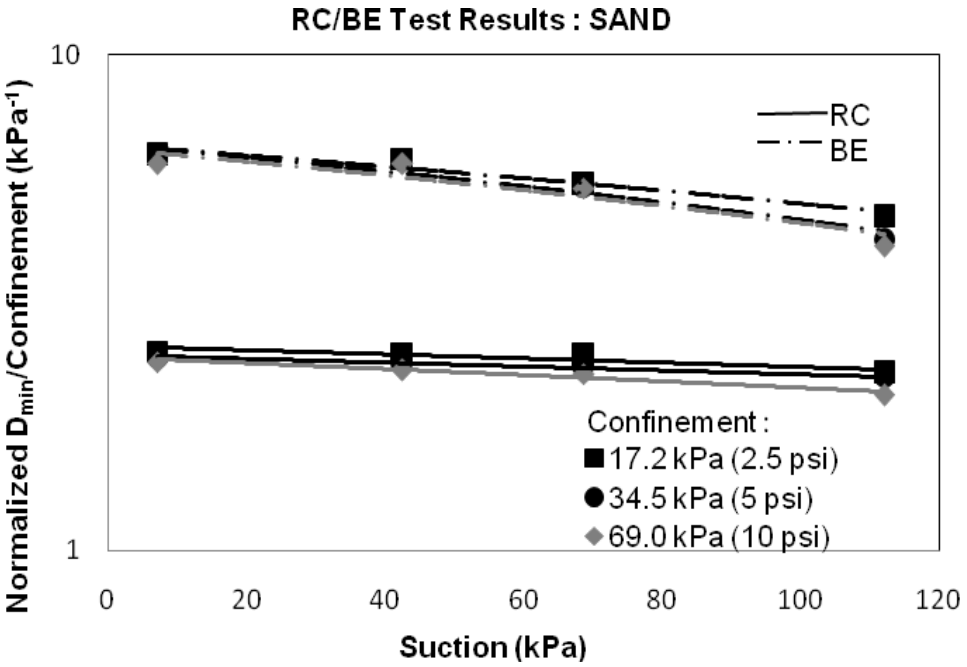

Figure 5.23 Normalized Damping Ratio as Function of Suction for Sand (RC/BE)

5.3 Shear Modulus Response: CLAY

A total of 48 RC/BE tests were performed on 12 specimens of high-plasticity clay compacted at four different moisture contents, 5, 10, 15, and 20%, in order to determine relationships between small strain shear modulus G_{max} with isotropic confining pressures and compaction-induced suction from RC and BE tests in the same confining chamber. Results are presented and analysed in the following sections.

5.3.1 Typical Response Curve

Figure 5.24 shows a typical RC test response at different confining pressures. In this figure we observe that the resonant frequency increases with increase in the confining pressure. This shows that the value of the shear modulus increases with increase in the confining pressure.

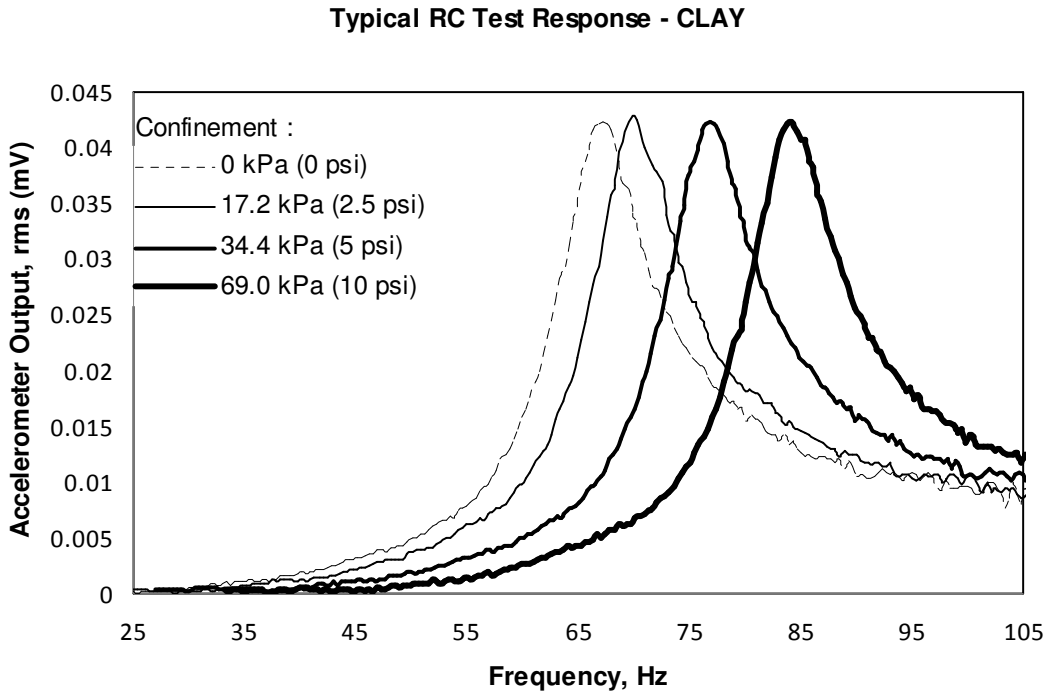

Figure 5.24 Typical RC Test Response from Clay at Different Confining Pressures

5.3.1 G_{max} Results from RC/BE Tests

Tables 5.9 to 5.12 summarize the results of small-strain shear modulus G_{max} of clay specimens at different isotropic confining pressures from both RC and BE methods.

A simple notation for specimen identification was adopted in order to facilitate the reading of all variables intervening in the fabrication/compaction of a specific specimen, particularly those variables referred to soil types, and confinements. For instance, a specimen identified as **"S-00-2"** indicates that this is a specimen made of **S**and, subjected to **0.0**-psi confinement, and labeled as trial specimen number **2**.

Figures 5.25 to 5.26 show the variation of small strain shear modulus at four moisture contents, i.e. at four different suctions, in RC and BE tests. From these figures it can be observed that the shear modulus decreases with decrease in the suction.

Figures 5.27 to 5.30 show the comparison of small strain shear modulus G_{max} from RC and BE tests. From these figures it can be observed that shear modulus increases with increase in confinement. It can also be noted that at low moisture content i.e. at high suction value, the shear modulus from BE test tends to be greater than that from the RC test; whereas shear modulus at higher moisture contents, i.e. at lower suction values, from both the RC and BE tests are similar. This explains that the higher the moisture content, the closer the shear modulus values from RC and BE methods.

Table 5.9 G_{max} Results from RC/BE Tests on Clay at w = 17.7% (S = 6000 kPa)

Specimen	f_r (Hz)	$G_{max(RC)}$ (MPa)	Avg $G_{max(RC)}$	$SD_{(RC)}$	Time (μs)	$G_{max(BE)}$ (Mpa)	Avg $G_{max(BE)}$	$SD_{(BE)}$
C-00-1	84.1	80.68	81.64	0.788	1216	175.51	174.90	0.493
C-00-2	84.6	81.64			1218	174.90		
C-00-3	85.1	82.61			1221	174.29		
C-2.5-1	84.8	82.03	83.13	0.875	1155	194.51	192.87	1.336
C-2.5-2	85.4	83.19			1160	192.86		
C-2.5-3	85.9	84.17			1165	191.23		
C-5.0-1	87.7	87.74	89.01	0.991	1025	247.09	245.20	1.537
C-5.0-2	88.4	89.14			1029	245.20		
C-5.0-3	88.9	90.15			1033	243.32		
C-10-1	88.3	88.94	90.02	0.832	989	265.53	263.49	1.657
C-10-2	88.9	90.15			993	263.49		
C-10-3	89.3	90.97			997	261.47		

Table 5.10 G_{max} Results from RC/BE Tests on Clay at w = 22.1% (S = 2400 kPa)

Specimen	f_r (Hz)	$G_{max(RC)}$ (MPa)	Avg $G_{max(RC)}$	$SD_{(RC)}$	Time (μs)	$G_{max(BE)}$ (MPa)	Avg $G_{max(BE)}$	$SD_{(BE)}$
C-00-1	70.2	54.28	52.85	1.076	1801	101.15	102.84	1.286
C-00-2	69.1	52.59			1397	104.27		
C-00-3	68.5	51.68			1599	103.10		
C-2.5-1	70.5	54.74	53.72	0.817	1691	104.32	105.79	1.067
C-2.5-2	69.8	53.66			1433	106.82		
C-2.5-3	69.2	52.74			1562	106.25		
C-5.0-1	76.1	63.79	64.18	0.285	1727	115.10	117.45	1.744
C-5.0-2	76.4	64.29			1250	118.01		
C-5.0-3	76.5	64.46			1489	119.27		
C-10-1	83.4	76.61	76.79	0.150	1507	134.99	136.57	1.252
C-10-2	83.5	76.79			1250	136.67		
C-10-3	83.6	76.98			1379	138.05		

Table 5.11 G_{max} Results from RC/BE Tests on Clay at w = 25.5% (S = 1500 kPa)

Specimen	f_r (Hz)	$G_{max(RC)}$ (MPa)	Avg $G_{max(RC)}$	$SD_{(RC)}$	Time (μs)	$G_{max(BE)}$ (MPa)	Avg $G_{max(BE)}$	$SD_{(BE)}$
C-00-1	68.1	49.62	49.28	0.298	1975	66.56	68.77	1.851
C-00-2	67.9	49.33			1911	71.09		
C-00-3	67.6	48.89			1943	68.70		
C-2.5-1	68.6	50.35	49.96	0.276	1864	74.72	73.50	0.990
C-2.5-2	68.2	49.76			1895	72.30		
C-2.5-3	68.2	49.76			1880	73.48		
C-5.0-1	69.2	51.23	50.69	0.422	1827	77.78	77.02	0.616
C-5.0-2	68.8	50.64			1845	76.27		
C-5.0-3	68.5	50.20			1836	77.01		
C-10-1	69.8	52.13	51.58	0.426	1791	80.94	81.21	0.222
C-10-2	69.4	51.53			1785	81.49		
C-10-3	69.1	51.08			1788	81.21		

Table 5.12 G_{max} Results from RC/BE Tests on Clay at w = 30.2% (S = 800 kPa)

Specimen	f_r (Hz)	$G_{max(RC)}$ (MPa)	Avg $G_{max(RC)}$	$SD_{(RC)}$	Time (μs)	$G_{max(BE)}$ (MPa)	Avg $G_{max(BE)}$	$SD_{(BE)}$
C-00-1	67.1	46.48	45.70	0.576	2173	65.98	65.10	0.654
C-00-2	66.4	45.52			1900	64.40		
C-00-3	66.1	45.11			2037	64.93		
C-2.5-1	68.2	48.02	47.09	0.741	2142	69.10	71.22	1.797
C-2.5-2	67.5	47.04			1617	71.09		
C-2.5-3	66.9	46.20			1880	73.50		
C-5.0-1	68.5	48.44	47.60	0.686	2142	75.85	75.07	0.571
C-5.0-2	67.9	47.60			1455	74.87		
C-5.0-3	67.3	46.76			1799	74.50		
C-10-1	69.1	49.29	48.07	0.931	1795	80.58	80.94	0.295
C-10-2	68.1	47.88			1787	81.30		
C-10-3	67.5	47.04			1791	80.94		

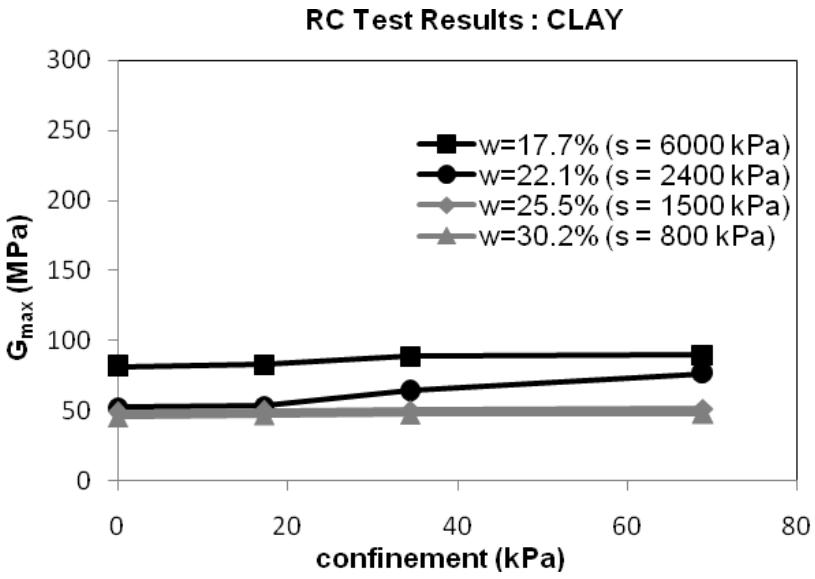

Figure 5.25 Variation of G_{max} with Confinement Using RC Method for Clay

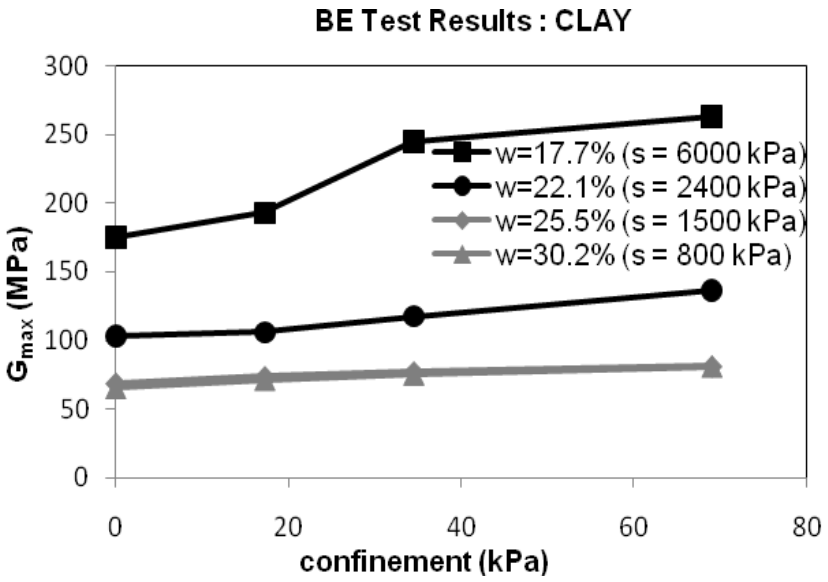

Figure 5.26 Variation of G_{max} with Confinement Using BE Method for Clay

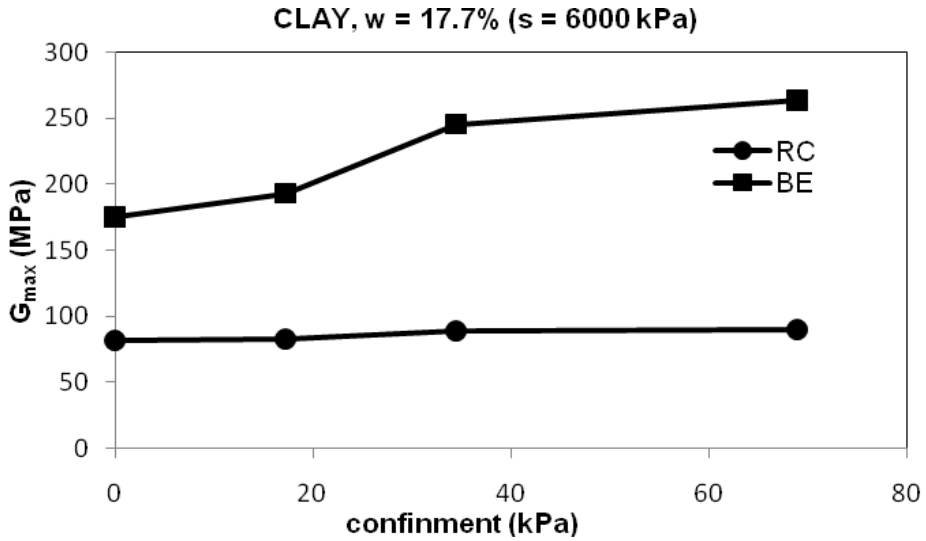

Figure 5.27 Comparison of G_{max} from RC and BE tests on Clay at w = 17.7% (S = 6000 kPa)

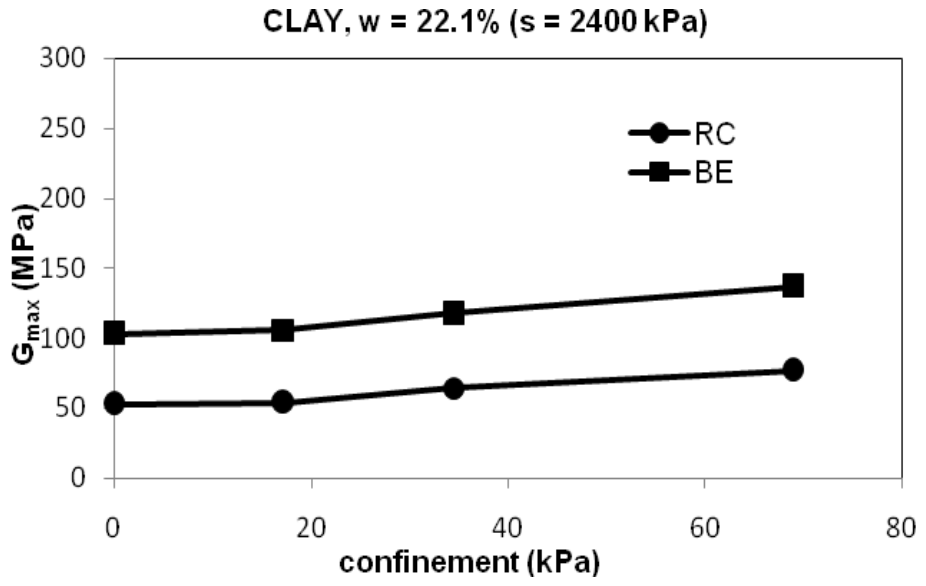

Figure 5.28 Comparison of G_{max} from RC and BE tests on Clay at w = 22.1% (S = 2400 kPa)

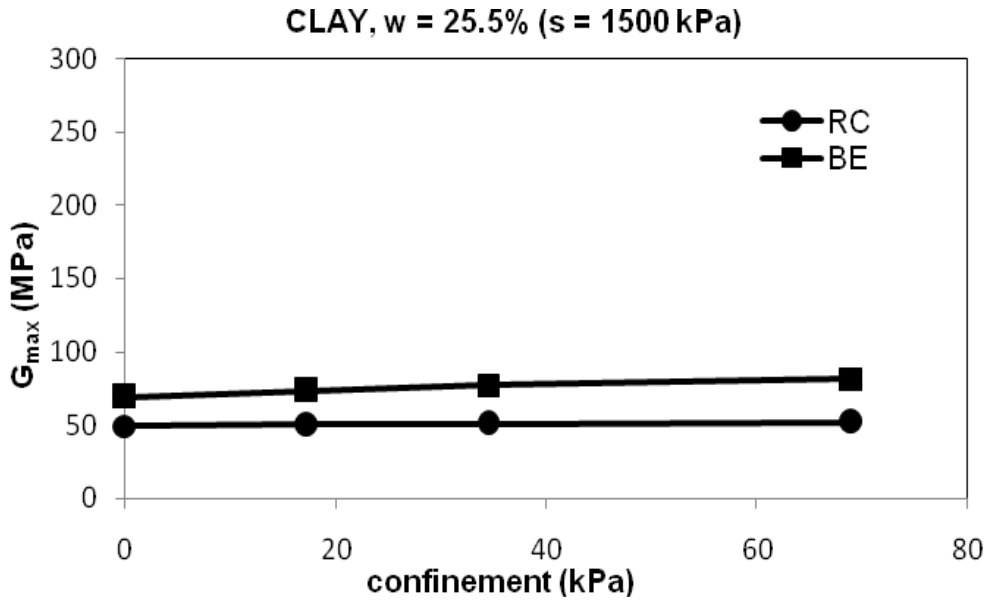

Figure 5.29 Comparison of G_{max} from RC and BE tests on Clay at w = 25.5% (S = 1500 kPa)

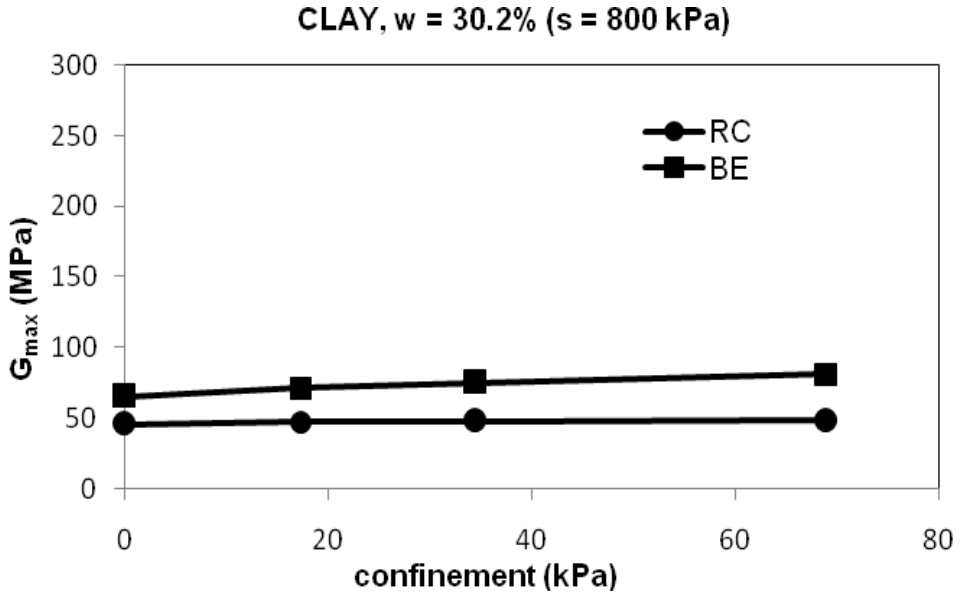

Figure 5.30 Comparison of G_{max} from RC and BE tests on Clay at w = 30.2% (S = 800 kPa)

5.3.2 Normalized G_{Max} /σ_o Data as Function of Suction

Figures 5.31 to 5.33 show values of small-strain shear modulus normalized by level of confinement, that is, G_{max}/Confinement from RC and BE tests presented as functions of compaction-induced suction. In general, the level of confinement has a significant effect on stiffness response of CH soil, i.e. as the confinement increases the normalized G_{max} decreases. It can also be noted the relatively significant influence of compaction-induced suction, there was a considerable increase in the shear modulus G_{max} at higher values of suction.

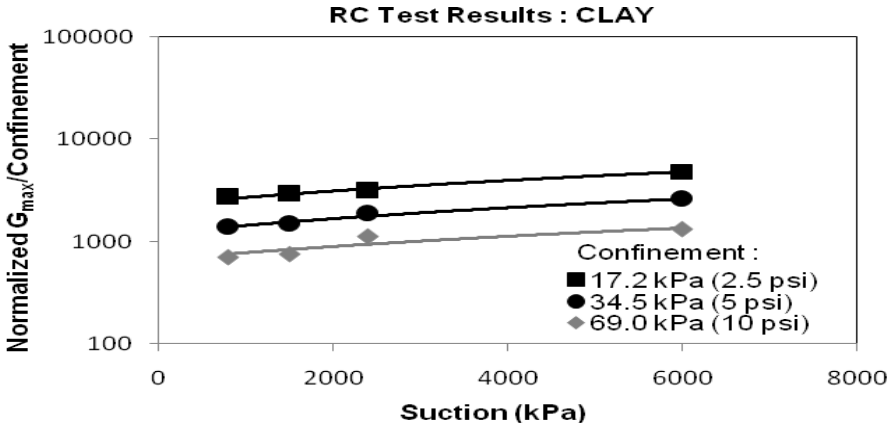

Figure 5.31 Normalized shear Modulus by Confinement with Suction for Clay (RC)

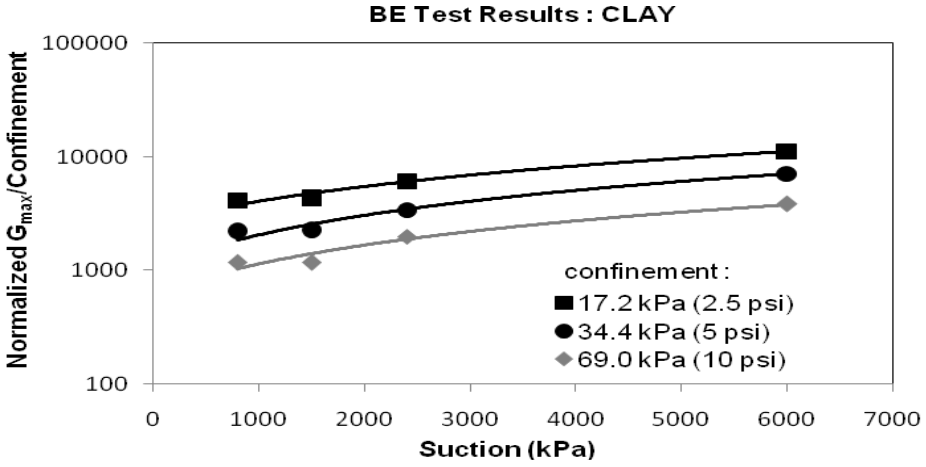

Figure 5.32 Normalized shear Modulus by Confinement with Suction for Clay (BE)

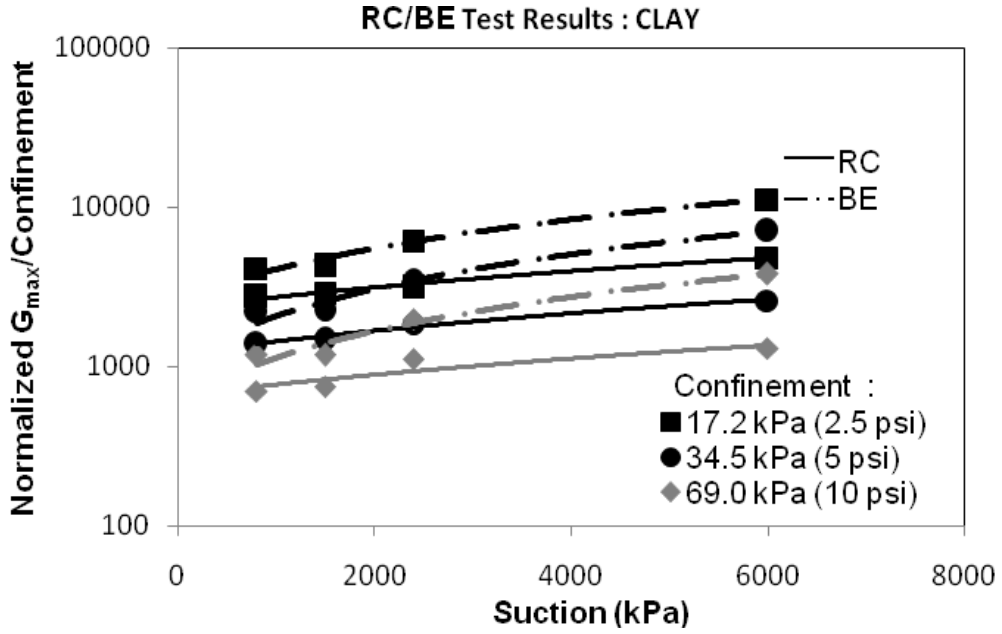

Figure 5.33 Normalized shear Modulus by Confinement with Suction for Clay (RC/BE)

5.4 Material Damping Response: CLAY

A total of 48 RC/BE tests were performed on 12 specimens of high-plasticity clay compacted at four different moisture contents, 5, 10, 15, and 20%, in order to determine relationships between damping ratio D_{min} with isotropic confining pressures and compaction-induced suction from RC and BE tests in the same confining chamber. Results are presented and analysed in the following sections.

5.4.1 Typical Response Curve

Figure 5.34 shows a typical BE test response at 17.2 kPa (2.5 psi) confining pressure and 68.7 kPa suction. The resonant frequency (f_r), corresponding to the peak of the frequency response curve and the half power points (f_1 and f_2) is used to determine matrial damping (D_{min}) for this particular specimen as described in chapter 3.

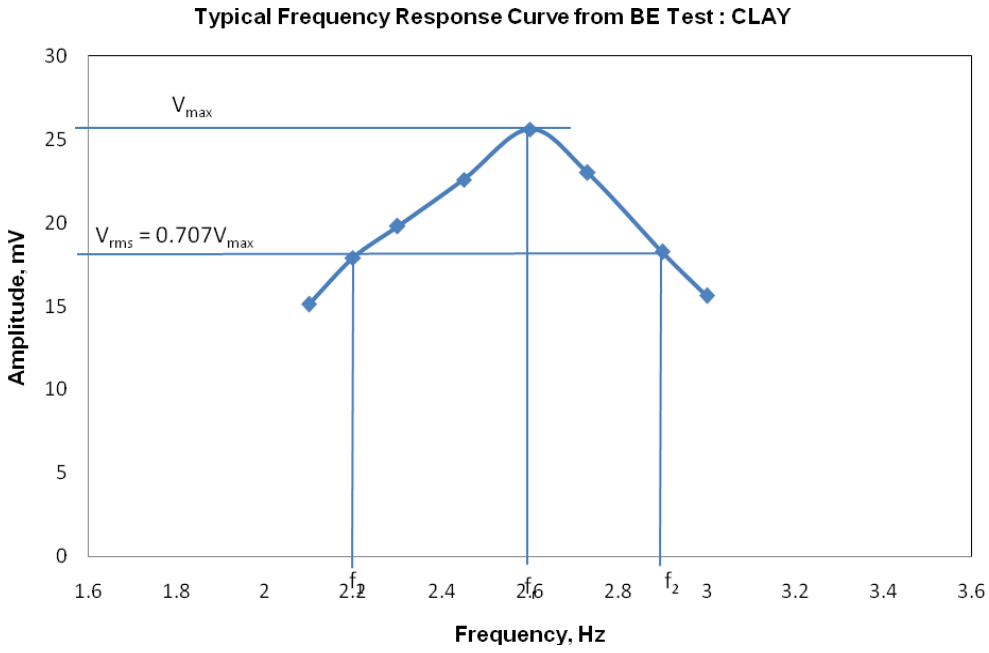

Figure 5.34 Typical BE Test Response from Clay for Damping Ratio

5.4.2 D_{min} Results from RC/BE Tests

Tables 5.13 to 5.16 demonstrate the results of material damping D_{min} of specimens at different isotropic confining pressures from both RC and BE methods.

Figures 5.35 to 5.36 show the variation of damping ratio at four moisture contents i.e. at four different suctions, in RC and BE tests. From these figures it can be observed that the damping ratio increases with decrease in the suction.

Figures 5.37 to 5.40 show the comparison of damping ratio D_{min} from RC and BE tests. From these figures it can be observed that damping ratio decreases with increase in confinement. It can also be noted that at low moisture content, i.e. at high suction value the damping ratio from BE test tends to be greater than that from the RC test and the difference increases with increase in moisture contents, i.e. with decrease in suction values. This explains

that the higher the moisture content, the farther the damping ratio values between both RC and BE methods.

Table 5.13 D_{min} Results from RC/BE Tests on Clay at w = 17.7% (S = 6000 kPa)

Specimen	$D_{min(RC)}$ (MPa)	Avg $D_{min(RC)}$	$SD_{(RC)}$	$D_{min(BE)}$ (MPa)	Avg $D_{min(BE)}$	$SD_{(BE)}$
C-00-1	4.16	4.13	0.02	4.76	4.72	0.03
C-00-2	4.13			4.69		
C-00-3	4.11			4.69		
C-2.5-1	3.59	3.46	0.11	4.65	4.32	0.24
C-2.5-2	3.46			4.22		
C-2.5-3	3.31			4.08		
C-5.0-1	2.16	2.15	0.04	3.61	3.77	0.12
C-5.0-2	2.09			3.79		
C-5.0-3	2.19			3.91		
C-10-1	1.76	1.91	0.11	2.53	2.40	0.27
C-10-2	2.02			2.65		
C-10-3	1.95			2.03		

Table 5.14 D_{min} Results from RC/BE Tests on Clay at w = 22.1% (S = 2400 kPa)

Specimen	$D_{min(RC)}$ (MPa)	Avg $D_{min(RC)}$	$SD_{(RC)}$	$D_{min(BE)}$ (MPa)	Avg $D_{min(BE)}$	$SD_{(BE)}$
C-00-1	4.98	5.29	0.23	7.53	7.71	0.33
C-00-2	5.35			7.43		
C-00-3	5.54			8.17		
C-2.5-1	4.89	4.99	0.07	7.54	7.32	0.19
C-2.5-2	5.01			7.35		
C-2.5-3	5.05			7.07		
C-5.0-1	4.79	4.91	0.08	7.07	7.05	0.01
C-5.0-2	4.97			7.05		
C-5.0-3	4.96			7.03		
C-10-1	4.79	4.75	0.03	6.68	6.67	0.10
C-10-2	4.73			6.78		
C-10-3	4.72			6.53		

Table 5.15 D_{min} Results from RC/BE Tests on Clay at w = 25.5% (S = 1500 kPa)

Specimen	$D_{min(RC)}$ (MPa)	Avg $D_{min(RC)}$	$SD_{(RC)}$	$D_{min(BE)}$ (MPa)	Avg $D_{min(BE)}$	$SD_{(BE)}$
C-00-1	5.87	5.86	0.02	9.84	8.68	0.81
C-00-2	5.89			8.06		
C-00-3	5.84			8.15		
C-2.5-1	5.68	5.73	0.04	8.14	7.97	0.19
C-2.5-2	5.79			7.70		
C-2.5-3	5.72			8.05		
C-5.0-1	5.49	5.54	0.04	7.69	7.71	0.04
C-5.0-2	5.59			7.67		
C-5.0-3	5.54			7.77		
C-10-1	5.51	5.54	0.02	6.13	6.85	0.51
C-10-2	5.55			7.31		
C-10-3	5.57			7.13		

Table5.16 D_{min} Results from RC/BE Tests on Clay at w = 30.2% (S = 800 kPa)

Specimen	$D_{min(RC)}$ (MPa)	Avg $D_{min(RC)}$	$SD_{(RC)}$	$D_{min(BE)}$ (MPa)	Avg $D_{min(BE)}$	$SD_{(BE)}$
C-00-1	6.11	6.26	0.13	12.55	12.41	0.15
C-00-2	6.25			12.20		
C-00-3	6.43			12.50		
C-2.5-1	5.86	5.99	0.09	12.40	11.91	0.50
C-2.5-2	6.07			12.11		
C-2.5-3	6.05			11.22		
C-5.0-1	5.91	5.88	0.07	12.40	11.85	0.54
C-5.0-2	5.78			12.04		
C-5.0-3	5.94			11.11		
C-10-1	5.79	5.87	0.09	11.79	11.50	0.58
C-10-2	5.83			11.02		
C-10-3	6.00			10.68		

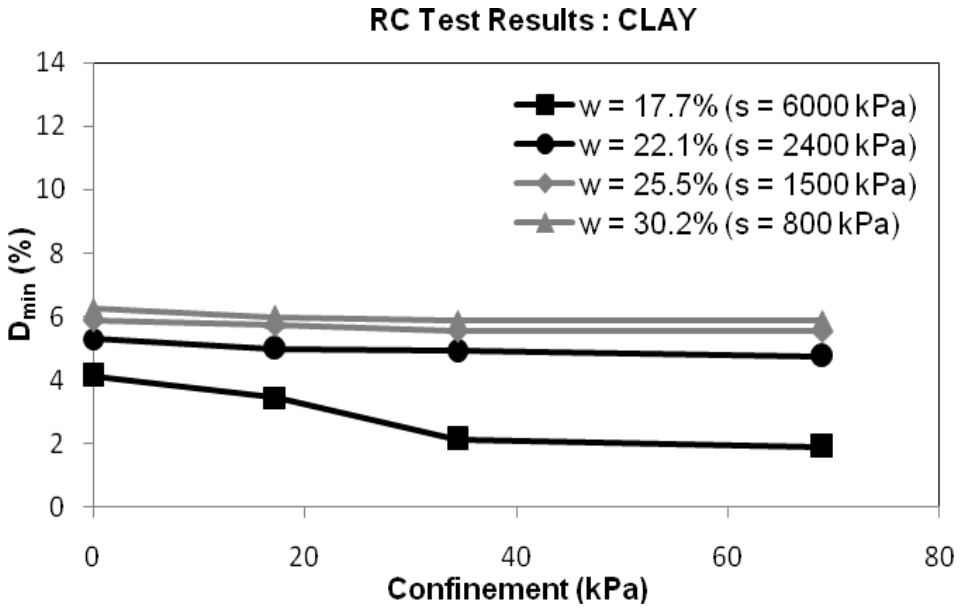

Figure 5.35 Variation of D_{min} with Confinement Using RC Method for Clay

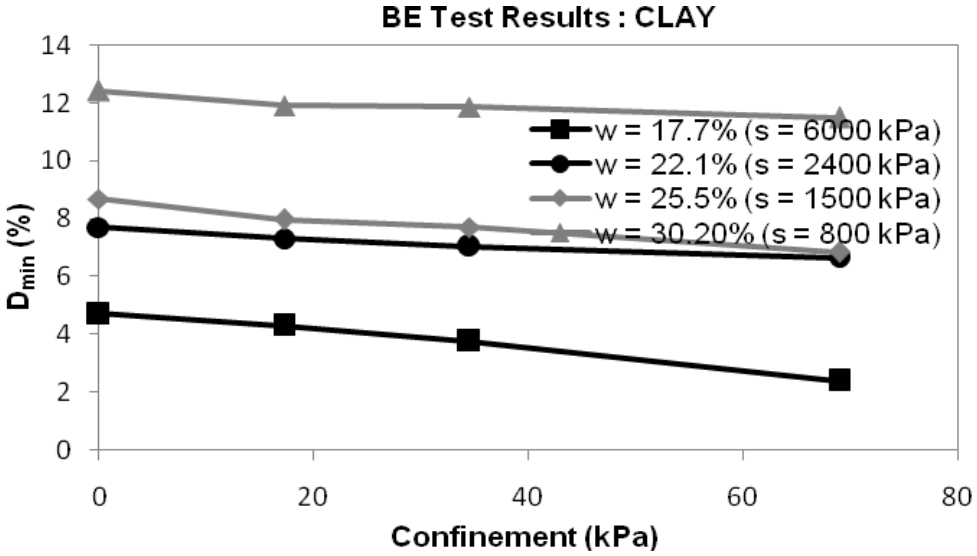

Figure 5.36 Variation of D_{min} with Confinement Using BE Method for Clay

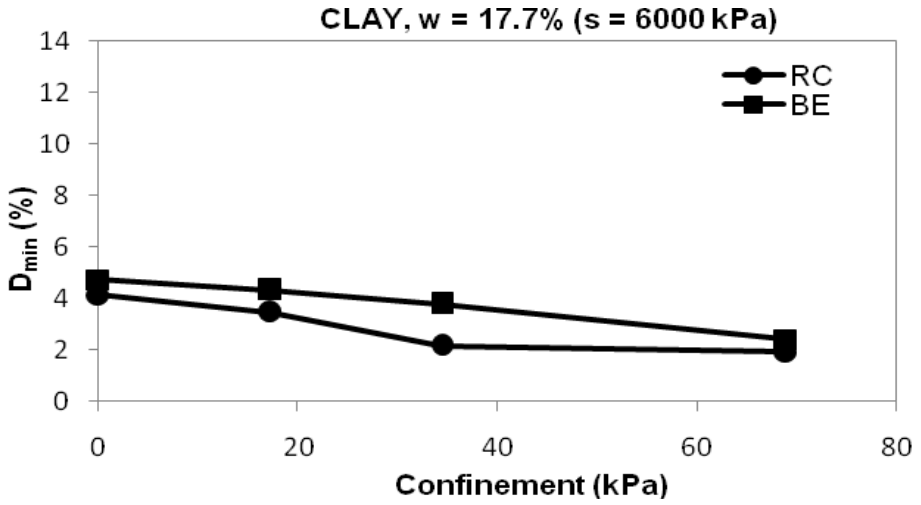

Figure 5.37 Comparison of D_{min} from RC and BE tests on Clay at w = 17.7% (S = 6000 kPa)

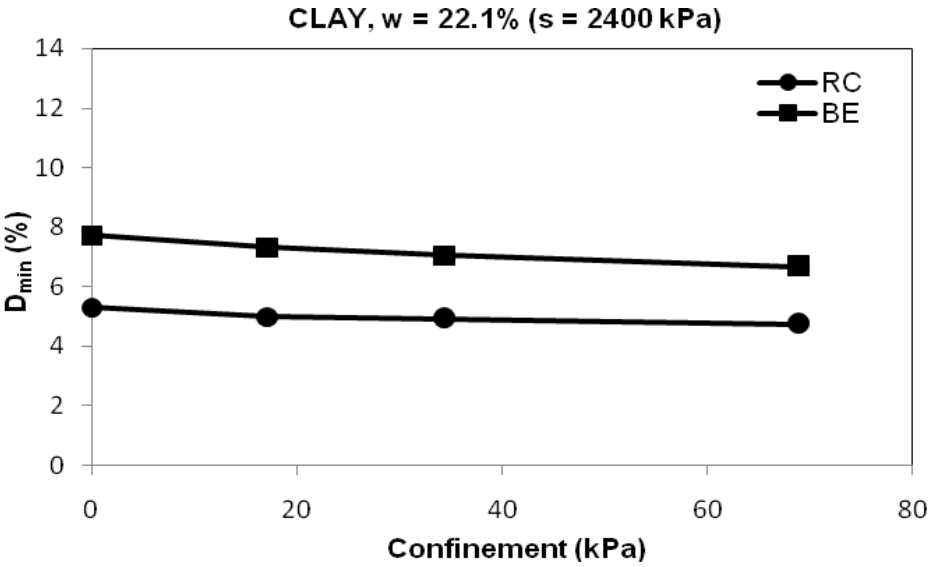

Figure 5.38 Comparison of D_{min} from RC and BE tests on Clay at w = 22.1% (S = 2400 kPa)

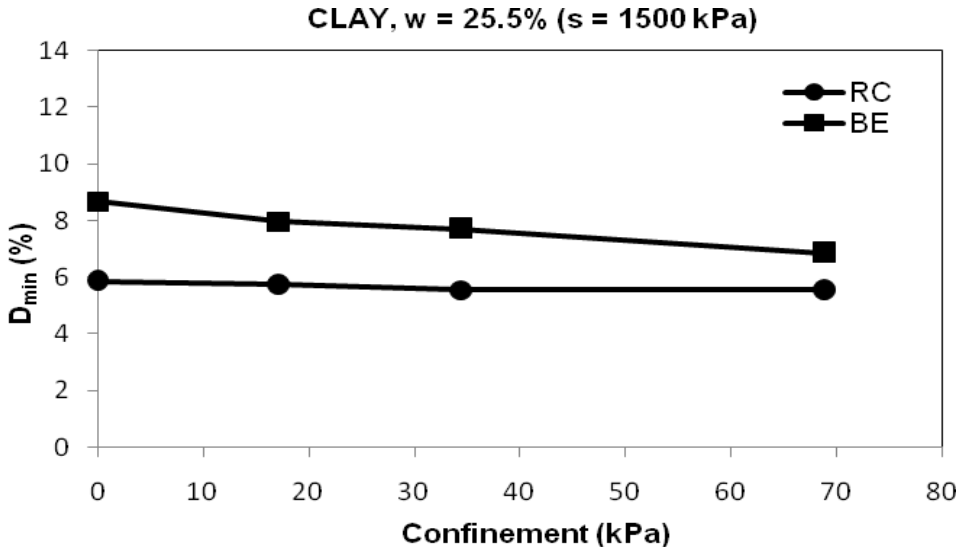

Figure 5.39 Comparison of D_{min} from RC and BE tests on Clay at w = 25.5% (S = 1500 kPa)

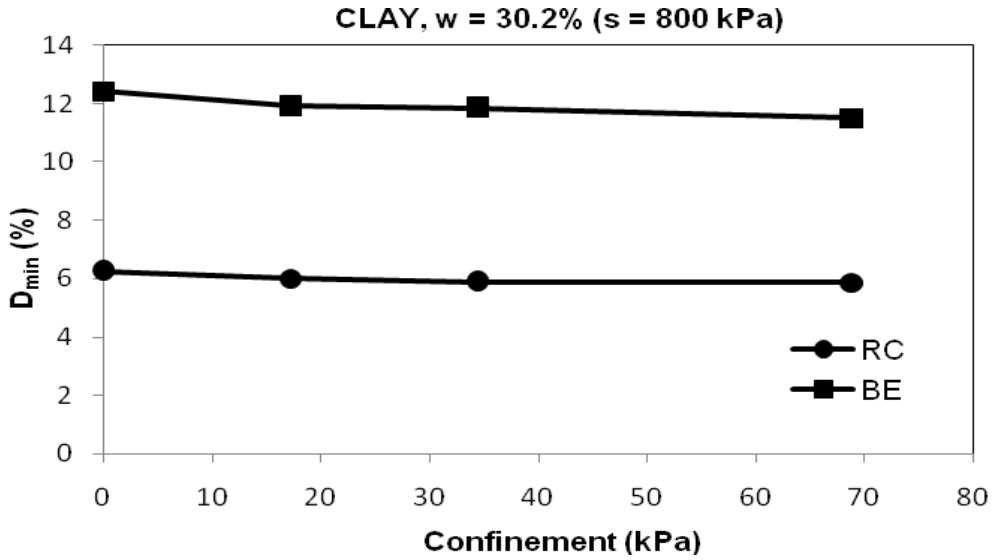

Figure 5.40 Comparison of D_{min} from RC and BE tests on Clay at w = 30.2% (S = 800 kPa)

5.4.3 Normalized D_{min}/σ_o Data as function of Suction

Figures 5.41 to 5.43 show values of material damping normalized by level of confinement, that is, D_{min}/Confinement from RC and BE tests presented as functions of compaction-induced suction. In general, the level of confinement has a significant effect on stiffness response of CH soil, i.e as the confinement increases the normalized D_{min} decreases. It can also be noted the relatively significant influence of compaction-induced suction, there was a considerable decrease in the damping ratio D_{min} at higher values of suction.

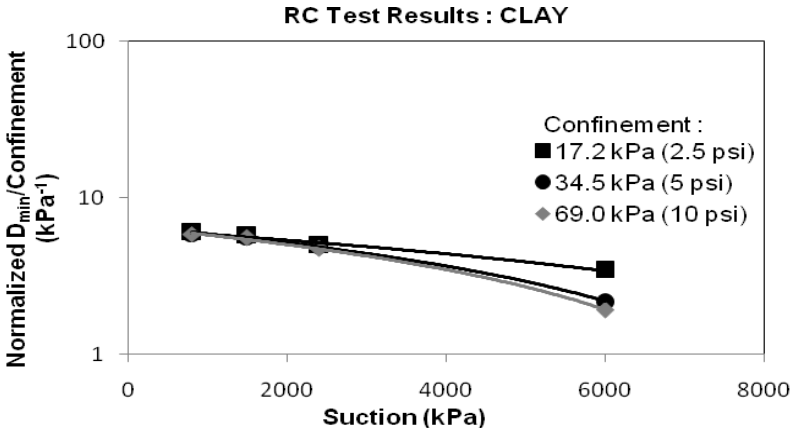

Figure 5.41 Normalized Damping Ratio as Function Suction for Clay (RC)

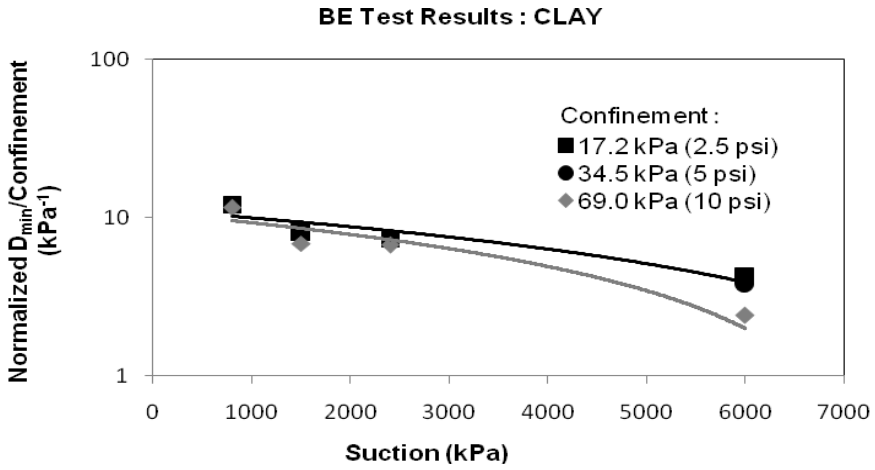

Figure 5.42 Normalized Damping Ratio as Function of Suction for Clay (BE)

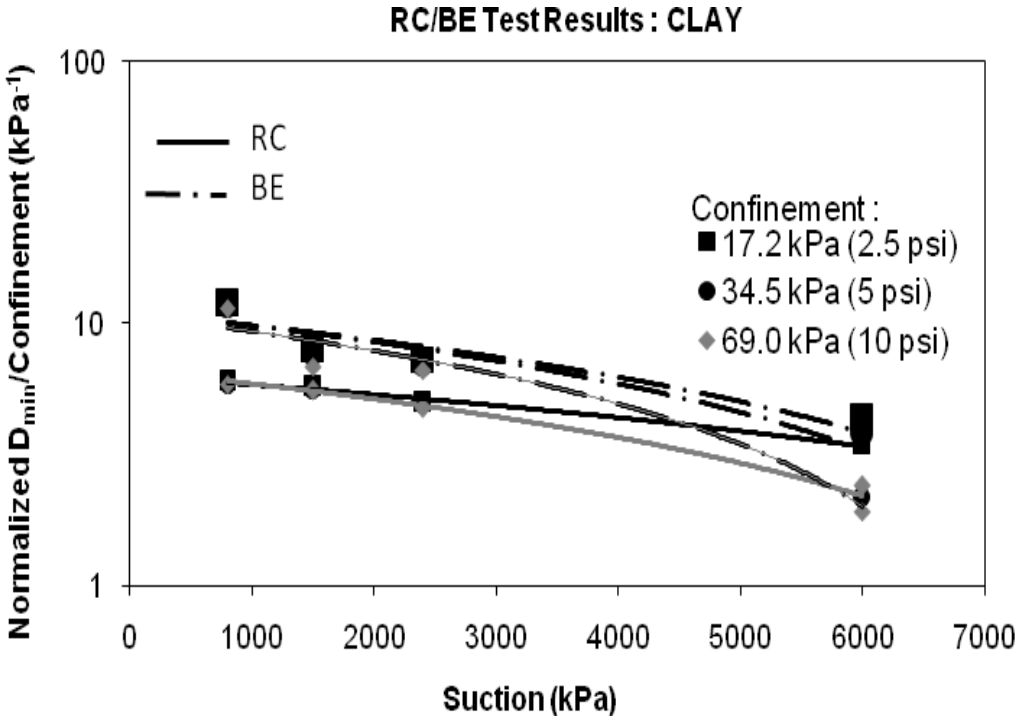

Figure 5.43 Normalized Damping Ratio as Function of Suction for Clay (RC/BE)

5.5 Correction Factor For BE Test Data

Figures 5.44 to 5.45 show the comparison of all G_{max} values obtained from RC and BE tests performed on sand and clay, respectively.

Results show a reasonable good matching between RC and BE tests in poorly-graded sand, with a slight overestimation of G_{max} from BE tests under higher suction conditions, i.e. low moisture content, as shown in figure 5.44.

On the other hand, G_{max} values from BE tests on clay are considerably overestimated, specially under higher suction conditions, i.e. at low moisture contents, as shown in figure 5.45 Differences between G_{max} from BE and RC tests can be as high as 250%.

Although the resonant column technique is a well established method for determining G_{max} in the laboratory, there is nothing that says these results are exactly correct, so the

resonant column and bender element techniques actually serve as a check on each other (Dyvik and Madshus, 1986).

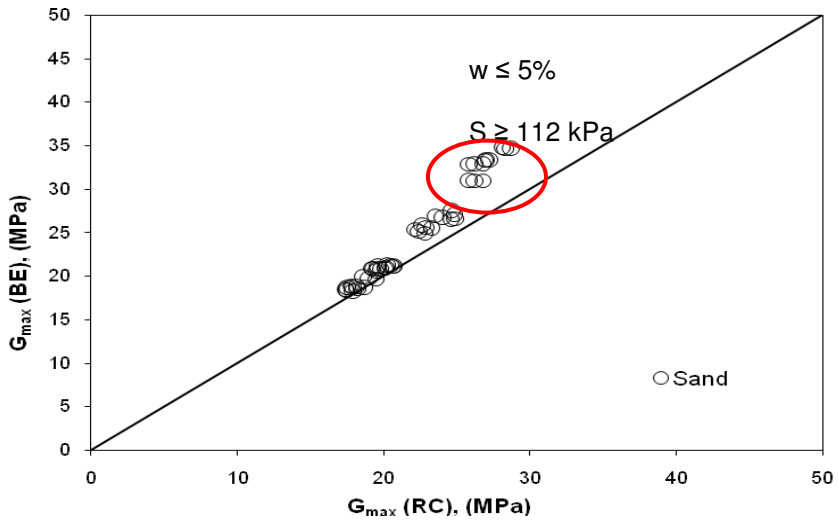

Figure 5.44 Comparison of G_{max} Values from RC and BE tests on Sand

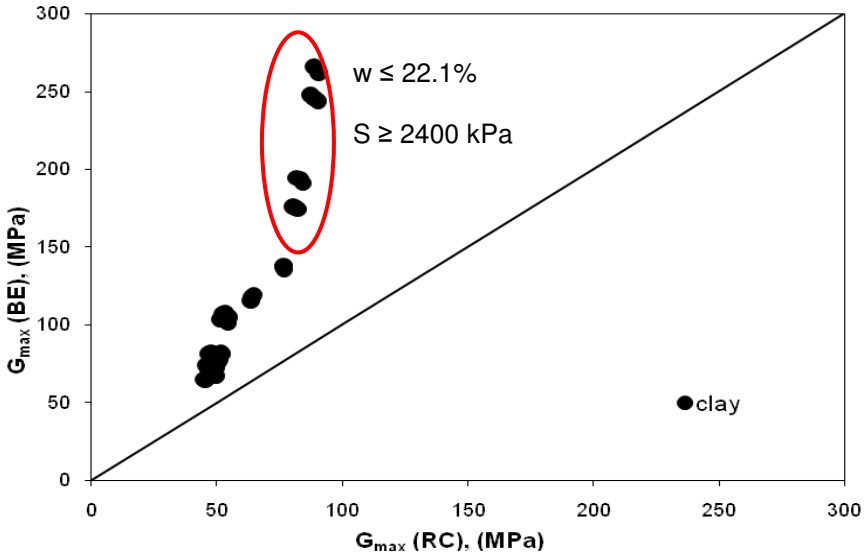

Figure 5.45 Comparison of G_{max} Values from RC and BE tests on Clay

The BE test technique does not appear to yield accurate D_{min} results in sand, as shown in figure 5.46.

Values of D_{min} from BE tests on clay show reasonable good agreement with those from RC tests for a wider range of moisture contents.

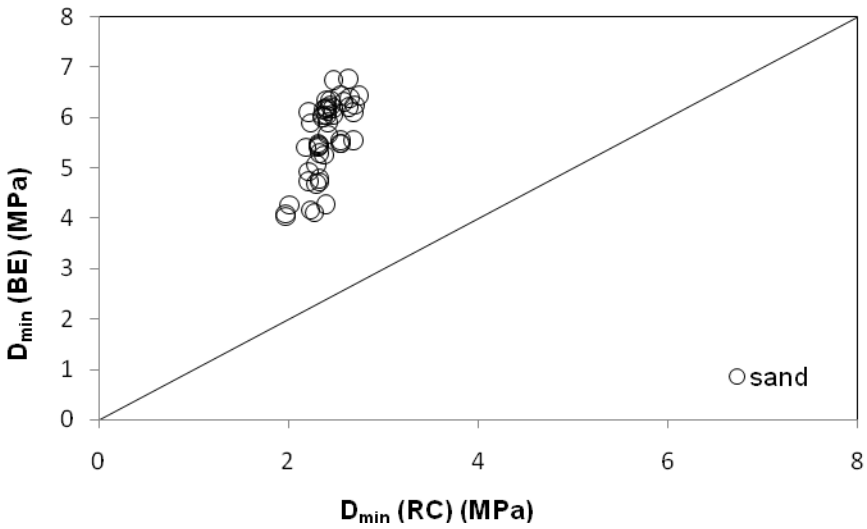

Figure 5.46 Comparison of D_{min} Values from RC and BE tests on Sand

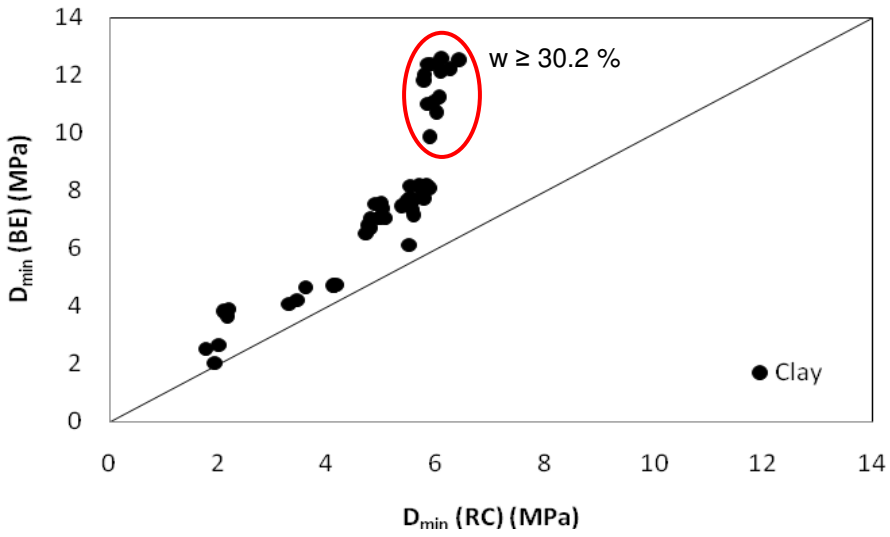

Figure 5.47 Comparison of D_{min} Values from RC and BE tests on Clay

In this work, an attempt was made to devise empirical correction factors to fine-tune experimental data from BE tests by taking RC tests as reference.

A correction factor for G values obtained from BE tests is given in equations 5.1 and 5.2. The equations are devised on the basis of soil suction and confinement.

Likewise, a correction factor for D values is also given by equations 5.3 and 5.4.

Best-fit constants are given in tables 5.17 and 5.18.

Shear Modulus

$$G_{(BE)\,corr} = CF_{BE,G} * G_{BE} \quad (5.1)$$

$$CF_{BE,G} = i(\sigma_o)^j[\Psi^{k.exp(m\sigma_o)}]exp(n\Psi) \quad (5.2)$$

Where:

$CF_{BE,G}$ = Bender element G correction factor

σ_o = Confinement (kPa), $\sigma_o \geq 1$ kPa

Ψ = Matric suction (kPa), S ≥ 1 kPa

I, j, k, m, and n = Constant as shown in table 5.17

Table 5.17 Best-fit Constants for Correction Factor $CF_{BE,\,G}$

Soil Type	i	j	k	m	n
Sand	2.2953	-0.0882	-0.2311	-0.0021	0.0034
Clay	1.5255E-3	0.6724	0.9243	0.0048	-0.0008

Damping Ratio

$$D_{(BE)\ corr} = CF_{BE,D} * D_{BE} \quad (5.3)$$

$$CF_{BE,D} = t(\sigma_o)^u \exp[v\Psi(w\sigma_o^x + y\sigma_o^z)] \quad (5.4)$$

Where:

$CF_{BE,D}$ = Bender Element correction factor

σ_o = Confinement (kPa), $\sigma_o \geq 1$ kPa

Ψ = Matric suction (kPa)

T, u, v, w, x, y, and z = Constant as shown in table 5.18

Table 5.18 Constant Values of BE Correction Factor for Damping Ratio

Soil Type	t	u	v	w	x	y	z
Sand	0.5482	0.0343	0.99	-0.0042	0.2546	0.0059	0.0375
Clay	0.3498	-0.0433	0.0003	0.43	0	0.5	0

Figures 5.48 and 5.51 show the comparison of the shear modulus and damping ratio resuts from resonant column (RC) and bender element (BE) tests after applying corresponding correction factors devised in equations 5.1 and 5.3.

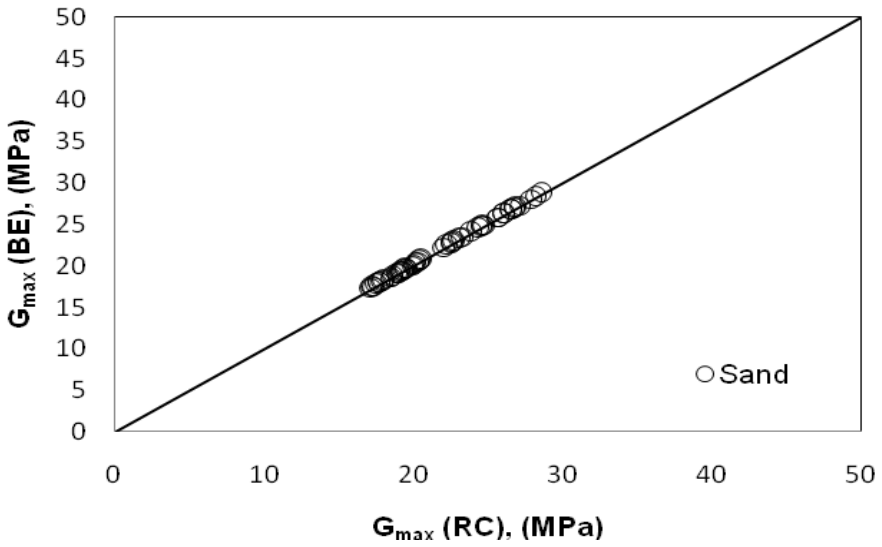

Figure 5.48 Comaprison of G_{RC} and $G_{BE,corr}$ Values for Sand

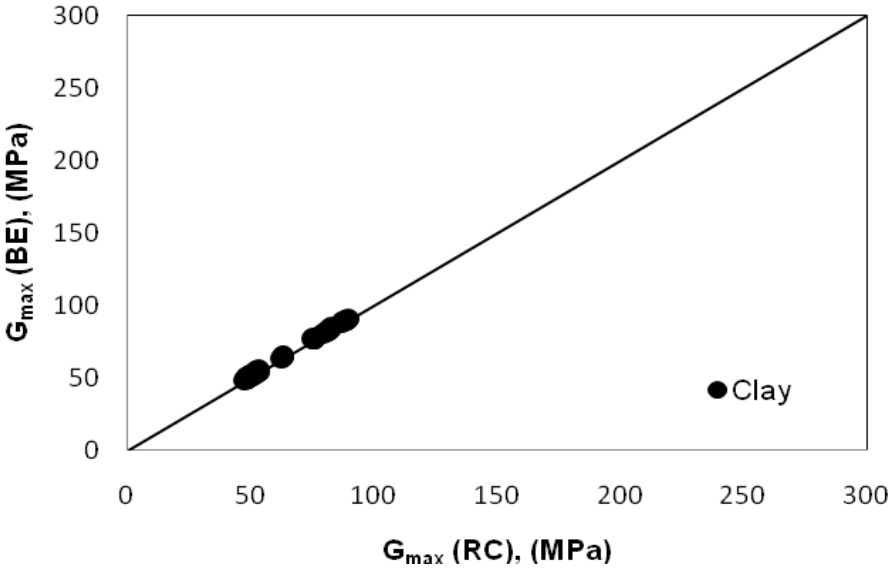

Figure 5.49 Comparison of G_{RC} and $G_{BE,corr}$ Values for Sand

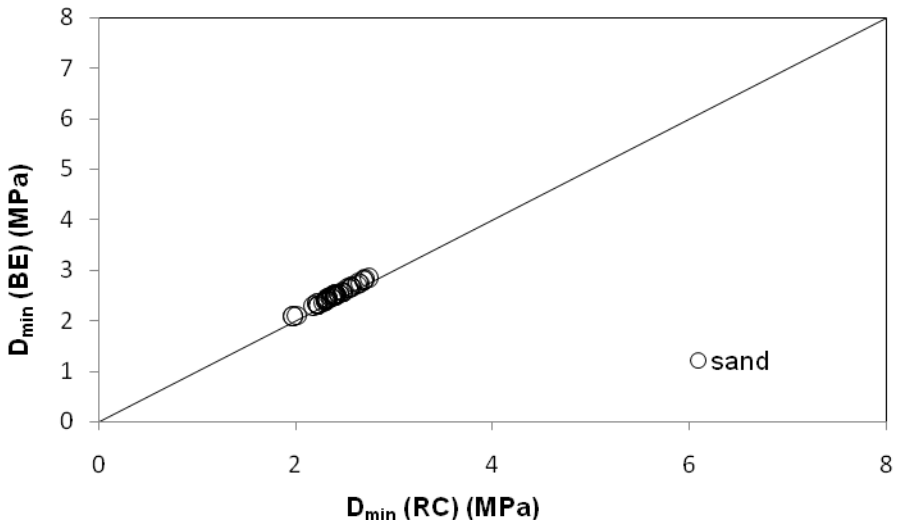

Figure 5.50 Comparison of D_{RC} and $D_{BE,corr}$ Values for Sand

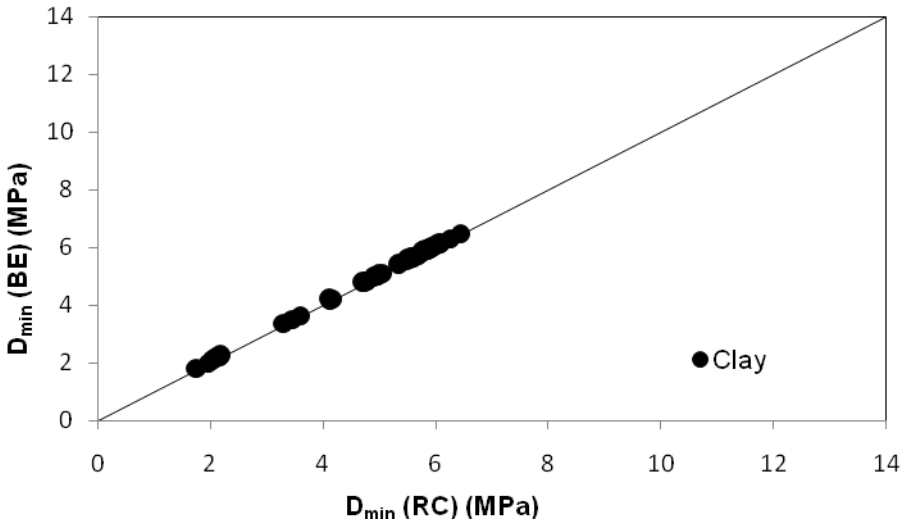

Figure 5.51 Comparison of D_{RC} and $D_{BE,corr}$ Values for Sand

CHAPTER 6

SUMMARY, CONCLUSIONS AND RECOMMENDATIONS

6.1 Summary

The main objective of the present thesis work was threefold: (1) To upgrade an existing resonant column device to accommodate piezoceramic bender elements, hereafter referred to as the RC/BE device; (2) To investigate the influence of key environmental factors, such as compaction-induced suction and confining pressure, on small-strain stiffness properties of unsaturated soils, such as shear modulus G_{max} and damping ratio D_{min}, via simultaneous RC and BE testing; and (3) To assess the feasibility of BE technique for a wide range of compaction-induced suction states.

In order to accomplish this goal a comprehensive series of resonant column and bender element test were simultaneously performed in the developed RC/BE apparatus. RC/BE tests were conducted on compacted specimens of poorly graded sand (SP) and high plasticity clay (CH) prepared at different moisture contents (17.7, 22.1, 25.5, and 30.2% by weight for clay, and 5, 10, 15, 20% by weight for sand) and under different confining pressures (0, 2.5, 5.0, and 10.0 psi, or 0, 17.2, 34.4, and 69.0 kPa).

The high PI clay used in this work was obtained from city of Paris, Texas, while poorly graded sand was obtained from a local supplier in the city of Arlington, Texas. Compaction-induced suction prior to RC/BE testing was assessed from soil-water characteristic curves (SWCC) obtained for SP and CH soils via PPE technique.

6.2 Conclusions

Based on the experimental findings and comprehensive analysis of the test results following conclusions can be drawn from the present thesis work.

1. The small-strain shear modulus (G_{max}) of both poorly graded sand (SP) and high plasticity clay (CH), tend to increase with an increase in the compaction-induced suction. This is because the suction in the soil specimen increases the effective stress which makes the soil sample stiffer.
2. The small-strain shear modulus (G_{max}) of both poorly graded sand (SP) and high plasticity clay (CH), tend to increase slightly with an increase in the isotropic confining pressure
3. On the contrary, damping ration (D_{min}) of both the poorly graded sand (SP) and high plasticity clay (CH), tend to decrease with an increase in the compaction-induced suction and isotropic confining pressure.
4. Results show a reasonable good matching between RC and BE tests in poorly-graded sand, with a slight overestimation of G_{max} from BE tests under higher suction conditions, i.e. low moisture content.
5. On the other hand, G_{max} values from BE tests on clay are considerably overestimated, specially under higher suction conditions, i.e. at low moisture contents. Differences between G_{max} from BE and RC tests can be as high as 250%.
6. The BE test technique does not appear to yield accurate D_{min} results in sand.Values of D_{min} from BE tests on clay show reasonable good agreement with those from RC tests for a wider range of moisture contents.

The range of shear strain amplitudes for which different techniques are suitable for are shown in table 6.1.

RC technique is applicable for shear strain amplitudes between 10^{-2} to 10^{-4}. Bender elements, however, may induce even smaller strains than those for which RC test is suitable for. This may partly explain the differences between RC and BE test results.

Table 6.1 Range and Applicability of Dynamic Laboratory Tests

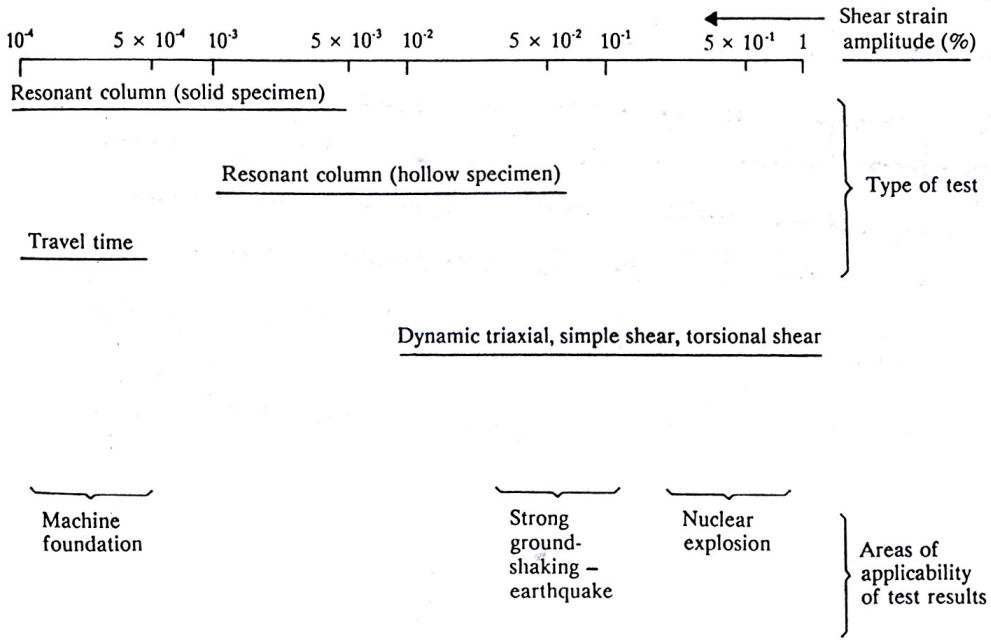

REFERENCES

1. AASHTO (1993). “Guide for design of pavement structures,” American Association of State Highway and Transportation Officials, Washington, DC.
2. Abbiss, C. P. (1981). “Shear wave measurements of the elasticity of the ground.” Geotechnique, 31(1), 91-104.
3. Arulnathan, R., Boulanger, R. W., Kutter, B.L., and Sluis, W. K. (2000). “New tool for shear wave velocity measurements in model tests.” Geotech. Test. J., 23(4), 444-453.
4. ASTM (1993) ‘Test methods for modulus and damping of soils by the resonant column method,” Standard D 4015-92, ASTM, Philadelphia, PA, 581-593
5. Baxter, C. D. P. (1999). “Experimental study on the aging of sands.” Ph.D. Dissertation, Virginia Tech.
6. Brignoli, E. G. M., Gotti, M., and Stokoe, K. H. II. (1996). “Measurement of shear waves in laboratory specimens by means of piezoelectric transducers.” Geotech. Test. J., 19(4), 384-397.
7. Chainuwat, P. (2001) “Effects of compaction moisture content on stiffness properties of chemically stabilized sulfate-rich expansive clays using the resonant column testing device.” M.S. Thesis, The University of Texas at Arlington, TX.
8. Dyvik, R. & Madshus, Ch. (1985). “Lab measurements of G_{max} using bender elements.” Advances in the Art of Testing Soils under Cyclic Conditions; Proc. ASCE, Detroit, 24 October 1985: 186-196. New York: ASCE.
9. Fam, M. A., Cascante, G., Dusseault, M. B. (2002). “Large and small strain properties of sands subjected to local void increase.” Journal of Geotechnical and Goeenvironmental Engineering, 128(12), 1019-1025.

10. Ferreira, Viana Da Fonseca, C., Santos, A. (2007). “Comparison of simultaneous bender elements and resonant column tests on Porto residual soil.” 146, 523-536.
11. Hardin, B. O., and Drnevich, V. P. (1972a). “Shear modulus and damping in soils: Measurement and parameter effects.” J. Soil Mech. and Found. Div., ASCE, 98(6), 603-624.
12. Hardin, B. O., and Drnevich, V. P. (1972b). “Shear modulus and damping in soils: Design equations and curves.” J. Soil Mech. and Found. Div., ASCE, 98(7), 667-692.
13. Hoyos, L. R. (1993). “Dynamic properties of puertorican residual soils using The resonant column device,” M.S. Thesis, The University. of Puerto Rico, Mayaguez, P.R., pp. 85-87.
14. Huoo-ni, S. (1987). “Dynamic properties of sand under true triaxial stress states from resonant-column/torsional-shear tests,” PhD dissertation, The University of Texas, Austin, TX.
15. Isenhower, W. M. (1979). “Torsional simple Shear/resonant column properties of San Francisco bay mud,” Thesis GT80-1, Geotech. Engg. Ctr., The University of Texas, Austin, TX.
16. Jovicic, M., Coop, R., and Simic, M. (1996), “Objective criteria for determining G_{max} from bender element tests,” Geotechnique, Vol. 46, No. 2, pp. 357-362. 285
17. Mancuso, C., Simonelli, A. L., and Vinale, F. (1998), “Numerical analysis of in situ S-wave measurements,” proceedings, Twelfth International Conference on Soil Mechanics and Foundation Engineering, Rio de Janeiro, Vol. 3, pp 277-280.
18. Phayak Takkabutr, (2006). “Experimental investigations on small-strain stiffness properties of partially saturated soils via resonant column and bender element testing.” Ph.D. Dissertation, The University of Texas at Arlington, TX.

19. Pyl, L, Degrade, G. (2000). “Measurement of material damping with bender elements in triaxial cell” Department of Civil Engineering, Structural Mechanics Division, K.U.Leuven, Belgium.
20. Richart, F. E., Hall, J. R. Jr., and Woods, R. D. (1970). “Vibration of soils and foundations,” Prentice-Hall, Inc., Englewood Cliffs, NJ.
21. Richart, F. E. (1975). “Some effects of dynamic soil properties on soil-structure interaction,” J. Geotech. Engg. Div., ASCE, 101(12), pp. 1193-1240.
22. Riemer, M. F., Gookin, W. B., Bray, J. D., and Wartman, J. (1998), “Using reflected shear waves to measure small strain dynamic properties.” Research Report No. UCG/GT-98-01, Department of civil engineering, University of California, Berkelay, CA.
23. Sanchez-Salinero, L., Reosset, J. M., and Stokoe, K. H. (1986). “Analytical studies of body wave propagation and attenuation.” Report GR 86-15 Department of civil engineering, University of Texas at Austin, TX.
24. Shirley, D.J. & Hampton, L.D. (1978), “Shear-wave measurements in laboratory sediments”, Journal of Acoustics Soc. Am., 63(2), 607-613.
25. Souto, A., Hartikainen, J., and Ozudogru, K. (1994). “Measurement of dynamic properties of road pavement materials by the bender element and resonant column tests.” Geotechnique, 44(3), 519-526.
26. Stokoe, K. H. II, Anderson, A. M., Hoar, R. J., and Isenhower, W. M. (1978). “Insitu and laboratory shear velocity and modulus,” Proceedings from Earthquake Engineering and Soil Dynamics Conference, ASCE, III, The University of Texas, Austin, TX, pp. 1498-1502.
27. Stoke, K. H. and Huoo-Ni, S. (1985). “Effects of stress state and strain amplitude on shear modulus of dry sand,” Proceedings of the Second Symposium on the Interaction of Non-Nuclear Munitions with Structures, Panama City, FL, pp. 407- 412.

28. Thomann, J. G. and Hryciw, R. D., 1990, “Laboratory measurement of small strain shear modulus under K0 conditions,” ASTM Geotechnical Testing Journal, Vol. 13, No. 2, pp. 97-105.
29. Viggiani, G., and Atkinson, J. H. (1995a). “Interpretation of bender element tests.” Geotechnique, 45(1), 149-154.

BIOGRAPHICAL INFORMATION

Roshnara Mohammad was born on October 6th, 1984 at the City of Khammam, India. she received her bachelor degree in Civil Engineering from Osmania University, India in June 2005. With the great motivation and enthusiasm for developing higher-level skills and knowledge in the area of civil engineering, she decided to pursue M.S. graduate studies majoring in geotechnical engineering at The University of Texas at Arlington. In August 2006, she was admitted to the Department of Civil Engineering at The University of Texas at Arlington as a Masters candidate. During her studies, she had the opportunity to work as a graduate research assistant under the supervision of Dr. Laureano Hoyos. Miss. Roshnara Mohammad has successfully completed all requirements for the Degree of Masters of Science in Civil Engineering and received the degree on May 10, 2008.